



www.ArabCalligraphy.com

*In the Name of Allah,
The Most Gracious, The Most Merciful.*

Computational Analysis for Nonlinear Boundary Value Problems



By

Arif Hussain

*Department of Mathematics
Quaid-i-Azam University
Islamabad, Pakistan
2019*

Computational Analysis for Nonlinear Boundary Value Problems



By

Arif Hussain

Supervised By

Prof. Dr. Muhammad Yousaf Malik

*Department of Mathematics
Quaid-i-Azam University
Islamabad, Pakistan
2019*

Computational Analysis for Nonlinear Boundary Value Problems



By

Arif Hussain

A THESIS SUBMITTED IN THE PARTIAL FULFILLMENT OF THE REQUIREMENT FOR THE

DEGREE OF

DOCTOR OF PHILOSOPHY

IN

MATHEMATICS

Supervised By

Prof. Dr. Muhammad Yousaf Malik

Department of Mathematics

Quaid-i-Azam University

Islamabad, Pakistan

2019

This thesis is dedicated to my ideal personalities

My Parents

And my dearest and beloved brother

Shaheed Zafar Ali
(LHC KP Police)

May Allah grant you highest place in Jannah.

Thanks to all of you for their support, love and encouragement. You are the personalities whom act like road to reach me at my destination.

Acknowledgement

I start my acknowledgement with the name of Almighty ALLAH (J.J) for his everlasting blessing, love and care. Bundle of thanks to Almighty (J.J) for giving me the strength, wisdom and confidence to complete this work. After Almighty (J.J), I pay my sincere gratitude to Holly Prophet Hazrat Muhammad (PBUH) for his gaudiness towards the seeking of knowledge. I also thanks to Holly Prophet (PBUH) family members (Hazrat Imam Ali (a.s), Hazrat Fatima (s.a), Hazrat Imam Hassan (a.s), Hazrat Imam Hussain (a.s) and specifically Hazrat Imam Mehdi (Alajal)).

I say thanks from core of my heart to my kind supervisor Prof. Muhammad Yousaf Malik for his loving and caring attitude, and providing me the excellent atmosphere to accomplish this work. His expert gaudiness, constructive criticism and continuous encouragement helped me in all time during my research and writing this thesis. I also say thanks to my IRSIP supervisor Prof. Andrew Hazel (School of Mathematics, University of Manchester, United Kingdom) for his gaudiness and expertise to prolong my research at foreign institute and his love and care during my stay at United Kingdom. I would also like to thanks my teachers who taught me able to overcome all the challenges, particularly Mr. Sajjad Hussain, Mr. Karim Khan (Late), Dr. M. Shafique, Dr. Sami, Dr. Rashid, Dr. Sohail Nadeem, Dr. M. Ayub and Dr. Tassarwar Hayat.

I would not imagine completing my acknowledgment without saying thanks to my colleagues and friends. I have no words to express my emotions and love to my dearest friend and colleague Mr. Muhammad Awias for his friendship and love during my Master and PhD studies. I am very pleased to acknowledge my senior lab fellows Dr. Naseer, Dr. Farzana, Dr. Taimoor and Dr. Bilal for their help during my research work. I would also say thanks to my precious and loving juniors Mr. Khalil, Mr. Imad, Mr. Mair and Mr. Usman for their supportive role during my PhD studies. Finally, I would like to thanks my fellows Mr. Rizwan, so-called Dr. Arif, Mr. Zahid and Mr. Zubair. This is injustice to completing this portion without saying thanks to my friends Mr. Safdar Bajwa, Mr. Ali Raza and Mr. Muhammad Ashraf.

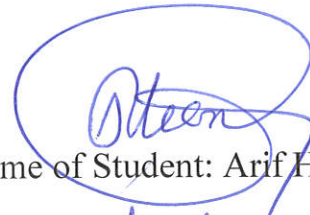
Last, but not least, I would like to thanks the personalities without whom my life is incomplete and colorless, my Parents, Brothers, Sisters, Sister-in-Law, Nephews and Nieces. I could not achieve any goal of my life without their support, love and prayers. Especially thanks to my Abu Jan, Ammi Jan and Bhai Jan (Late) who encouraged me at every moment when I was struggling. I found myself is the luckiest person on the planet having such loving and caring family.

Arif Hussain

Author's Declaration

I **Mr. Arif Hussain** hereby state that my PhD thesis entitled "**Computational Analysis for Nonlinear Boundary Value Problems**" is my own work and has not been submitted previously by me for tacking any degree from this University (**Quaid-I-Azam University**) or anywhere else in the country/world.

At any time if my statement is found to be incorrect even after completion, the university has the right to withdraw my PhD degree.



Name of Student: Arif Hussain

Date: 07/06/2019

Plagiarism Undertaking

I solemnly declare that research work presented in the thesis entitled “**Computational Analysis for Nonlinear Boundary Value Problems**” is solely my research work with no significant contribution from any other person. Small contribution/help wherever taken has been duly acknowledged and that complete thesis has been written by me.

I understand the zero tolerance policy of the HEC and Quaid-I-Azam University, Islamabad towards plagiarism. Therefore I as an Author of the above titled thesis declare that no portion of my thesis has been plagiarized and any material used as reference is properly referred/cited.

I undertake that if I am found guilty of any formal plagiarism in the above titled thesis even after ward of PhD degree, the University reserved the rights to withdraw/revoke my PhD degree and that HEC and the University has the right to publish my name on the HEC/University Website on which names of student are placed who submitted plagiarized thesis.

Signature/Author Signature:



Name: Arif Hussain

17/06/2019

Computational Analysis for Nonlinear Boundary Value Problems

By

Arif Hussain

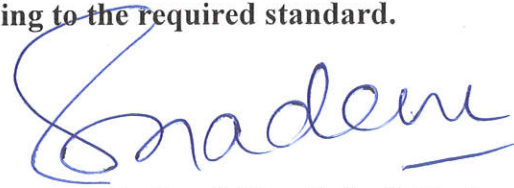
CERTIFICATE

A DISSERTATION SUBMITTED IN THE PARTIAL FULFILMENT OF THE REQUIREMENT FOR THE DEGREE OF THE DOCTOR OF PHILOSOPHY

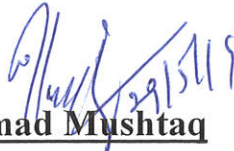
We accept this dissertation as confirming to the required standard.



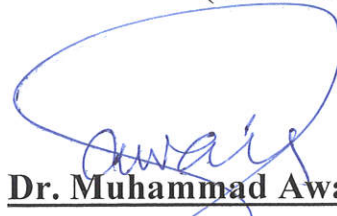
1. **Prof. Dr. Muhammad Yousaf Malik**
(Supervisor)



2. **Prof. Dr. Sohail Nadeem**
(Chairman)



3. **Dr. Muhammad Mushtaq**
Assistant Professor
Department of Mathematics,
COMSATS University,
Islamabad Campus
Park Road, Islamabad
(External Examiner)



4. **Dr. Muhammad Awais**
Assistant Professor
Department of Mathematics,
COMSATS University, Attock
Campus, Attock
(External Examiner)

Department of Mathematics
Quaid-I-Azam University
Islamabad, Pakistan
2019

Certificate of Approval

This is to certify that the research work presented in this thesis entitled Computational Analysis for Nonlinear Boundary Value Problems was conducted by Mr. Arif Hussain under the kind supervision of Prof. Dr. Muhammad Yousaf Malik. No part of this thesis has been submitted anywhere else for any other degree. This thesis is submitted to the Department of Mathematics, Quaid-i-Azam University, Islamabad in partial fulfillment of the requirements for the degree of Doctor of Philosophy in field of Mathematics from Department of Mathematics, Quaid-i-Azam University Islamabad, Pakistan.

Student Name: Arif Hussain

Signature: 

External committee:

a) External Examiner 1:

Name: Dr. Muhammad Mushtaq

Designation: Assistant Professor

Office Address: Department of Mathematics, COMSATS University
Islamabad Campus, Park Road ChackShehzad, Islamabad.

Signature: 

b) External Examiner 2:

Name: Dr. Muhammad Awais

Designation: Assistant Professor

Office Address: Department of Mathematics, COMSATS University, Attock
Campus, Attock.

Signature: 

c) Internal Examiner

Name: Dr. Muhammad Yousaf Malik

Designation: Professor

Office Address: Department of Mathematics, QAU Islamabad.

Supervisor Name:

Prof. Dr. Muhammad Yousaf Malik

Signature: 

Signature: 

Name of Dean/ HOD

Prof. Dr. Sohail Nadeem

Signature: 

Preface

Mostly fluids which are very useful in our daily life and industry do not obey the Newtonian law of viscosity. These fluids are called non-Newtonian fluids, these can be subdivided into two categories i.e. viscoelastic and viscoinelastic fluids. Viscoinelastic fluids are those in which viscosity is prominent factor regarding internal opposition of molecules. Viscoinelastic fluids are further categorized with shear thinning and shear thickening etc. The common examples of these fluids are lubricating greases, waterborne coatings, multiphase mixers, paints, suspensions, emulsions, blood, polymer sheets and biological fluids etc. The flow of electrically conducting fluids is encountered in almost every branch of science e.g. astrophysics, geophysics, mechanical engineering, aerospace engineering, nuclear engineering and bio engineering etc. Also, this concept is incorporated in many industrial processes and daily use devices such as MHD pumps, MHD power generator and electromagnetic propulsion etc. Additionally, turbulence of fluid is also handled with magnetic field. Hall current effects are noteworthy in electrically conducting fluids when applied magnetic field is strong or fluids with low density. This is an important phenomenon having many applications such as Hall accelerates, Hall sensors etc. Heat transfer over stretching surfaces is encountered in many practical applications, because cooling/heating is an important factor to achieve the desired quality of product. For instance many processes/products like extrusion, paper production, fiber-glass production, hot rolling, condensation process, crystal growing, polymer sheets, artificial fibers and plastic films etc. based on heat transfer of boundary layer flows. Thermal conductivity of fluids enlarges by increasing the temperature of fluid and vice versa. Thus fluids having low thermal conductivity are used for cooling in many industrial or daily life products. Experimentally, it is observed that when fluid particles move, the viscosity of fluid alters some part of kinetic energy into thermal energy i.e. dissipate energy. Such type of dissipation is called viscous dissipation. In heat transfer of many practical problems, it plays an important role. Joule heating is an important factor in heat transfer of electrically conducting fluid flows. This phenomenon has a lot of applications such as electric stoves, electric heaters, cartridge heaters, electric fuses, electronic cigarettes, vaporizing propylene glycol and vegetable glycerin etc. Also, it is utilized in some food processing equipment. Nanofluids are modern type of fluids which are combination of base fluid and nano-sized metal particles. The principal objective of including these particles to enlarge the thermal conductivity of base fluids, because it is observed that mostly fluids (water, oil, ethylene glycol, engine oil etc.) which are traditionally utilized in thermal processes possessing low thermal conductivity.

Recently, nanofluids are found very useful in bio-medicine and bio-engineering. Thus due to substantial importance of these phenomena has motivated to explore these important features of fluid flows in current work. Since Sisko fluid and Prandtl-Eyring fluid models have great importance in industry but have not been discussed for stretching cylinder so far. Thus, present work has main focus on these models. Numerical solutions are obtained through robust numerical techniques (Keller Box method, Finite element method and Shooting method).

The layout of this thesis is as follows:

Literature review of present work is presented in chapter 0.

In chapter 1, the boundary layer flow of MHD Sisko fluid over stretching cylinder along with heat transfer is investigated. The cylindrical polar co-ordinates are used to model the physical problems. This modeling yields the nonlinear set of partial differential equations. The modelled equations are transferred to non-dimensional form after application of appropriate similarity transformations. The obtained equations are solved numerically with the aid of shooting technique in conjunction with Runge-Kutta fifth order scheme. The expressions for velocity and temperature are computed under different parametric conditions and deliberated in graphical manner. The local Nusselt number and wall friction coefficient are calculated and described in quantitative sense through graphs and tables. The contents of this chapter are published in **International Journal of Numerical Methods for Heat & Fluid Flow 26(2016)1787-1801**.

Chapter 2 extends chapter 1 by factoring thermal conductivity effects into account. This chapter addresses the influences of variable thermal conductivity and applied magnetic field on boundary layer flow of electrically conducting Sisko fluid over stretching cylinder. The modelled partial differential equations are highly nonlinear. A set of ordinary differential equations is obtained after applying appropriate similarity transforms. The attained equations are solved with efficient numerical technique (i.e. shooting method). Impact of flow controlling parameters on velocity, temperature, coefficient of wall friction and wall heat flux is delineated via graphical and tabular manners. A comparison with literature is made to ensure the validity of computed results. The contents of this chapter are published in **AIP Advances 6 (2016) 025316, DOI: 10.1063/1.4942476**.

Chapter 3 focuses on the physical aspects of viscous dissipation and variable thermal conductivity on non-Newtonian Sisko fluid flow over stretching cylinder under the influence of normally impinging magnetic field. The modelled partial differential equations are transfigured into ordinary differential equations with the aid of scaling group of transforms. The highly nonlinear ordinary differential equations are tackled with numerical scheme Runge-Kutta-Fehlberg method. The focused physical quantities (velocity, temperature, coefficient of wall friction and wall heat flux) are calculated and variations in these quantities are displayed

graphically as well as tabular by choosing feasible values of involving physical parameters. The accuracy of adapted method is certified by comparing present results with reported literature. The contents of this chapter are published in **Results in Physics 7(2017)139-146**.

Chapter 4 explicates the combined effects of viscous dissipation and Joule heating on boundary layer flow of MHD Sisko nanofluid over stretching cylinder. The flow governing equations are highly nonlinear set of partial differential equations with appropriate boundary conditions. These equations are converted into system of ordinary differential equations by using suitable similarity transformations and then solved the resulting boundary value problem with the help of shooting technique. The velocity, temperature and nanoparticle concentration are computed numerically in dimensionless form. The effects of pertinent flow parameters on these quantities are displayed with the help of graphs. Physical phenomena in vicinity of stretching surface are explained with the help of skin friction coefficient, local Nusselt number and local Sherwood number. Also, effects of physical parameters are depicted with the assistance of graphs and tables. The comparison of present and previous results exhibits good agreement which leads to validation of the presented model. The contents of this chapter are published in **Journal of Molecular Liquids 231(2017)341-352**.

In chapter 5, a computational study has been established to explore the physical aspects of non-Newtonian Prandtl-Eyring fluid flow over stretching sheet under the influence of normally applied magnetic field. The mathematical formulation of this flow configuration produces highly nonlinear system of simultaneous partial differential equations. The formulated problem is transformed to non-dimensional model by applying suitable scaling variables. The numerical solution of resulting nonlinear boundary value problem is computed with the assistance of finite difference scheme Keller-Box method. The concerned physical quantities i.e. velocity and coefficient of wall friction are computed and discussed under different parametric conditions. The graphs and tables are developed to deliver the effects of involved physical parameters on focused physical quantities. A comparative study has been made of obtained results with the literature. The contents of this chapter are published in **Neural Computing & Applications 31(2019)425-433**.

Applications of generalized Fourier law of heat conduction on MHD Prandtl-Eyring fluid flow over stretching sheet with temperature dependent thermal conductivity has been made in chapter 6. Modelled system of nonlinear partial differential equations is transformed to system of ordinary differential equations by using similarity transformations after simplifying through boundary layer assumptions. Shooting method is applied to compute numerical results for the obtained nonlinear system of ordinary differential equations. The graphs are adorned to investigate the influences of governing parameters on fluid velocity and

temperature. Local wall friction coefficient and local Nusselt number are computed to explore physical aspects near the stretched surface. The impacts of controlling parameters on these physical quantities are revealed through tables. Additionally, a correlation between present and previous results is presented to justify the validation of present results. The contents of this chapter are published in **International Journal of Numerical Methods for Heat & Fluid Flow (2019), DOI: 10.1108/HFF-02-2019-0161.**

Chapter 7 spotlights the effects of Hall current on Christove-Cattaneo heat flux model for viscous fluid flow over stretching sheet with variable thickness. The modelled problem comprises highly nonlinear partial differential equations with presubscribed boundary conditions. To facilitate the computation process, an appropriate group of similar variables is utilized to transfigure governing flow equations into dimensionless form. To find more compatible and realistic solution of obtained non-dimensional boundary value problem well-known numerical scheme shooting method is used. Numerical results are accomplished and interesting aspects of axial velocity, normal velocity and temperature are visualized via graphs by varying involving physical parameters. A comprehensive discussion is presented to delineate the effects of flow parameters on axial wall friction, transverse wall friction and wall heat flux in tabular form. A comparison of computed results (in limiting case) is presented to authenticate the present computations. The contents of this chapter are under review in peer-reviewed journal.

Chapter 8 narrates the physical features of gravity-driven swimming microorganisms in the boundary layer regime of MHD viscous nanofluid flow over stretching surface. The mathematical configuration of flow problem yields the nonlinear simultaneous partial differential equations. These equations are then transformed to non-dimensional form by applying scaling variables on it. The numerical solution of resulting system of non-dimensional partial differential equations is computed with finite element method. The deviations in interesting physical quantities are demonstrated through graphs by varying the flow governing parameters.

Contents

0	Introduction	4
1	Numerical solution of MHD Sisko fluid over a stretching cylinder and heat transfer analysis	15
1.1	Problem formulation	15
1.2	Shooting method	24
1.3	Results and discussion	27
1.4	Concluding remarks	38
2	Magnetohydrodynamic flow of Sisko fluid over a stretching cylinder with variable thermal conductivity: A numerical study	39
2.1	Mathematical formulation	40
2.2	Numerical solution	43
2.3	Results and discussion	44
2.4	Concluding remarks	55
3	Computational analysis of magnetohydrodynamic Sisko fluid flow over a stretching cylinder in the presence of viscous dissipation and temperature dependent thermal conductivity	57
3.1	Development of problem	58
3.2	Numerical solution	61
3.3	Results and discussion	63
3.4	Concluding remarks	73

4	Combined effects of viscous dissipation and Joule heating on MHD Sisko nanofluid over a stretching cylinder	74
4.1	Problem formulation	75
4.2	Numerical solution	79
4.3	Results and discussion	81
4.4	Concluding remarks	93
5	Computational and physical aspects of MHD Prandtl-Eyring fluid flow analysis over a stretching sheet	95
5.1	Formulation of physical problem	95
5.2	Keller-box method	102
5.3	Results and discussion	108
5.4	Conclusions	113
6	Application of generalized Fourier heat conduction law on MHD viscoelastic fluid flow over stretching surface	114
6.1	Physical configuration of problem	115
6.2	Computational algorithm	119
6.3	Results and discussion	120
6.3.1	Validation of present results	120
6.3.2	Velocity profile	121
6.3.3	Temperature profile	123
6.3.4	Wall friction factor and wall heat flux	126
6.4	Enumerated key findings	127
7	Thermal energy change in Christov-Cattaneo heat flux model for MHD fluid flow over variable thickened sheet with Hall current effects: A computational study	128
7.1	Problem development	129
7.2	Numerical solution	135
7.3	Results and discussion	136

7.3.1	Validity of computed results	136
7.3.2	Effects of wall thickness parameter	137
7.3.3	Effects of Hartmann number	138
7.3.4	Effects of Hall parameter	140
7.3.5	Effects of nonlinearity parameter	142
7.3.6	Effects of thermal relaxation parameter and Prandtl number	144
7.3.7	Radial and transverse friction factors and local Nusselt number	145
7.4	Enumerated key results	151
8	On the movement of gravity-driven swimming microorganisms in viscous nanofluid flow	152
8.1	Configuration of physical problem	153
8.2	Finite element method	156
8.3	Results and discussion	161
8.3.1	Validity of computed results	161
8.3.2	Axial Velocity Profile	165
8.3.3	Concentration profile	170
8.3.4	Motile microorganisms density	173
8.3.5	Wall friction factor, wall heat flux, wall mass flux and wall microorganism density flux	175
8.4	Concluding remarks	178

Chapter 0

Introduction

Most of processes occurred in nature are nonlinear i.e. this phenomenon encountered in many disciplines of universe (nature science, life science, social science etc.). The salient features of nonlinear phenomena have been explored with the help of applied mathematics. Mathematical formulations of these phenomena yield nonlinear mathematical systems. These nonlinear systems consist on algebraic equations, recurrence relations and/or differential equations. In natural sciences, specifically in physics, mostly nonlinear problems are handled with differential equations e.g. Navier-Stokes equations(fluid dynamics), Nonlinear Schrödinger equations(optics), Sine-Gorden equations(differential geometry), Einstein field equations(general relativity), Korteweg–de Vries equation(wave phenomenon) etc. In current analysis, Navier-Stokes equations are studied, these are nonlinear partial differential equations (even in one-dimensional flow case). These equations explicate the dynamics of fluids in different physical situations. Two kinds of problems usually occurred in fluid dynamics i.e. initial and/or boundary value problems. In present analysis, the designed problems are nonlinear boundary value problems. As these problems are highly nonlinear, thus numerical techniques are applied to analyze more compatible and realistic situations. Because analytic solution for conducting equations is intractable in order to illustrate the behaviour of interesting physical quantities.

Many fluids experienced in daily life did not obey the Newton viscosity law i.e. deformation rate and shear stress are not linearly related for these fluids e.g. lubricating greases, oil, polymer sheets, rubber sheets, paints, emulsions, ketchup, toothpaste, blood, slurries and silly putty etc., called non-Newtonian fluids. Hence these fluids are an influential issue in few recent years

which attracted researchers attentions. As, in Newtonian fluids shear properties are discussed with deformation rate but in non-Newtonian fluids this concept is not feasible. In addition, non-Newtonian fluids comprises different varieties e.g. viscoelastic, nonlinear viscoelastic, shear thinning, shear thickening, rheopectic, thixotropic etc. Also, important characteristics of these fluid with single constitutive system is useless. So, numerous constitutive equations were proposed to examine the physical properties of these fluids. These fluids are subdivided into two major types i.e. viscoelastic and viscoinelastic. Current analysis focuses on viscoinelastic fluids. These fluids have similar behaviour at zero shear stress while properties of these fluids are quite dissimilar against applied stress. Thus, researchers proposed various models to investigate the physical aspects of viscoinelastic fluids more accurately. Few among them are power law model, Prandtl fluid model, Powell-Eyring model, Sisko fluid model and Prandtl-Eyring fluid model etc. Among these fluid models power law fluid model is most felicitous model to presage attitude of non-Newtonian fluids. But, it can predicts fluid properties in the power law region only while it fails to analyze flow characteristics when shear rate become very small or large. This deficiency overcomes in Sisko fluid model by adding high shear rate effects, (this model was proposed by Sisko [1] in 1958). In his investigation, he considered three different greases and compared the results of Bingham and Ree-Eyring fluid models with experimental data. But he found that these models fail to describe flow properties of lubricating greases. Thus he proposed the Sisko model. The results of this model were matched with the experimental data. Also, it is experimentally verified that Sisko fluid model predicts the properties of many real fluids which are used in chemical engineering. Recently, this model was investigated by many researchers under different physical environments. Akyildiz et al. [2] investigated the two dimensional Sisko fluid flow over thin film. The approximate analytic solution was found by using homotopy analysis method. They perceived that shear thinning fluid velocity inclines for both power law index and material parameters. Mekhimer and El-Kot [3] analyzed the Sisko fluid flow passing through tapered elastic arteries with time-variant overlapping stenosis. They concluded that magnitude of velocity is substantially large for Sisko fluid when compared with Newtonian fluids. Additionally, pressure of Newtonian fluid is extremely immense than Sisko fluid while shear thickening fluids have low pressure than shear thinning fluids. Nadeem and Akbar [4] studied the peristaltic motion in Sisko fluid flow through uniform inclined tube. The

analytical solution was computed with HAM and regular perturbation method. The peristaltic motion in Sisko fluid flow is analyzed in the endoscope by Nadeem et al. [5]. They computed numerical as well as analytical solutions and found that Newtonian fluid has best peristaltic transference than both Sisko and power law fluids. Akbar [6] delineated the flow of Sisko nanofluid passing through asymmetric channel. Khan et al. [7] inspected Sisko fluid flow in the annular pipe with heat transfer. Khan et al. [8] studied the MHD flow of Sisko fluid in annular pipe. They predicted that material parameter decelerates the motion of fluid. Additionally, Newtonian fluid has lesser velocity than Sisko fluid. Khan and Shahzad [9] delineated the Sisko fluid flow over radially stretching sheet. They proved that both fluid velocity and wall friction are increased against Sisko parameter. Additionally, Sisko fluid has larger wall friction than both power law and Newtonian fluids. Khan and Shahzad [10] studied Sisko fluid flow over stretching surface. They found that the linear momentum is decelerated versus power law index while Sisko parameter increases it. Malik et al. [11] firstly investigated the Sisko fluid flow over continuously stretching cylinder along with temperature dependent thermal conductivity. They computed solution with the aid of shooting method and discussed the problem by varying controlling physical parameters. Present work also focuses on the Prandtl-Eyring fluid model to describe viscoelastic fluid properties. Prandtl-Eyring model relates shear stress to sine hyperbolic function of deformation rate. This model is capable to investigate the fluid properties of shear thinning fluids. Darji and Timol [12] studied the viscoelastic fluid flows and established the similar solutions of modeled problems. The modeled equations for Prandtl-Eyring fluid are solved and deliberated the fluid parameter effects on velocity and its slope. Akbar et al. [13] described the blood flow through tapered arteries by using constitutive law of Prandtl-Eyring. They calculated solution with regular perturbation method and predicts that both fluid parameters accelerate momentum. Akbar [14] analyzed the peristaltic motion of Prandtl-Eyring fluid in small intestine. They computed solution via perturbation method and show that fluid parameter decelerates fluid motion away from wall.

Magnetohydrodynamics (MHD) elaborates the characteristics of electrically conducting fluids. There a lot of natural MHD fluids e.g. plasma, electrolysis, salt water and solar wind are MHD fluids. Applied magnetic field produces current in fluid flow, as a result, a significantly opposing force called Lorentz force is produced. Alfven [15] discovered electromagnetic-

hydrodynamic waves in their experiments. This discovery opens a vast area of interest for researchers. This work acquires a lot of importance very soon, because it has many applications in every subdivision of science specifically in geophysics, astrophysics, electrical engineering, mechanical engineering and aerospace engineering. MHD pumps, MHD sensors, MHD flow meters, MHD power generators, electrostatic filters, electromagnetic propulsion, purification of crude oil, fluid droplets are some engineering and industrial products/processes which are based on the phenomenon of magnetohydrodynamics. Also, MHD phenomenon is utilized to control thermal equilibrium in interstellar medium and interplanetary medium. Additionally, radio propagation and geothermal extraction also utilized MHD phenomenon. Since rate of cooling is an important factor corresponds to quality of product, hence magnetohydrodynamic fluids are used in many manufacturing processes to control rate of cooling. For instance, it is applied to control cooling/heating of nuclear reactor walls, fusing metals in electric furnace, crystal growth and metal casting. Recently, MHD was found very useful in bioengineering, because it is utilized in many disease diagnostic processes. While turbulence comportment of fluid is also handled with magnetic field. MHD phenomenon is mathematical formulation by adding Maxwell equations with Navier-Stokes equations. Rossow [16] investigated the MHD viscous fluid flow over flat plate. Chakrabarti and Gupta [17] computed the similarity solutions of MHD Newtonian fluid flow over a stretching sheet with uniform suction. Andersson [18] calculated numerical solutions of MHD viscous fluid flow past a stretching surface. He formulated and solved analytically this model. He also proved the validity of computed solutions for large values of Reynolds number. Yih [19] studied free convection flow of MHD Newtonian fluid past through permeable vertical sheet. Liao [20] investigated the MHD effects on non-Newtonian fluid flow past a stretching sheet. They shows that MHD effects on shear thinning are prominent than shear thickening fluids. Abo-Eldahab and Salem [21] studied diffusion and chemical reaction effects on MHD power-law nanofluid on a moving cylinder. They computed numerical solution and observed that magnetic field decelerates fluid motion while rises temperature. Additionally, they suggested that magnetic field enhances wall temperature gradient while it reduces both skin friction coefficient and Sherwood number. Cortell [22] deliberated the physical features of power law fluid flow past a stretching surface under magnetic field effects. They proved that the Hartmann number effects are opposing on fluids velocity.

Ishak et al. [23] studied the hydrodynamics flow of Newtonian fluid through vertical stretching sheet. They found that fluid momentum are decreased versus applied magnetic field while friction coefficient enlarges against it. Akbar et al. [24] described the MHD characteristics on Powell-Eyring fluid past a stretching surface. MHD flow of Williamson fluid passing through stretching surface was studied by Malik and Salahuddin [25]. The numerical solution of fluid model was computed via shooting method. Malik et al. [26] utilized Keller-Box integration scheme to solve the flow governing system of MHD tangent hyperbolic fluid over a stretching cylinder. They predicted that both local wall stress and velocity reduces versus applied magnetic field. In all above mentioned studies, the Hall current effects are ignored, because for low magnetic field these effects are inconsequential while Hall current phenomenon is prominent when intensity of applied magnetic field is strong or density of fluid is low. It happens because electron carries the induced current and moves faster than ions. This phenomenon generates an isotropic conductivity which is known as Hall current. The occurrence of Hall current demands the modification of Ohm's law, also the consequences of this phenomenon enhance the order of flow govern differential equations. Hall current has many practical applications e.g. Hall accelerators, Hall sensors and turbine etc. The importance of Hall current in electrically conducting fluid under the strong magnetic field was analyzed by Lighthill [27]. The study of Hall current effects in viscous fluid between parallel plates was initiated by Sato [28]. The exact solution of the problem was found against low Reynolds number and he proved that Hall current effects are noticeable. Jana et al. [29] investigated the MHD Newtonian fluid flow passing through an infinite porous plate with Hall current effects. They found that shear rate neither depends on magnetic parameter nor on Hall parameter. Hall current effects and pressure gradient on time-dependent hydrodynamic fluid flow through rotating channel were studied by Seth and Ghosh [30]. Chaudhary and Jha [31] elaborated the impacts of Hall current on free convection flow of viscous fluid past an infinite plate. Salem and Abd El-Aziz [32] discussed the influences of Hall current phenomenon on MHD flow of Newtonian fluid past a vertical stretching sheet. They recommended that Hall parameter affected tangential velocity component slightly while lateral velocity component enhances very rapidly against it. Ali et al. [33] captured the significance of Hall current phenomenon on viscous fluid flow over vertical flat plate with mixed convection. Shateyi and Motsa [34] investigated the unsteady flow of viscous fluid past through a stretch-

ing sheet with Hall current effects. Reddy [35] delineated the impacts of Hall current on flow of Newtonian fluid over vertical surface with other physical effects. They prevailed that Hall parameter accelerates velocity while it has opponent effects on temperature. Parsad et al. [36] analyzed the Hall current phenomenon on MHD Newtonian fluid flow over variable stretching surface. They observed that Hall parameter effects are insignificant on horizontal velocity and temperature while the behavior of transverse velocity is periodic against it. Recently, Sreedevi et al. [37] and Chandra and Misra [38] inspected the Hall current effects with different physical situations.

Heat transfer in fluid flow plays remarkable role due to its widespread uses in applied sciences e.g. biomedicine, meteorology, plasma physics, astrophysics, physical chemistry, oceanography etc. Heat transfer plays a sensible role on the quality of many industrial products, thus liquid cooling/heating is the major concern of modern days researchers. For instance, controlling the heat transfer during the processes like crystal growing, polymer sheets, artificial fibers, plastic films, filtration of liquid metal, glass fiber production and cooling/heating in heat exchangers or chambers etc. is a crucial factor regarding achievement of desired quality products. Gupta and Gupta [39] was firstly analyzed the heat transfer phenomenon in flow of Newtonian fluid past through porous sheet. Also, Dutta and Roy [40] analyzed the heat transfer problem by assuming uniform heat flux in flow of Newtonian fluid past a stretching sheet. Heat transfer of fluid flows was also discussed by number of researchers (e.g. Grubka and Bobba [41], Hassanien et al. [42], Cortell [43], Andersson and Kumran [44]). The heat conductance capacity of any material called its thermal conductivity, according to Fourier law, it is directly related to heat flux while it has inverse variation with temperature gradient. Thus, thermal conductivity of fluid varies by increasing or decreasing temperature. For fluids, thermal conductivity increases with increase in fluid temperature from 0 to $400F$. As thermal conductivity varies by increasing temperature, thus temperature dependent thermal conductivity is provides more suitable results of heat transfer. Chiam [45] considered primarily the temperature dependent thermal conductivity in his problem. He analyzed the consequences of variable thermal conductivity on Newtonian fluid flow over a porous stretched surface. In this investigation, they found that the variable thermal conductivity enhances temperature while it declines wall temperature gradient. Abel and Mahesha [46] inspected the consequences of variable thermal conductivity on MHD

viscoelastic fluid by considering various physical effects. It was found that variable thermal conductivity increases temperature profile i.e. fluid with less thermal conductivity are better for cooling. Abel et al. [47] also examined flow of power law fluid past a stretching sheet with variable thermal conductivity and found analytical expressions for temperature profile. Mishra et al. [48] discussed the variable thermal conductivity effects on unsteady viscous fluid flow past a stretching plate. Rangi and Ahmad [49] investigated the variable thermal conductivity features on viscous fluid flow past a stretching surface. They recommended that the variations in thermal conductivity significantly affected the temperature. In literature, there are some other investigations related to variable thermal conductivity (Singh [50], Miao et al. [51] and Jhankal [52]).

It has been observed that viscosity of the fluid provides resistance to the motion, this process converted some amount of mechanical energy into thermal energy i.e. energy is dissipated. Since, this dissipation is because of viscous force hence its called viscous dissipation and it behaves like an energy source. Brinkman [53] was initially factored the influences of viscous dissipation in viscous fluid flow through capillary. Lin et al. [54] described the energy dissipation effects in viscous fluid flow through pipe. Vajravelu and Hadjinicolaou [55] analyzed the viscous dissipation impacts on viscous fluid flow past a stretching sheet with variable heat flux. Shigechi et al. [56] described the characteristics of energy dissipation in Couette-Poiseuille flow of Newtonian fluid. Both viscous dissipation and MHD effects on viscous fluid flow past a stretching surface with suction/injection was investigated by Anjali Devi and Ganga [57]. They utilized hypergeometric functions to solve the problem for linear stretching case and shows that viscous dissipation effects are insignificant on temperature. Recently, Singh [58], Alinejad and Samarbakhsh [59], Reddy et al. [60] and Mabood et al. [61] delineated the influences of energy dissipation in viscous fluid flows with physical assumptions. Another important factor affecting the heat transfer of hydrodynamics fluid flow is Joule heating. It is experimentally proved that when current passes through the hydrodynamics fluid flow, its temperature rises. This phenomenon occurs due to interaction between the moving particles and atomic ions which make the body like conductor. The charged particle accelerated and produced electrostatic potential energy. These particles strike with ions and release the energy which escalates temperature of the fluid. Joule heating has a lot of applications such as incandescent light bulb, electric stoves,

electric heaters, soldering irons, cartridge heaters, electric fuses, electronic cigarettes, vaporizing propylene glycol and vegetable glycerine. Also, some food processing equipment utilized Joule heating phenomenon. Because of its frequent use in daily-life devices, a lot of investigations have been performed to delineate Joule heating phenomenon. Aissa and Mohammadein [62] examined the flow of micropolar fluid over a stretched surface along with Joule heating effects and found numerical solution. They shown that Eckert number and magnetic parameter enlarge the temperature. Alim et al. [63] computed numerical solution of Joule heating impacts on hydrodynamic flow of viscous fluid past a flat plate. Recently, Kaladhar [64] and Harish Babu and Satya Narayana [65] were discussed Joule heating effects on Couple stress and Jeffrey fluids. Additionally to figure out the physical problem in more realistic way, many researchers factored Joule heating effects along with viscous dissipation. Fillo [66] initially factored the viscous dissipation and Joule heating impacts collectively on flow of viscous fluid. Hossain [67] studied thermophysical aspects of energy dissipation and Joule heating on viscous fluid flow. El-Amin [68] discussed the both Joule heating as well as energy dissipation impacts on viscous fluid flow past a horizontal cylinder. Recently, Das et al. [69], Ibrahim and Suneetha [70] discussed the viscous dissipation along with Joule heating effects on Newtonian fluid with various physical assumptions.

The transfer of heat happens due to difference of temperature (known as thermal conduction), it takes place in every type of matter (solid, liquid, gas and plasma). The observations proved that the heat always marched towards frosty region from warmer region. The transportation of heat transfer through fluid flow is interpreted via thermodynamic first law (it relates internal energy with heat flux). Fourier [71] proposed the most popular heat conduction law to anticipate the heat flux, this law is found to be very helpful for estimation of heat flux for many materials but in the context of fluid this law is incompetent. One of the major fault in this law is its mathematical formulation which yields a parabolic equation i.e. according to this, an initial disturbance is felt very effective throughout the system which does not make sense in practice. To affix this unrealistic property, plenty of attempts have been made, but Maxwell-Cattaneo model eradicates this imperfection very significantly. Cattaneo [72 – 73] included the thermal relaxation time and put partial time derivative into account and named this term as thermal inertia. The addition of this term resolves the main issue of the Fourier

law and this transformed the heat equation into damped hyperbolic equation. This gives the direction to generalize Fourier law and correct the behaviour of solution. But this law needs still modifications in partial time derivative, thus a lot of modifications have been proposed for time derivative (see Fox [74], Straughan and Franchi [75], Lebon and Cloot [76]) but their solutions faced some critical problems in physical sense. Haupt [77] suggested that Oldroyd derivative would be better approximation for partial time derivative. Christov [78] revised the Maxwell-Cattaneo heat flux law and utilized the Oldroyd upper convective derivative (instead of partial time derivative) and showed that proposed model is invariant under different coordinates systems, and also, it is reducible to classical Fourier law under special circumstances. Ciarletta and Straughan [79] proved uniqueness and stability of Christov-Cattaneo equation solution. Further, Straughan [80] studied the application of Christov-Cattaneo model for thermal convection effects in Newtonian fluid flow. He found that thermal relaxation effects are so strong in case of large Cattaneo number. Straughan [81] extended their previous work and analyzed the thermal convection in gravity-driven incompressible Newtonian fluid flow in porous media. He discussed the heat transfer by using Christov-Cattaneo and Christov-Fox models. He recommended that in both cases the influences of thermal relaxation is noteworthy for large Cattaneo number while stationary convection is preferred in case of low Cattaneo number. Tibullo and Zampoli [82] discussed the Christov-Cattaneo model for incompressible fluid flow and constructed the unique solution of initial-boundary value problem. They found that the computed solution is trivially deduced to Cattaneo results as a special case. Recently, many researchers discussed the heat transfer by using Christov-Cattaneo heat flux model. Application of Christov-Cattaneo equation on flow of Williamson fluid past through stretching cylinder was discussed by Salahuddin et al. [83]. Malik et al. [84] implemented Christov-Cattaneo theory to illustrate the thermal energy on Casson fluid over variable stretching sheet with various thermophysical effects. They solved the governing boundary value problem with Keller-Box method and extracted that addition of thermal relaxation effects corresponds to fall down in temperature. Tanveer et al. [85] studied the heat transfer in channel flow with Christov-Cattaneo heat flux model.

Nanofluid is a modern type fluid which is the combination of base fluid and nano size particles. These nano particles are of different metals like copper, aluminum, silicon etc. The main purpose of including nanoparticles is to enhance the thermal conductivity. Because, many

conventional heat transfer fluids have poor thermal conductance (e.g. ethylene glycol, water and engine oil etc.). Many experiments are performed to overcome this deficiency, e.g. geometry is modified, small size (e.g. milli, micro etc.) metallic particles are dropped into base fluid to enhance the thermal conductivity but these experiments did not give the required results. Two decades ago, Chio [86 – 87] inserted nano sized particles and surprisingly found that nanofluid have many times greater thermal conductivity than base fluid. After this successful experiment, many theoretical and experimental studied are performed to analyze nanofluids, because of nanofluid utilization in many thermal engineering processes. Kang et al. [88] and Yoo et al. [89] performed experiments to investigate thermal conductivity variations in nanofluids. They analyzed the thermal conductivity by considering different base fluids (water, glycol etc.) and nano particles (ultra-dispersed diamond, iron, aluminum, copper etc.) and concluded that nanofluid have much larger thermal conductivity. Maiga et al. [90] studied the water based nanofluids(water- γ Al₂O₃ and Ethylene Glycol- γ Al₂O₃) by considering different geometries. The results show that nanofluids have very better heat transfer rate than their respective base fluid. Also, the comparison of two nanofluids shows that Ethylene Glycol- γ Al₂O₃ has more capability of heat transfer than water- γ Al₂O₃. A comprehensive review on nanofluid was written by Wang and Mujumdar [91]. They compared viscosity, thermal conductivity and heat transfer coefficient of many proposed models. They suggested that many other effects like Brownian motion, size and shape of nanoparticles should be considered to obtain better results. Finally, they summarized that prediction of physical characteristics of nanofluids is very difficult by using theoretical models. Till now, for mathematical formulation of nanofluids two different approaches (Two-phase model and Buongiorno model) have been adopted in literature. Two-phase model elaborated the base fluid and nano particles particularly, but this model is not common. On the other hand, Buongiorno [92] suggested the model which based on continuum assumption of fluid with nanoparticles. He studied the influences of seven factors (inertia, Brownian diffusion, thermophoresis, diffusiophoresis, Magnus effect, fluid drainage and gravity) in nanofluids. He observed that only thermophoresis and Brownian diffusion have significant effects. Additionally, this model is simpler and efficient in computational point of view, so Buongiorno model is considered to deliberate thermo-physical properties of nanofluids in this work. Bachok et al. [93] utilized the Buongiorno model to describe properties of nanofluid

past a semi infinite flat plate. Keller-Box technique was implemented to find solution of flow governing equations. Khan and Pop [94] discussed viscous nanofluid flow past a stretching sheet. The solution of similar equations was calculated numerically. Rana and Bhargava [95] computed numerical solution of Newtonian nanofluid flow through nonlinear stretched sheet. Zaimi et al. [96] designed the problem on viscous nanofluid flow passing through permeable nonlinear stretching/shrinking sheet. Mabood et al. [97] theoretically analyzed the viscous nanofluid flow on stretching surface. Recently, Malik et al. [98] and Narmgari and Sulochna [99] presented the similarity solution of MHD nanofluid flow in different physical situations.

Chapter 1

Numerical solution of MHD Sisko fluid over a stretching cylinder and heat transfer analysis

The physical features of Sisko fluid flow past over a stretching cylinder under magnetic field. The electrically conducting fluids have been encountered in various industrial applications such as electrostatic filters, cooling reactors, MHD power generation, fluid droplets and geothermal energy extraction. So, this chapter discusses the MHD flow of Sisko fluid passing over a stretching cylinder. A suitable set of transformations is employed to transfigure the governing partial differential system into ordinary differential system. Ordinary differential system is then solved via Runge-Kutta-Fehlberg scheme. The involved parameters effects on momentum and thermal energy are shown via graphs.

1.1 Problem formulation

Consider 2D, axisymmetric, steady state, incompressible electrically conducting flow of Sisko fluid over a stretching cylinder in the boundary layer regime. The fluid occupied the semi-infinite region $r > 0$, also the movement in fluid is made due to stretching of cylinder along x -direction with velocity $U(x) = cx$, where $c > 0$. An orthogonal magnetic field of strength B_0 is utilized to the x -direction i.e. along radial direction. Electric field and induced magnetic

field effects are not taken into account(see **Fig. 1**). Governing equations for under consider problem are

Fig. 1.1

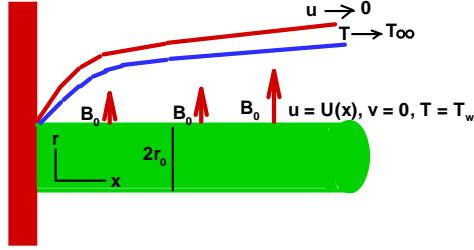


Fig. 1.1: Physical configuration of flow problem.

$$\nabla \cdot \mathbf{V} = 0, \quad (1.1)$$

$$\rho \frac{D\mathbf{V}}{Dt} = \nabla \cdot \mathbf{T} + \mathbf{J} \times \mathbf{B}, \quad (1.2)$$

$$\rho c_p \frac{DT}{Dt} = \kappa \nabla^2 T, \quad (1.3)$$

in the above-defined system, ∇ is differential operator, material time derivative is symbolized by $\frac{D}{Dt}$, $\mathbf{V} = (u, v, 0)$ is velocity vector, \mathbf{T} is mathematical symbol of Cauchy stress tensor, $\mathbf{B} = (0, B_0, 0)$ is strength of magnetic field, $\mathbf{J} = \sigma(\mathbf{V} \times \mathbf{B})$ represents the magnetic flux (in the absence of electric field), T denotes temperature field, ρ is density of non-Newtonian fluid, c_p is specific heat while κ defines the thermal conductivity. The mathematical quantities ∇ and $\frac{D}{Dt}$ are given below (in polar cylindrical coordinates)

$$\nabla = \frac{\partial(\cdot)}{\partial x} \hat{e}_x + \frac{\partial(\cdot)}{\partial r} \hat{e}_r + \frac{1}{r} \frac{\partial(\cdot)}{\partial \theta} \hat{e}_\theta, \quad (1.4)$$

$$\frac{D}{Dt} = \mathbf{V} \cdot \nabla. \quad (1.5)$$

As for steady flow the term $\frac{\partial}{\partial t}$ is neglected in material time derivative. The stress tensor of defined as

$$\mathbf{T} = -p\mathbf{I} + \mathbf{S}. \quad (1.6)$$

in above relation p shows pressure, identity tensor is represented with \mathbf{I} while \mathbf{S} called the extra stress tensor of Sisko fluid. Extra stress tensor is defined below

$$\mathbf{S} = \left(a + b \left| \sqrt{\frac{1}{2} \text{tr}(\mathbf{A}_1^2)} \right|^{n-1} \right) \mathbf{A}_1. \quad (1.7)$$

The symbols a , b and n denote the viscosity at high shear rate, power law region viscosity and power law index respectively. Additionally, \mathbf{A}_1 called first Rivlin-Ericksen tensor defined below

$$\mathbf{A}_1 = \nabla \mathbf{V} + (\nabla \mathbf{V})^t. \quad (1.8)$$

After interposing the all concerned variables, the first Rivlin-Ericksen tensor converted into

$$\mathbf{A}_1 = \begin{bmatrix} 2\frac{\partial v}{\partial r} & 0 & \frac{\partial v}{\partial x} + \frac{\partial u}{\partial r} \\ 0 & 2\frac{u}{r} & 0 \\ \frac{\partial v}{\partial x} + \frac{\partial u}{\partial r} & 0 & 2\frac{\partial u}{\partial x} \end{bmatrix}. \quad (1.9)$$

Now the $tr(\mathbf{A}_1^2)$ is computed, it is given by

$$tr(\mathbf{A}_1^2) = 4\left(\frac{\partial u}{\partial x}\right)^2 + 4\left(\frac{\partial v}{\partial r}\right)^2 + 4\frac{v^2}{r^2} + 2\left(\frac{\partial v}{\partial x} + \frac{\partial u}{\partial r}\right)^2. \quad (1.10)$$

Incorporating *Eqs.* (1.9) – (1.10) into *Eq.* (1.7), extra stress tensor takes the form

$$\mathbf{S} = \left(a + b \left| \sqrt{2\left(\frac{\partial u}{\partial x}\right)^2 + 2\left(\frac{\partial v}{\partial r}\right)^2 + 2\left(\frac{v}{r}\right)^2 + \left(\frac{\partial v}{\partial x} + \frac{\partial u}{\partial r}\right)^2} \right|^{n-1} \right) \begin{bmatrix} 2\frac{\partial v}{\partial r} & 0 & \frac{\partial v}{\partial x} + \frac{\partial u}{\partial r} \\ 0 & 2\frac{v}{r} & 0 \\ \frac{\partial v}{\partial x} + \frac{\partial u}{\partial r} & 0 & 2\frac{\partial u}{\partial x} \end{bmatrix}. \quad (1.11)$$

Also, after simplification, $\mathbf{J} \times \mathbf{B} = \sigma(-B_0^2 u, 0, 0)$. Now substituting the concerned variables in *Eq.* (1.1) (continuity equation), it is converted to

$$\frac{\partial(ru)}{\partial x} + \frac{\partial(rv)}{\partial r} = 0. \quad (1.12)$$

After inserting \mathbf{T} , momentum equation (by neglecting pressure gradient) takes the below defined form

$$\rho \frac{D\mathbf{V}}{Dt} = \nabla \cdot \mathbf{S} + \mathbf{J} \times \mathbf{B}. \quad (1.13)$$

The derivative of velocity field \mathbf{V} in components form is given below

$$\left(\frac{D\mathbf{V}}{Dt}\right)_x = \frac{Du}{Dt} = u\frac{\partial u}{\partial x} + v\frac{\partial u}{\partial r}, \quad (1.14)$$

$$\left(\frac{D\mathbf{V}}{Dt}\right)_r = \frac{Dv}{Dt} = u\frac{\partial v}{\partial x} + v\frac{\partial v}{\partial r}, \quad (1.15)$$

$$\left(\frac{D\mathbf{V}}{Dt}\right)_\theta = \frac{Dw}{Dt} = 0. \quad (1.16)$$

The divergence of extra stress tensor is given as

$$\begin{aligned} (\nabla \cdot \mathbf{S})_x &= a\left(\frac{1}{r}\frac{\partial}{\partial r}\left(r\frac{\partial u}{\partial r}\right) + 2\frac{\partial^2 u}{\partial x^2} + \frac{\partial^2 v}{\partial x\partial r} + \frac{1}{r}\frac{\partial v}{\partial x}\right) \\ &\quad + b\left(\frac{1}{r}\frac{\partial}{\partial r}\left(r\frac{\partial u}{\partial r}\right) \left| \sqrt{2\left(\frac{\partial u}{\partial x}\right)^2 + 2\left(\frac{\partial v}{\partial r}\right)^2 + 2\frac{v^2}{r^2} + \left(\frac{\partial v}{\partial x} + \frac{\partial u}{\partial r}\right)^2} \right|^{n-1}\right) \\ &\quad + 2\frac{\partial}{\partial x}\left(\frac{\partial u}{\partial x} \left| \sqrt{2\left(\frac{\partial u}{\partial x}\right)^2 + 2\left(\frac{\partial v}{\partial r}\right)^2 + 2\frac{v^2}{r^2} + \left(\frac{\partial v}{\partial x} + \frac{\partial u}{\partial r}\right)^2} \right|^{n-1}\right) \\ &\quad + \frac{\partial}{\partial r}\left(\frac{\partial v}{\partial x} \left| \sqrt{2\left(\frac{\partial u}{\partial x}\right)^2 + 2\left(\frac{\partial v}{\partial r}\right)^2 + 2\frac{v^2}{r^2} + \left(\frac{\partial v}{\partial x} + \frac{\partial u}{\partial r}\right)^2} \right|^{n-1}\right) \\ &\quad + \frac{1}{r}\frac{\partial v}{\partial x} \left| \sqrt{2\left(\frac{\partial u}{\partial x}\right)^2 + 2\left(\frac{\partial v}{\partial r}\right)^2 + 2\frac{v^2}{r^2} + \left(\frac{\partial v}{\partial x} + \frac{\partial u}{\partial r}\right)^2} \right|^{n-1}, \end{aligned} \quad (1.17)$$

$$\begin{aligned} (\nabla \cdot \mathbf{S})_r &= a\left(\frac{2}{r}\frac{\partial}{\partial r}\left(r\frac{\partial v}{\partial r}\right) + \frac{\partial}{\partial x}\left(\frac{\partial v}{\partial x} + \frac{\partial u}{\partial r}\right) - \frac{2v}{r^2}\right) \\ &\quad + b\left(\frac{2}{r}\frac{\partial}{\partial r}\left(r\frac{\partial v}{\partial r}\right) \left| \sqrt{2\left(\frac{\partial u}{\partial x}\right)^2 + 2\left(\frac{\partial v}{\partial r}\right)^2 + 2\frac{v^2}{r^2} + \left(\frac{\partial v}{\partial x} + \frac{\partial u}{\partial r}\right)^2} \right|^{n-1}\right) \\ &\quad + \frac{\partial}{\partial x}\left(\left(\frac{\partial v}{\partial x} + \frac{\partial u}{\partial r}\right) \left| \sqrt{2\left(\frac{\partial u}{\partial x}\right)^2 + 2\left(\frac{\partial v}{\partial r}\right)^2 + 2\frac{v^2}{r^2} + \left(\frac{\partial v}{\partial x} + \frac{\partial u}{\partial r}\right)^2} \right|^{n-1}\right) \\ &\quad - \frac{2v}{r^2} \left| \sqrt{2\left(\frac{\partial u}{\partial x}\right)^2 + 2\left(\frac{\partial v}{\partial r}\right)^2 + 2\frac{v^2}{r^2} + \left(\frac{\partial v}{\partial x} + \frac{\partial u}{\partial r}\right)^2} \right|^{n-1}, \end{aligned} \quad (1.18)$$

$$(\nabla \cdot \mathbf{S})_\theta = 0. \quad (1.19)$$

After inserting the *Eqs.* (1.14) – (1.19) and expression of $\mathbf{J} \times \mathbf{B}$ in *Eq.* (1.13), the fluid momentum governing equation transfigured to the following form

$$\begin{aligned}
u \frac{\partial u}{\partial x} + v \frac{\partial u}{\partial r} &= \frac{a}{\rho} \left(\frac{1}{r} \frac{\partial}{\partial r} \left(r \frac{\partial u}{\partial r} \right) + 2 \frac{\partial^2 u}{\partial x^2} + \frac{\partial^2 v}{\partial x \partial r} + \frac{1}{r} \frac{\partial v}{\partial x} \right) \\
&+ \frac{b}{\rho} \left(+b \left(\frac{1}{r} \frac{\partial}{\partial r} \left(r \frac{\partial u}{\partial r} \right) \left| \sqrt{2 \left(\frac{\partial u}{\partial x} \right)^2 + 2 \left(\frac{\partial v}{\partial r} \right)^2 + 2 \frac{v^2}{r^2} + \left(\frac{\partial v}{\partial x} + \frac{\partial u}{\partial r} \right)^2} \right|^{n-1} \right) \right. \\
&+ 2 \frac{\partial}{\partial x} \left(\frac{\partial u}{\partial x} \left| \sqrt{2 \left(\frac{\partial u}{\partial x} \right)^2 + 2 \left(\frac{\partial v}{\partial r} \right)^2 + 2 \frac{v^2}{r^2} + \left(\frac{\partial v}{\partial x} + \frac{\partial u}{\partial r} \right)^2} \right|^{n-1} \right) \\
&+ \frac{\partial}{\partial r} \left(\frac{\partial v}{\partial x} \left| \sqrt{2 \left(\frac{\partial u}{\partial x} \right)^2 + 2 \left(\frac{\partial v}{\partial r} \right)^2 + 2 \frac{v^2}{r^2} + \left(\frac{\partial v}{\partial x} + \frac{\partial u}{\partial r} \right)^2} \right|^{n-1} \right) \\
&\left. + \frac{1}{r} \frac{\partial v}{\partial x} \left| \sqrt{2 \left(\frac{\partial u}{\partial x} \right)^2 + 2 \left(\frac{\partial v}{\partial r} \right)^2 + 2 \frac{v^2}{r^2} + \left(\frac{\partial v}{\partial x} + \frac{\partial u}{\partial r} \right)^2} \right|^{n-1} \right) - \frac{\sigma}{\rho} B_0^2 u, \quad (1.20)
\end{aligned}$$

$$\begin{aligned}
u \frac{\partial v}{\partial x} + v \frac{\partial v}{\partial r} &= \frac{a}{\rho} \left(\frac{2}{r} \frac{\partial}{\partial r} \left(r \frac{\partial v}{\partial r} \right) + \frac{\partial^2 v}{\partial x^2} + \frac{\partial^2 u}{\partial x \partial r} - \frac{2v}{r^2} \right) \\
&+ b \left(\frac{2}{r} \frac{\partial}{\partial r} \left(r \frac{\partial v}{\partial r} \right) \left| \sqrt{2 \left(\frac{\partial u}{\partial x} \right)^2 + 2 \left(\frac{\partial v}{\partial r} \right)^2 + 2 \frac{v^2}{r^2} + \left(\frac{\partial v}{\partial x} + \frac{\partial u}{\partial r} \right)^2} \right|^{n-1} \right) \\
&+ \frac{\partial}{\partial x} \left(\left(\frac{\partial v}{\partial x} + \frac{\partial u}{\partial r} \right) \left| \sqrt{2 \left(\frac{\partial u}{\partial x} \right)^2 + 2 \left(\frac{\partial v}{\partial r} \right)^2 + 2 \frac{v^2}{r^2} + \left(\frac{\partial v}{\partial x} + \frac{\partial u}{\partial r} \right)^2} \right|^{n-1} \right) \\
&- \frac{2v}{r^2} \left| \sqrt{2 \left(\frac{\partial u}{\partial x} \right)^2 + 2 \left(\frac{\partial v}{\partial r} \right)^2 + 2 \frac{v^2}{r^2} + \left(\frac{\partial v}{\partial x} + \frac{\partial u}{\partial r} \right)^2} \right|^{n-1}. \quad (1.21)
\end{aligned}$$

Now simplifying the energy equation, the material time derivative of temperature field is

$$\frac{DT}{Dt} = u \frac{\partial T}{\partial x} + v \frac{\partial T}{\partial r}. \quad (1.22)$$

Also, Laplacian of fluid temperature is given as

$$\nabla^2 T = \frac{1}{r} \frac{\partial}{\partial r} \left(r \frac{\partial T}{\partial r} \right) + \frac{\partial^2 T}{\partial x^2}. \quad (1.23)$$

After using *Eqs.* (1.22) – (1.23) in *Eq.* (1.3), the energy equation of non-Newtonian fluid is transmuted to

$$u \frac{\partial T}{\partial x} + v \frac{\partial T}{\partial r} = \alpha \left(\frac{1}{r} \frac{\partial}{\partial r} \left(r \frac{\partial T}{\partial r} \right) + \frac{\partial^2 T}{\partial x^2} \right), \quad (1.24)$$

where $\alpha = \frac{\kappa}{\rho c_p}$ symbolized the thermal diffusivity.

After inserting the boundary layer approximations (Prandtl theory) in *Eqs.* (1.12), (1.20), (1.21), (1.24), these are transformed to

$$\frac{\partial(rv)}{\partial r} + \frac{\partial(ru)}{\partial x} = 0, \quad (1.25)$$

$$u \frac{\partial u}{\partial x} + v \frac{\partial u}{\partial r} = \frac{a}{\rho} \left(\frac{1}{r} \frac{\partial}{\partial r} \left(r \frac{\partial u}{\partial r} \right) \right) + \frac{b}{\rho} \left(\frac{1}{r} \frac{\partial}{\partial r} \left(r \frac{\partial u}{\partial r} \left| \frac{\partial u}{\partial r} \right|^{n-1} \right) \right) - \frac{\sigma}{\rho} B_0^2 u,$$

After rearranging, the momentum equation takes the form

$$u \frac{\partial u}{\partial x} + v \frac{\partial u}{\partial r} = \frac{a}{\rho} \left(\frac{1}{r} \frac{\partial}{\partial r} \left(r \frac{\partial u}{\partial r} \right) \right) - \frac{b}{r\rho} \left(-\frac{\partial u}{\partial r} \right)^n + \frac{nb}{\rho} \left(-\frac{\partial u}{\partial r} \right)^{n-1} \frac{\partial^2 u}{\partial r^2} - \frac{\sigma}{\rho} B_0^2 u, \quad (1.26)$$

$$u \frac{\partial T}{\partial x} + v \frac{\partial T}{\partial r} = \frac{\alpha}{r} \frac{\partial}{\partial r} \left(r \frac{\partial T}{\partial r} \right), \quad (1.27)$$

along with boundary conditions

$$u(x, r) = U(x), \quad v(x, r) = 0, \quad T(x, r) = T_w \text{ at } r = r_0, \quad (1.28)$$

$$u(x, r) \rightarrow 0, \quad T(x, r) \rightarrow T_\infty \text{ as } r \rightarrow \infty.$$

The stream function Ψ of flow velocity is defined as

$$u = \frac{1}{r} \frac{\partial \Psi}{\partial r}, \quad v = -\frac{1}{r} \frac{\partial \Psi}{\partial x}. \quad (1.29)$$

The modified form of *Eqs.* (1.25) – (1.27) along with the boundary conditions (1.28) is obtained using the following similarity transformations

$$\begin{aligned} \eta &= \frac{r^2 - r_0^2}{2xr_0} \text{Re}_b^{\frac{1}{n+1}}, \quad \Psi = xr_0 U \text{Re}_b^{\frac{-1}{n+1}} f(\eta), \\ \theta(\eta) &= \frac{T - T_\infty}{T_w - T_\infty}, \quad \text{Re}_b = \frac{\rho x^n U^{2-n}}{b}. \end{aligned} \quad (1.30)$$

The mass equation is satisfied identically while momentum and energy equations will take the form

$$\begin{aligned} A(1 + 2\gamma\eta)f''' + n(1 + 2\gamma\eta)^{\frac{n+1}{2}}(-f'')^{n-1}f''' - (n+1)\gamma(1 + 2\gamma\eta)^{\frac{n-1}{2}}(-f'')^n \\ + 2A\gamma f'' - f'^2 + \frac{2n}{n+1}ff'' - Mf' = 0, \end{aligned} \quad (1.31)$$

$$(1 + 2\gamma\eta)\theta'' + 2\gamma\theta' + \frac{2n}{n+1}\text{Pr}f\theta' = 0, \quad (1.32)$$

along with the boundary conditions

$$\begin{aligned} f(0) &= 0, \quad f'(0) = 1, \quad \theta(0) = 1, \\ f'(\infty) &\rightarrow 0, \quad \theta(\infty) \rightarrow 0, \end{aligned} \quad (1.33)$$

where the symbols M , γ , A and Pr denote material parameter, curvature parameter, magnetic field parameter and Prandtl number respectively. These are defined as follows

$$\begin{aligned}\gamma &= \frac{x}{r_0} \text{Re}_b^{-\frac{1}{n+1}}, \quad \text{Re}_a = \frac{\rho U x}{a}, \quad A = \frac{\text{Re}_b^{\frac{2}{n+1}}}{\text{Re}_a}, \\ M &= \frac{\sigma x B_0^2}{\rho U}, \quad \text{Pr} = \frac{x U}{\alpha} \text{Re}_b^{\frac{-2}{1+n}}.\end{aligned}\tag{1.34}$$

The coefficient of wall friction and local heat flux (i.e. quantities of practical interest) are introduced as

$$C_{fx} = \frac{\tau_w}{\frac{1}{2}\rho U^2}, \quad Nu_x = \frac{x q_w}{\kappa(T_w - T_\infty)},\tag{1.35}$$

where τ_w is surface shear stress and q_w is surface heat flux, these are defined below

$$\tau_w = a\left(\frac{\partial u}{\partial r}\right)_{r=r_0} - b\left(-\frac{\partial u}{\partial r}\right)_{r=r_0}^n, \quad q_w = -\kappa\left(\frac{\partial T}{\partial r}\right)_{r=r_0}.\tag{1.36}$$

Using similarity transformations, the above equations are converted to

$$\tau_w = \frac{aU}{x} \text{Re}_b^{\frac{1}{n+1}} f''(0) - b\left[-\frac{U}{x} \text{Re}_b^{\frac{1}{n+1}} f''(0)\right]^n, \quad q_w = -k\left(\frac{T_w - T_\infty}{x}\right) \text{Re}_b^{\frac{1}{n+1}} \theta'(0).\tag{1.37}$$

Using Eq. (1.37) into Eq. (1.35), the coefficients of surface friction and surface heat flux are transfigured into following dimensionless form

$$\frac{1}{2}C_{fx} \text{Re}_b^{\frac{1}{n+1}} = A f''(0) - (-f''(0))^n, \quad Nu_x \text{Re}_b^{-\frac{1}{n+1}} = -\theta'(0).\tag{1.38}$$

1.2 Shooting method

Eqs. (1.31) – (1.32) is nonlinear ordinary differential system subject to conditions (1.33). Thus solution of this system is computed with the help of efficient numerical technique, that is, shooting method by considering distinct values of physical parameter γ , A , M and Pr .

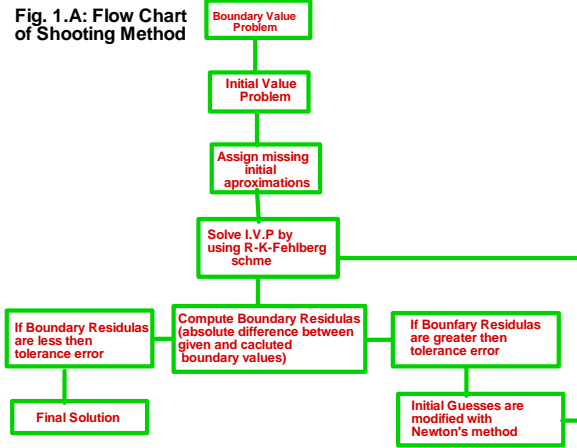


Fig. 1.A: Flow chart of numerical scheme

Since first step of the procedure is convert BVP into IVP, so *Eqs. (1.31) – (1.32)* are re-written as

$$f''' = \frac{(n+1)\gamma(1+2\gamma\eta)^{\frac{n-1}{2}}(-f'')^n - 2A\gamma f'' + f'^2 - \frac{2n}{n+1}f f'' + Mf'}{A(1+2\gamma\eta) + n(1+2\gamma\eta)^{\frac{n+1}{2}}(-f'')^{n-1}}, \quad (1.39)$$

$$\theta'' = -\frac{\frac{2n}{n+1}\text{Pr} f\theta' + 2\gamma\theta'}{(1+2\gamma\eta)}. \quad (1.40)$$

Above equations i.e. *Eqs. (1.39)–(1.40)* are transfigured into first order ordinary differential equations by substituting variables defined below

$$f = y_1, f' = y_2, f'' = y_3, \theta = y_4 \text{ and } \theta' = y_5, \quad (1.41)$$

into

$$y'_1 = y_2, \quad (1.42)$$

$$y'_2 = y_3, \quad (1.43)$$

$$y'_3 = \frac{(n+1)\gamma(1+2\gamma\eta)^{\frac{n-1}{2}}(-y_3)^n - 2\gamma y_3 + y_1^2 - \frac{2n}{n+1}y_1y_3 + My_2}{A(1+2\gamma\eta) + n(1+2\gamma\eta)^{\frac{n+1}{2}}(-y_3)^{n-1}}, \quad (1.44)$$

$$y'_4 = y_5, \quad (1.45)$$

$$y'_5 = -\frac{\frac{2n}{n+1}Pr y_1y_5 + 2\gamma y_5}{(1+2\gamma\eta)}. \quad (1.46)$$

The given conditions are converted to

$$y_1(0) = 0, y_2(0) = 1, y_2(\infty) = 0, y_4(0) = 1, y_4(\infty) = 0.$$

Now missing initial conditions $y_3(0)$ and $y_5(0)$ are added instead of $y_2(\infty)$ and $y_4(\infty)$. So above-defined conditions can be re-written as

$$y_1(0) = 0, y_2(0) = 1, y_3(0) = u_1, y_4(0) = 1, y_5(0) = u_2. \quad (1.47)$$

To solve the initial value problem (*Eqs.* (1.42) – (1.46)) subject to initial conditions (1.47) Runge–Kutta–Fehlberg formula is used. Fehlberg proposed the following formulas for Runge–Kutta 4th and 5th order integration schemes

$$\mathbf{y}_5(\eta + h) = \mathbf{y}(\eta) + \sum C_i \mathbf{K}_i, \text{ where } i = 1, 2, 3, 4, 5, 6 \text{ (5th-order)} \quad (1.48)$$

$$\mathbf{y}_4(\eta + h) = \mathbf{y}(\eta) + \sum D_i \mathbf{K}_i, \text{ where } i = 1, 2, 3, 4, 5, 6 \text{ (4th-order)} \quad (1.49)$$

where \mathbf{y}_5 and \mathbf{y}_4 correspond to the solution of 4th and 5th order integration formulas. Also, $\mathbf{y}(\eta) = (y_1, y_2, y_3, y_4, y_5)^t$ denotes solution while \mathbf{K}_i are defined in following equation

$$\begin{aligned} \mathbf{K}_1 &= h\mathbf{F}(\eta, \mathbf{y}), \\ \mathbf{K}_i &= h\mathbf{F}(\eta + A_i h, \mathbf{y} + \sum B_{ij} \mathbf{K}_j), \quad i = 2, 3, \dots, 6 \text{ and } j = 0, 1, \dots, i-1, \end{aligned} \quad (1.50)$$

h is the step size and \mathbf{F} is vector defined as

$$\mathbf{F}(\eta, \mathbf{y}) = \begin{pmatrix} y_2 \\ y_3 \\ \frac{(n+1)\gamma(1+2\gamma\eta)^{\frac{n-1}{2}}(-y_3)^n - 2A\gamma y_3 + y_1^2 - \frac{2n}{n+1}y_1 y_3 + M y_2}{A(1+2\gamma\eta) + n(1+2\gamma\eta)^{\frac{n+1}{2}}(-y_3)^{n-1}} \\ y_4 \\ -\frac{\frac{2n}{n+1} \text{Pr } y_1 y_5 + 2\gamma y_5}{(1+2\gamma\eta)} \end{pmatrix}.$$

According to this method, fifth-order formula defined in Eq. (1.48) is utilized to solve the considered problem while truncation error is computed with the aid of fourth order formula.

$$\mathbf{E}(h) = \mathbf{y}_5(\eta + h) - \mathbf{y}_4(\eta + h) = \sum (C_i - D_i) \mathbf{K}_i \text{ where } i = 1, 2, 3, 4, 5, 6, \quad (1.51)$$

the error in fifth order integration scheme is computed with above defined equation. Here coefficients A_i , B_{ij} , C_i and D_i are used which proposed by Cash and Karp [108] (see **Table 1.1**).

Table 1.1: Coefficients proposed by Cash and Karp[108].

i	A_i	B_{ij}	C_i	D_i
1	-	- - - - -	$\frac{37}{378}$	$\frac{2825}{27648}$
2	$\frac{1}{5}$	$\frac{1}{5}$ - - - -	0	0
3	$\frac{3}{10}$	$\frac{3}{40}$ $\frac{9}{40}$ - - -	$\frac{250}{261}$	$\frac{18575}{48384}$
4	$\frac{3}{5}$	$\frac{3}{10}$ $\frac{-9}{10}$ $\frac{6}{5}$ - -	$\frac{125}{594}$	$\frac{13525}{55296}$
5	1	$\frac{-11}{54}$ $\frac{5}{2}$ $\frac{-70}{27}$ $\frac{35}{27}$ -	0	$\frac{277}{14336}$
6	$\frac{7}{8}$	$\frac{1631}{55296}$ $\frac{175}{512}$ $\frac{575}{13824}$ $\frac{44275}{110592}$ $\frac{253}{4096}$	$\frac{512}{1771}$	$\frac{1}{4}$

Now Runge-Kutta-Fehlberg formula is utilized to solve the initial value problem by selecting both u_1 and u_2 as -1 and $\eta_\infty = 5$. Now boundary residuals are calculated to test the accuracy of computed solution. They are mathematically given below

$$r_1(u_1, u_2) = |\hat{y}_2(\infty) - y_2(\infty)|, \quad r_2(u_1, u_2) = |\hat{y}_4(\infty) - y_4(\infty)|, \quad (1.52)$$

here $r_1(u_1, u_2)$ and $r_2(u_1, u_2)$ are residuals of momentum and heat equations respectively and $\hat{y}_2(\infty)$ and $\hat{y}_4(\infty)$ are computed values.

The computed solution converges only if boundary residuals are less than tolerance error i.e. $\epsilon = 10^{-6}$. On the other hand, if boundary residuals do not meet the criteria then initial values are modified with Newton method. The process of computation is started unless the boundary residuals meet the required criteria.

1.3 Results and discussion

The flow governing problem is solved numerically by varying involved parameters. The calculated solution is compared through tables with previous results. **Table 1.2** represents the comparison of wall friction factor with Akbar et al. [24] results for variations in magnetic field parameter M . This table reflects that both results have good agree upto desired number of digits. Additionally, comparison of local Nusselt number is presented via **Table 1.3** with the

existing literature i.e. Cortell [43], Rana and Bhargava [95] and Zaimi et al. [96]. Nusselt number is calculated for several values of power law index n by taking $Pr = 1, 5$. It is found that present result has slight variations from previous. These results proved that computed solution is accurate.

Table 1.2: Wall friction coefficient i.e. $f''(0)$ by varying magnetic field parameter M when $A = \gamma = 0$ and $n = 1$.

M	Akbar et al. [24]	Present Results
0	-1	-1
0.5	-1.11803	-1.11809
1.0	-1.41421	-1.41532
5.0	-2.44949	-2.44954
10	-3.31663	-3.31661
100	-10.04988	-10.05001
500	-22.38303	-22.38901
1000	-31.63859	-31.63901

Table 1.3: Comparison of surface heat flux i.e. $-\theta'(0)$ versus power law index and Prandtl number while keeping $A = M = \gamma = 0$.

Pr	n	Cortell [43]	Rana and Bhargava [95]	Zaimi et al. [96]	Current Results
1.0	0.2	0.610262	0.6133	0.61131	0.61416
	0.5	0.595277	0.5967	0.59668	0.59663
	1.5	0.574537	0.5768	0.57668	0.57405
	2.0			0.57245	0.57240
	3.0	0.564472	0.5672	0.56719	0.56451
	4.0			0.56415	0.56411
	8.0			0.55897	0.55803
	10.0	0.55460	0.5578	0.55783	0.55721
5.0	0.1			1.61805	1.61361
	0.2	1.607175	1.5910	1.60757	1.59115
	0.3			1.59919	1.58919
	0.5	1.586744	1.5839	1.58658	1.58496
	0.8			1.57389	1.57342
	1.0			1.56787	1.56657
	1.5	1.557463	1.5461	1.55751	1.55529
	2.0			1.55093	1.55106
	2.5			1.54636	1.54660
	3.0	1.542337	1.5372	1.54271	1.54229
	10.0	1.528573	1.5260	1.52877	1.52951

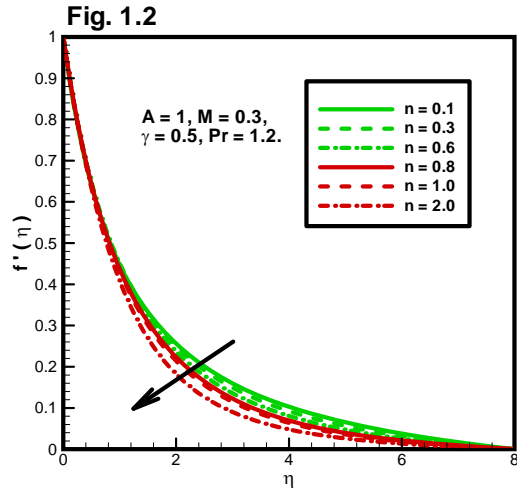


Fig. 1.2: Fluid velocity $f'(\eta)$ versus power law index n .

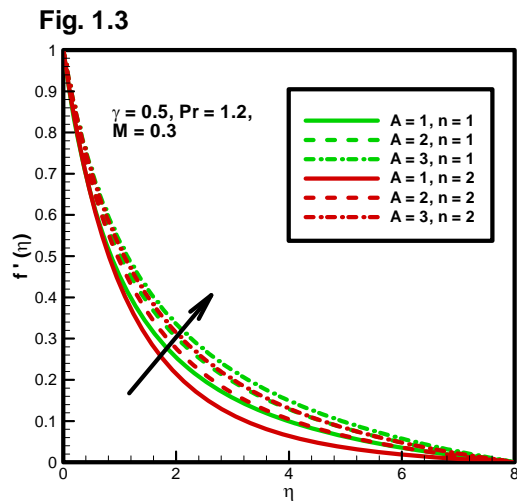


Fig. 1.3: Material parameter A effects on $f'(\eta)$ by keeping power law index $n = 1$ and 2 .

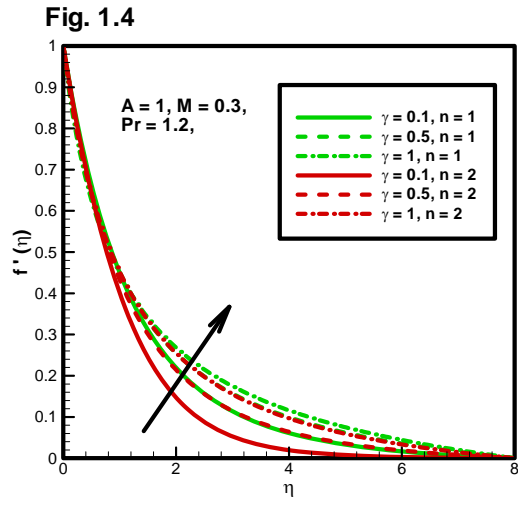


Fig. 1.4: Curvature parameter γ effects on velocity profile $f'(\eta)$ for power law index $n = 1$ and 2.

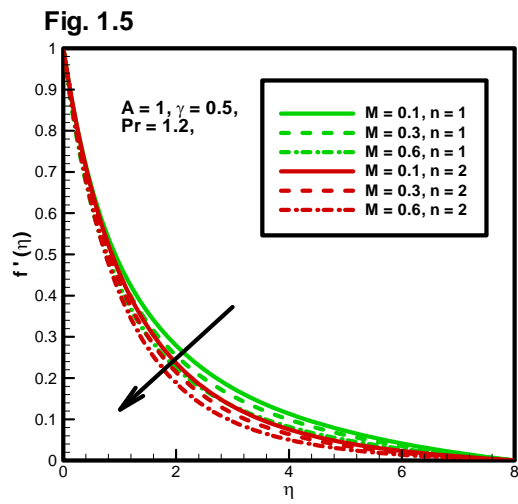


Fig. 1.5: Deviations in fluid velocity $f'(\eta)$ versus M and power law index $n = 1$ and 2.

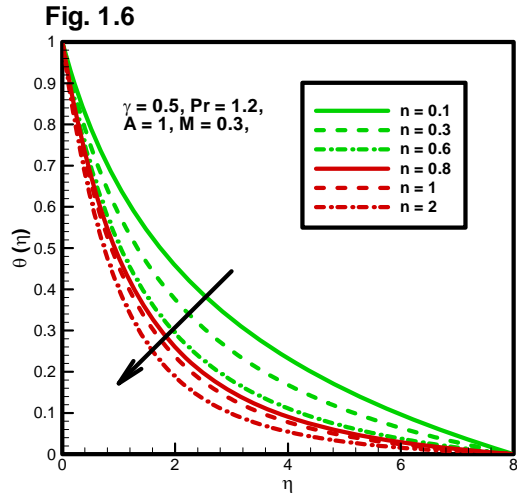


Fig. 1.6: Temperature profile $\theta(\eta)$ by varying power law index n .

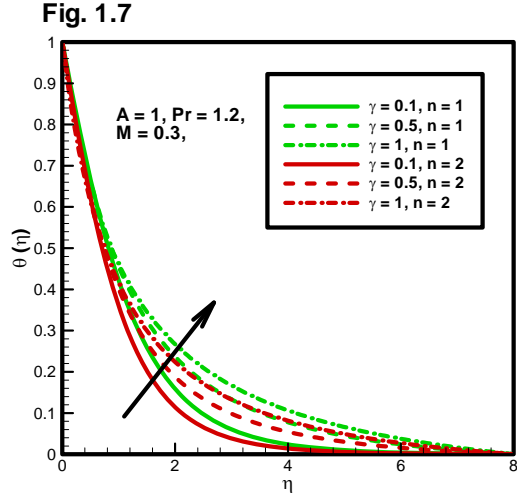


Fig. 1.7: Temperature profile $\theta(\eta)$ behaviour versus γ and n .

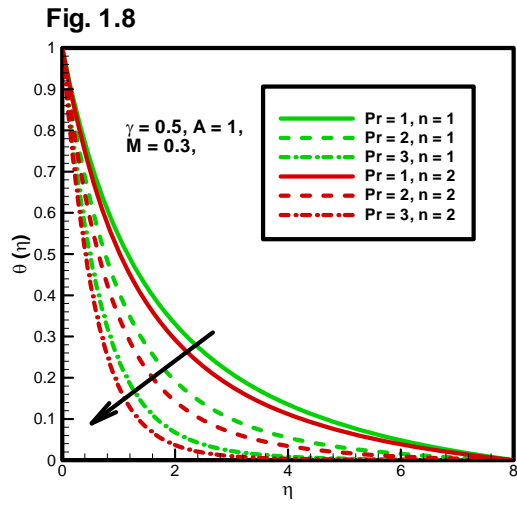


Fig. 1.8: Effects of Prandtl number Pr on temperature profile $\theta(\eta)$ for $n = 1, 2$.

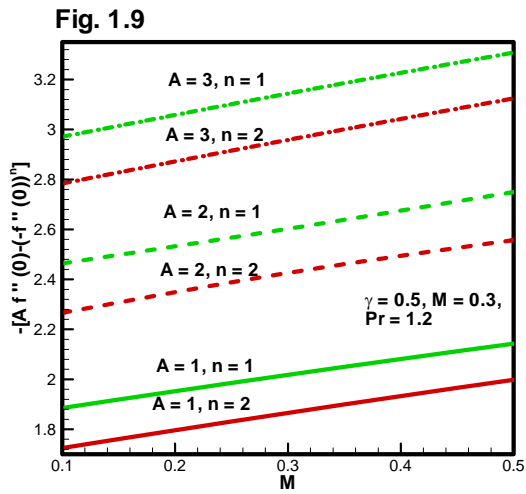


Fig. 1.9: Variations in wall friction coefficient versus governing parameters A , M and n .

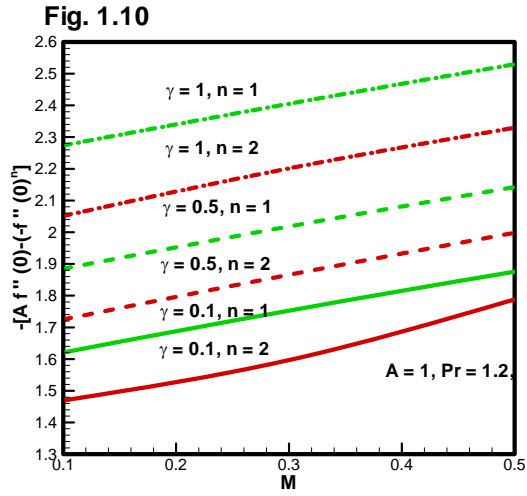


Fig. 1.10: Variations in wall friction factor versus governing parameters M , γ and n .

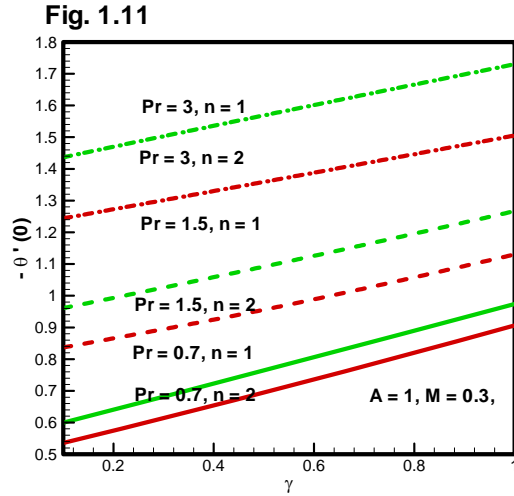


Fig. 1.11: Variations in Nusselt number against thermophysical parameters Pr , γ and n .

Table 1.4: Wall friction coefficient for variations in physical parameters A , γ , n and M .

n	A	M	γ	$Af''(0) - (-f''(0))^n$
0.1	1.0	0.3	0.5	-2.4215
0.5				-2.2533
0.8				-2.2190
1.0				-2.0648
1.3				-1.9913
1.6				-1.9398
1.8				-1.9125
2.0				-1.8911
1.0	1.0			-2.0648
1.0	2.0			-2.1792
1.0	3.0			-3.3138
2.0	1.0			-1.8911
2.0	2.0			-2.5017
2.0	3.0			-3.0976
1.0	1.0	0.1		-1.9443
1.0		0.3		-2.0648
1.0		0.5		-2.1792
2.0		0.1		-1.7595
2.0		0.3		-1.8911
2.0		0.5		-2.0168
1.0		0.3	0.1	-1.7072
1.0			0.5	-2.0648
1.0			1.0	-2.4980
2.0			0.1	-1.5994
2.0			0.5	-1.8911
2.0			1.0	-2.2740

Table 1.5: Effects of physical parameters γ , Pr and n on Nusselt number.

		$-\theta'(0)$	$-\theta'(0)$
γ	Pr	$n = 1$	$n = 2$
0.1	1.2	0.8390	0.7278
0.4		0.9396	0.8257
0.7		1.0486	0.9349
1.0		1.1601	1.0474
0.5	0.3	0.5862	0.5567
	0.7	0.8080	0.7286
	1.2	0.6574	0.8614
	2.0	1.2684	1.1021

Effects of power law index n on fluid momentum are depicted via **Fig. 1.2**. It can be observed that velocity of fluid declines when power law index n increases. It practically holds because when power law index enhances, fluid become more viscous and the velocity decelerates. Also, velocity of shear thinning fluids is higher than both Newtonian and shear thickening fluids which can be observed in graph. Influence of material parameter A on $f'(\eta)$ is represented through **Fig. 1.3** for $n = 1$ and 2. One can see that material parameter A accelerates the fluid movement. Since increment in material parameter A reduces the viscosity which respond by enhancing velocity. It is observed that fluid movement decelerate when power law index n increases. **Fig. 1.4** indicates the effects of curvature parameter γ on $f'(\eta)$ for $n = 1$ and 2. When curvature parameter γ enhances, it reduces radius of cylinder and hence its surface area. Thus contact area of cylinder with particles is deducted, so less opposing force is offered. This produces more acceleration in fluid movement. **Fig. 1.5** shows variations in horizontal velocity $f'(\eta)$ by varying magnetic field parameter M and keeping $n = 1, 2$. When magnetic field strength is increased, it generates Lorentz force which decelerates fluid velocity.

Fig. 1.6 reflects variations in temperature profile $\theta(\eta)$ for power law index n . It can be shown that temperature of fluid decayed against power law index n . Variations in temperature profile is shown via **Fig. 1.7** by altering curvature parameter γ . The fluid temperature rises

when curvature parameter γ increases (see graph). **Fig. 1.8** captures the variations in temperature versus Prandtl number Pr . Since Prandtl number is quotient of momentum to thermal diffusivities. So, for $Pr < 1$ corresponds to dominant momentum diffusivity i.e. convective heat transfer is prominent than conduction, as a result, temperature of fluid is high. On the other hand if $Pr > 1$ then conduction is dominant heat transfer mode, so it causes reduction in fluid temperature. Hence temperature falls down versus Prandtl number.

Skin friction coefficient is computed through formula given in *Eq. (1.38)*, the influences of different parameters are shown in **Figs. 1.9-1.10**. **Fig. 1.9** shows variations in wall friction factor versus magnetic field parameter M , Sisko parameter A and power law index n . As imposed magnetic field increases thickness of momentum boundary layer, it increases skin friction coefficient. Also, material parameter A enhances boundary layer thickness. It causes enhancement in skin friction coefficient. Finally, this graph shows that wall friction factor is larger in case of $n = 2$. Effects of curvature parameter γ along with magnetic field parameter M on wall friction factor are explored via **Fig. 1.10**. This graph depicts that curvature parameter γ increases wall friction. This is true because curvature parameter is related with Reynolds number in inverse relation and *Eq. (1.38)* expresses that skin friction coefficient is also inversely proportional to Reynolds number. Thus an increment in curvature parameter γ reduces the Reynolds number which alternatively increases wall friction.

Variations in wall heat flux coefficient are shown via **Fig. 1.11** by varying governing parameters γ , Pr and n . As Prandtl number enhances momentum transport which reflects the behavior of convective heat transfer and Nusselt number as well. Lastly, this graph demonstrates that curvature parameter γ accelerates the wall temperature gradient i.e. $-\theta'(0)$.

Table 1.4 displays the wall friction coefficient by varying governing parameters A , M , n and γ . This table exhibits that skin friction is larger for shear thinning fluids as compared to Newtonian or shear thickening fluids. Also, magnetic field enhances momentum boundary layer and skin friction coefficient. Also, similar results are observed for material parameter A and curvature parameter γ .

Variations in local Nusselt number against deviations in γ , Pr and n are presented in **Table 1.5**. It is found that the Nusselt number inclines when physical parameters γ and Pr increases but opposing behaviour has been recorded against n .

1.4 Concluding remarks

In current investigation boundary layer flow of MHD Sisko fluid past a stretching cylinder is presented. The results are calculated with shooting technique are shown via graphs and tables. It is observed that the applied magnetic field controls momentum boundary layer and decelerates velocity of fluid. Also, fluid velocity enhances versus both curvature parameter γ and Sisko parameter A . Curvature parameter γ rises fluid temperature while Prandtl number Pr causes reduction in it. Both velocity and temperature decline versus power law index n .

Chapter 2

Magnetohydrodynamic flow of Sisko fluid over a stretching cylinder with variable thermal conductivity: A numerical study

This chapter extends the previous work by taking temperature dependent thermal conductivity. Experimentally, it is validated that thermal conductivity of fluid changes when temperature rises from 0 to 400F. As thermal conductivity is an important thermal property which measures the capability of conductance, hence this property plays a paramount role in heat transfer analysis. Thus major concern of present chapter is to discuss the variable thermal conductivity effects on MHD Sisko fluid flow over stretching cylinder. Appropriate group of local similar transforms are utilized to transform the modelled partial differential equations into ordinary differential system and then resulting system is tackled with Runge-Kutta-Fehlberg scheme. Physical aspects of interesting physical quantities are depicted through graphs versus involved parameters. Additionally, variations in local wall friction and local heat flux are exhibited with figures and tables. For validation of computed results, a comparison has been made with literature.

2.1 Mathematical formulation

Let us assume the axisymmetric, 2-dimensional flow of Sisko fluid over stretching cylinder. Surface is stretching along x - axis (axial direction of cylinder) with velocity $U(x) = cx$. The upper half of the plane i.e. $r > 0$ is filled with fluid. A magnetic field of strength B_0 is imposed on the fluid particles in radial direction by neglecting induced magnetic field and electric field. Thermal conductivity of the fluid is considered as temperature dependent (i.e. variable). The governing equations after boundary layer approximations are given by

Fig. 2.1

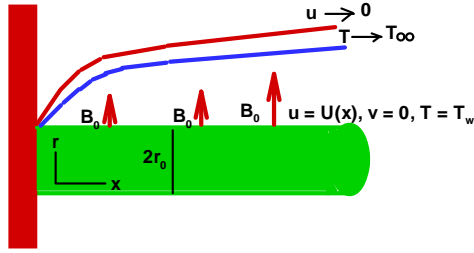


Fig. 2.1: Geometry of the problem.

$$\frac{\partial(rv)}{\partial r} + \frac{\partial(ru)}{\partial x} = 0, \quad (2.1)$$

$$u \frac{\partial u}{\partial x} + v \frac{\partial u}{\partial r} = \frac{a}{\rho} \left(\frac{1}{r} \frac{\partial}{\partial r} \left(r \frac{\partial u}{\partial r} \right) \right) - \frac{b}{r\rho} \left(-\frac{\partial u}{\partial r} \right)^n + \frac{nb}{\rho} \left(-\frac{\partial u}{\partial r} \right)^{n-1} \frac{\partial^2 u}{\partial r^2} - \frac{\sigma}{\rho} B_0^2 u, \quad (2.2)$$

$$u \frac{\partial T}{\partial x} + v \frac{\partial T}{\partial r} = \frac{1}{r} \frac{\partial}{\partial r} \left(\alpha r \frac{\partial T}{\partial r} \right), \quad (2.3)$$

subject to the boundary conditions

$$\begin{aligned}
u(x, r) &= U(x), \quad v(x, r) = 0, \quad T(x, r) = T_w \text{ at } r = r_0, \\
u(x, r) &\rightarrow 0, \quad T(x, r) \rightarrow T_\infty \text{ as } r \rightarrow \infty.
\end{aligned} \tag{2.4}$$

In above system u and v represent the components of velocity along x -axis and r -axis. Also, a called the high shear rate viscosity, consistency index is denoted with b , n represents the power law index, σ is the electrical conductivity and ρ is the density of fluid particles. In last equation, T is temperature while T_w , T_∞ and $\alpha = \frac{\kappa}{\rho c_p}$ represent wall temperature, extreme temperature and thermal diffusivity respectively.

Define the stream function Ψ such that

$$u = \frac{1}{r} \frac{\partial \Psi}{\partial r}, \quad v = -\frac{1}{r} \frac{\partial \Psi}{\partial x}, \tag{2.5}$$

which satisfies the continuity equation identically.

Modelled differential system is converted into non-dimensional form by using the following transformations

$$\begin{aligned}
\eta &= \frac{r^2 - r_0^2}{2xr_0} \text{Re}_b^{\frac{1}{n+1}}, \quad \Psi = xr_0 U \text{Re}_b^{\frac{-1}{n+1}} f(\eta), \\
\theta(\eta) &= \frac{T - T_\infty}{T_w - T_\infty}, \quad \alpha = \alpha_\infty (1 + \epsilon\theta),
\end{aligned} \tag{2.6}$$

where $\text{Re}_b = \frac{\rho x^n U^{2-n}}{b}$ is the Reynolds number, α_∞ is thermal diffusivity when $r \rightarrow \infty$ and ϵ is a positive number called thermal conductivity parameter.

Using above similarity transformations into *Eqs.* (2.1) – (2.3), following system of equations is obtained

$$A(1 + 2\gamma\eta)f''' + n(1 + 2\gamma\eta)^{\frac{n+1}{2}}(-f'')^{n-1}f''' - (n+1)\gamma(1 + 2\gamma\eta)^{\frac{n-1}{2}}(-f'')^n$$

$$+2A\gamma f'' - f'^2 + \frac{2n}{n+1} f f'' - M f' = 0, \quad (2.7)$$

$$(1 + 2\gamma\eta)(\theta'' + \epsilon(\theta\theta'' + \theta'^2)) + 2\gamma(1 + \epsilon\theta)\theta' + \frac{2n}{n+1} \text{Pr} f\theta' = 0, \quad (2.8)$$

and the boundary conditions of the problem reduces to

$$\begin{aligned} f(0) &= 0, \quad f'(0) = 1, \quad \theta(0) = 1, \\ f'(\infty) &= 0, \quad \theta(\infty) = 0. \end{aligned} \quad (2.9)$$

Here the curvature parameter γ , Hartmann parameter M , Sisko fluid parameter A and Prandtl number Pr are defined as

$$\begin{aligned} \text{Re}_a &= \frac{\rho U x}{a}, \quad \gamma = \frac{x}{r_0} \text{Re}_b^{\frac{-1}{n+1}}, \quad M = \frac{\sigma x B_0^2}{\rho U}, \\ A &= \frac{\text{Re}_b^{\frac{2}{n+1}}}{\text{Re}_a}, \quad \text{Pr} = \frac{x U}{\alpha_\infty} \text{Re}_b^{\frac{-2}{1+n}}. \end{aligned} \quad (2.10)$$

The quantities of practical interest i.e. local wall friction and local wall heat flux are defined as

$$C_{fx} = \frac{\tau_w}{\frac{1}{2}\rho U^2} \quad \text{and} \quad Nu_x = \frac{x q_w}{\kappa(T_w - T_\infty)}, \quad (2.11)$$

where τ_w is surface shear stress while q_w called wall heat flux. These quantities are defined below

$$\tau_w = a\left(\frac{\partial u}{\partial r}\right)_{r=r_0} - b\left(-\frac{\partial u}{\partial r}\right)_{r=r_0}^n \quad \text{and} \quad q_w = -\kappa\left(\frac{\partial T}{\partial r}\right)_{r=r_0}. \quad (2.12)$$

The non-dimensional form of wall friction and heat flux coefficients are take the following form

$$\frac{1}{2}C_{f_x} \text{Re}_b^{\frac{1}{n+1}} = Af''(0) - [-f''(0)]^n \text{ and } Nu_x \text{Re}_b^{\frac{-1}{n+1}} = -\theta'(0). \quad (2.13)$$

2.2 Numerical solution

In this chapter, the problem on MHD non-Newtonian Sisko fluid with varying thermal conductivity is formulated. Since governing system i.e. *Eqs.* (2.7) – (2.8) of this problem are highly nonlinear. For computation of numerical solution shooting method is implemented. The variations in model are discussed for different values of curvature parameter γ , material parameter A , magnetic field parameter M , variable thermal conductivity parameter ϵ and Prandtl number Pr . Initially higher order equations are transformed to:

$$f''' = \frac{(n+1)\gamma(1+2\gamma\eta)^{\frac{n-1}{2}}(-f'')^n - 2A\gamma f'' + f'^2 - \frac{2n}{n+1}f f'' + Mf'}{A(1+2\gamma\eta) + n(1+2\gamma\eta)^{\frac{n+1}{2}}(-f'')^{n-1}}, \quad (2.14)$$

$$\theta'' = -\frac{\frac{2n}{n+1}\text{Pr} f\theta' + 2\gamma(1+\epsilon\theta)\theta' + \epsilon(1+2\gamma\eta)\theta'^2}{(1+2\gamma\eta)(1+\epsilon\theta)}, \quad (2.15)$$

A new set of variables is defined as

$$f = y_1, f' = y_2, f'' = y_3, f''' = y_3', \theta = y_4, \theta' = y_5 \text{ and } \theta'' = y_5'. \quad (2.16)$$

Using *Eq.* (2.16) in governing equations i.e. *Eqs.* (2.14) – (2.15), these are transformed to first order ordinary differential system

$$y_1' = y_2, \quad (2.17)$$

$$y_2' = y_3, \quad (2.18)$$

$$y_3' = \frac{(n+1)\gamma(1+2\gamma\eta)^{\frac{n-1}{2}}(-y_3)^n - 2A\gamma y_3 + y_2^2 - \frac{2n}{n+1}y_1y_3 + My_2}{A(1+2\gamma\eta) + n(1+2\gamma\eta)^{\frac{n+1}{2}}(-y_3)^{n-1}}, \quad (2.19)$$

$$y_4' = y_5, \quad (2.20)$$

$$y_5' = -\frac{\frac{2n}{n+1}\text{Pr}y_1y_5 + 2\gamma(1+\epsilon y_4)y_5 + \epsilon(1+2\gamma\eta)y_5^2}{(1+2\gamma\eta)(1+\epsilon y_4)}. \quad (2.21)$$

and the subjected boundary conditions are

$$y_1(0) = 0, \quad y_2(0) = 1, \quad y_2(\infty) = 0, \quad y_4(0) = 1 \quad \text{and} \quad y_4(\infty) = 0. \quad (2.22)$$

Now to compute the solution of above system i.e. *Eqs.* (2.17) – (2.21) with Runge-Kutta Fehlberg method, it requires five initial values, but *Eq.* (2.22) has only three initial conditions, so it lacks two initial approximations for dependent variables y_3 and y_5 . Thus before proceeding towards solution procedure first missing initial conditions must be chosen, $y_3(0) = \gamma_1$ and $y_5(0) = \gamma_2$ are chosen initially. Additionally, the domain of independent variable is semi-infinite, so finite upper limit of η i.e. η_∞ must be chosen. Now solution process is started for computation of fluid velocity and temperature. The process of solution will be terminated after satisfying the tolerance criteria which is 10^{-6} in this problem. If error differences is larger then initial values are modified by using Newton method.

2.3 Results and discussion

MHD flow of Sisko fluid over stretching cylinder is described under the impacts of variable thermal conductivity. The solution was found numerically and compared with reported data to check accuracy. In **Table 2.1**, numerical values of skin friction coefficient are compared with Hassanien et al. [42], Cortell [43], Liao [20], Andreson and Kumran [44] and Abel et al. [47]. It can be observed from the table that results agree upto desired significant digits. Additionally, comparison of wall heat flux i.e. $-\theta'(0)$ is presented via **Table 2.2** by varying Prandtl number. This graph reveals that present values are quite similar with reported data i.e. results of Yih

[19], Ali et al. [33] and Reddy et al. [35].

Table 2.1: Comparison of wall friction coefficient by varying n and considering $M = 0$, $A = 0$ and $\gamma = 0$.

	Hassanien et al.	Cortell [43]	Laio [20]	Andreson and	Abel et al.	Present
n	[42]			Kumran [44]	[47]	Results
0.6			1.0280	1.0951	1.095166	1.0961
0.8	1.02883	1.0000	1.0000	1.0284	1.028713	1.0285
1	1.00000			1.0000	1.000000	1.0000
1.2	0.98737			0.9874	0.987372	0.9874
1.4				0.9819	0.981884	0.9824
1.5	0.98090		0.9820	0.9806	0.980653	0.9806
1.6				0.9798	0.979827	0.9798
1.8	0.97971			0.9794	0.979469	0.9797
2		0.9797	0.9820	0.9800	0.979991	0.9791

Table 2.2: Local Nusselt number comparison with reported data by varying Pr and keeping $n = 1$, $A = 0$, $\gamma = 0$, $\epsilon = 0$.

Pr	Yih [19]	Ali et al. [33]	Reddy et al. [35]	Present
0.71	0.8686	0.8686	0.86864	0.8685
1	1.0000	1.0000	1.001	1.0000
3	1.9237	1.9237	1.9230	1.9229
10	3.7207	3.7208	3.72028	3.7221

Fig. 2.2 shows the fluid velocity curves $f'(\eta)$ for different values of Sisko fluid parameter A and $n = 1, 2$. This figure discloses that enhancement in Sisko fluid parameter A causes increase in both velocity and momentum boundary layer. These results are physically valid because Sisko parameter has inverse relation with consistency index b i.e. fluid viscosity of power law region. So, when material parameter A increases, viscous force become weaker, as a result, the fluid motion is accelerated. To figure out the influences of magnetic field parameter

M on fluid velocity, **Fig. 2.3** is constructed. This figure divulges that when magnetic field strength increases, it decays fluid velocity. It is true because the Lorentz force (resisting force) become stronger when magnetic field parameter M increases. Effects of curvature parameter γ on velocity profile $f'(\eta)$ are displayed through **Fig. 2.4** for power law index $n = 1$ and 2. It can be perceived that when bending of cylinder enhances it reduces both radius of cylinder and surface area. Hence the surface of the cylinder provides less, as a result, fluid velocity enlarges.

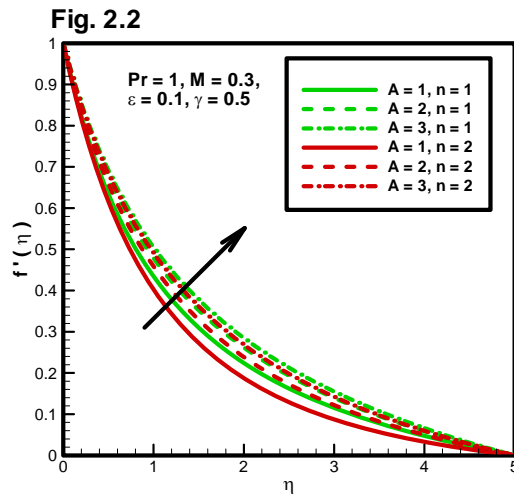


Fig. 2.2: Fluid velocity $f'(\eta)$ variations against Sisko parameter A and $n = 1$ and 2.

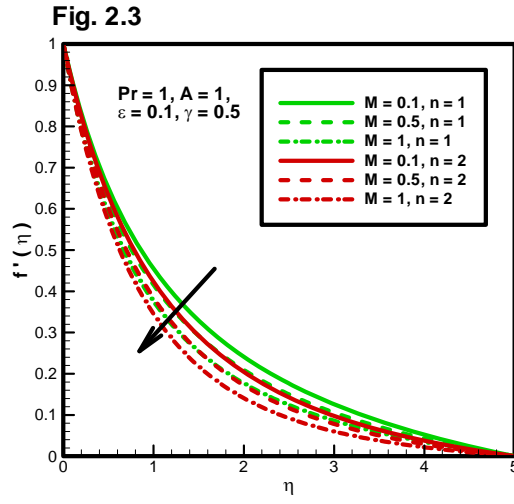


Fig. 2.3: Magnetic field parameter M influences on $f'(\eta)$ for $n = 1$ and 2.

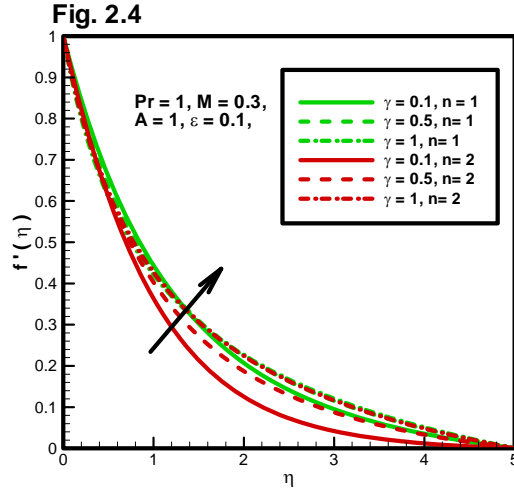


Fig. 2.4: Velocity profile $f'(\eta)$ for variation in curvature parameter γ and $n = 1, 2$.

Fig. 2.5 depicts the behavior of thermal conductivity parameter ϵ on heat equation for $n = 1$ and 2. This figure indicates that when thermal conductivity of fluid increases, it rises the fluid temperature. The reason behind that when thermal conductivity enhances, then fluid

conducts heat more rapidly and consequently temperature increases. Temperature curves are shown for different values of Prandtl number Pr and $n = 1, 2$ in **Fig. 2.6**. It can be observe that temperature profile declines for larger values of Prandtl number Pr . It holds practically since Pr is the ratio of momentum to thermal diffusivity. Thus by increasing Pr , momentum transport accelerates which enhances convective heat transfer and declines conductive heat transfer, hence it reduces the fluid temperature. The influence of curvature parameter γ on temperature profile for $n = 1$ and 2 is shown via **Fig. 2.7**. This graph illustrates that curvature parameter γ enhances fluid temperature and hence thermal boundary layer as well. This is physically true because when curvature of cylinder increases, it reduces radius of the cylinder which accelerates the heat transfer rate. **Fig. 2.8** depicts magnetic field parameter M effects on temperature profile by keeping $n = 1, 2$. Here fluid temperature enhances by increasing the strength of magnetic field. The fact behind that when magnetic field strength increases, it produced heat in the fluid which causes enhancement in fluid temperature.

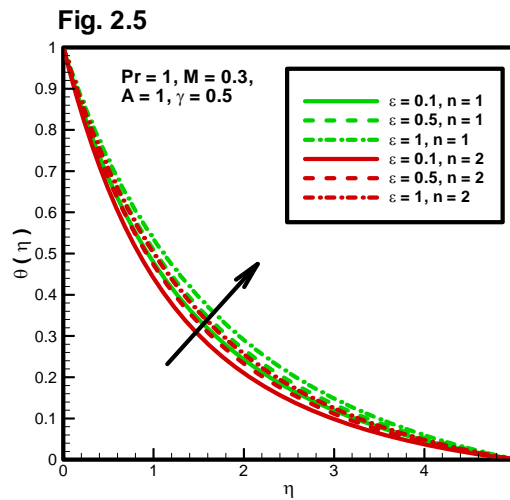


Fig. 2.5: Temperature curves against thermal conductivity parameter ϵ and keeping $n = 1, 2$.

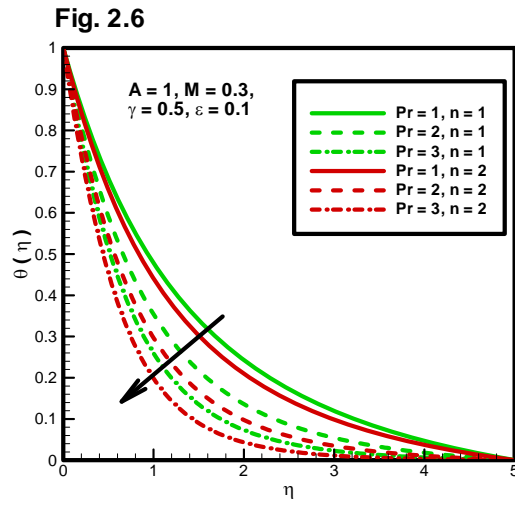


Fig. 2.6: Temperature profile $\theta(\eta)$ versus Prandtl number Pr while fixing $n = 1, 2$.

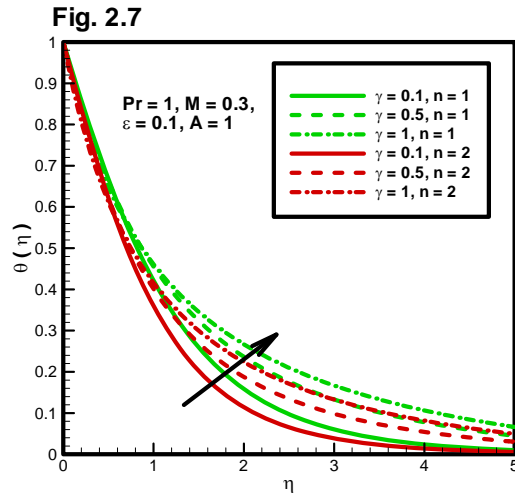


Fig. 2.7: Curvature parameter γ impacts on temperature $\theta(\eta)$ for $n = 1, 2$.

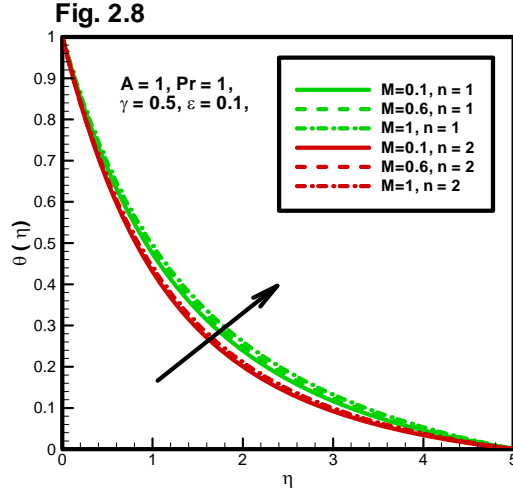


Fig. 2.8: Temperature profile $\theta(\eta)$ for magnetic field parameter M and keeping fixed n .

Fig. 2.9 reflects combined impacts of fluid parameter A , magnetic field parameter M and power law index n on skin friction coefficient. This graph demonstrates that wall friction enhances versus magnetic field parameter M and Sisko parameter A . The results hold practically because enhancement in A and M increase momentum boundary layer and coefficient of wall friction. Also, this figure proves that wall shear stress of pseudoplastic fluid is hotter than dilatant and Newtonian fluids. **Fig. 2.10** delineates the fluctuations in skin friction coefficient by altering power law index n , Sisko parameter A and curvature parameter γ . It shows that curvature parameter γ increases wall friction coefficient. It is true because inclination in curvature parameter γ decrease Reynolds number which causes enhancement in wall shear stress.

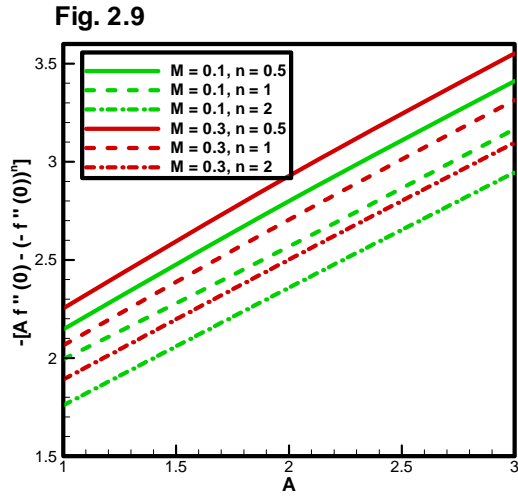


Fig. 2.9: Effects of magnetic field parameter M and Sisko parameter A on wall friction coefficient for $n = 1, 2$.

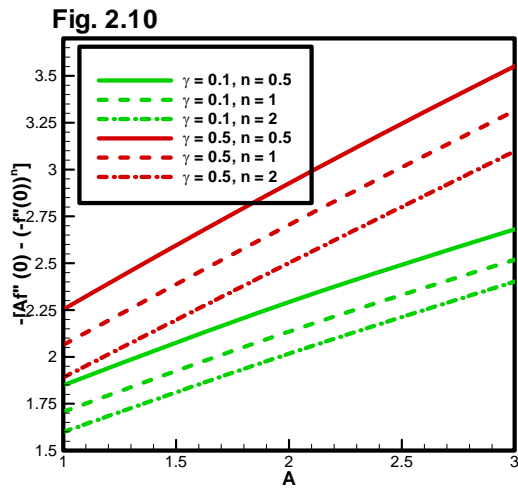


Fig. 2.10: Wall shear stress by varying curvature parameter γ and material parameter A while $n = 0.5, 1, 2$.

The impacts of governing parameters A, M, γ and n on skin friction coefficient is displayed

in **Table 2.3**. In this table a comparison is presented between power law fluid ($A = 0$) and Sisko fluid ($A = 1$). It is observed that Sisko fluid has larger skin friction coefficient than power law fluid for all values of n . Also, wall shear stress declines for larger values of power law index n while it inclines for physical parameters M and γ .

Table 2.3: Influences of M , γ and n on skin friction coefficient.

A	n	M	γ	$Af''(0) - (-f''(0))^n$
0	0.7	0.3	0.5	-1.3929
	1			-1.3485
	1.6			-1.2873
	1	0.1		-1.2558
		0.4		-1.3924
		0.7		-1.5160
		0.3	0.1	-1.1825
			0.6	-1.3839
			1	-1.5504
1	0.5	0.3	0.5	-2.2533
	1			-2.0648
	2			-1.8911
	1	0.1		-1.9943
		0.4		-2.1228
		0.7		-2.2880
		0.3	0.1	-1.7270
			0.6	-2.1528
			1	-2.4980

Fig. 2.11 exemplifies the effects of both curvature parameter γ and variable thermal conductivity parameter ϵ on wall temperature gradient. Curvature parameter γ accelerates heat transfer from the wall, while the influence of thermal conductivity parameter ϵ is opposite on it

(see figure). These results are true because Nusselt number varies inversely to heat conduction. Thus high thermal conductivity decreases the Nusselt number. Also, it can be analyzed that power law index n causes decline in wall temperature gradient. **Fig. 2.12** expresses variations in local wall heat flux versus variable thermal conductivity parameter ϵ , Prandtl number Pr and power law index n . This figure illustrates that Prandtl number enhances local Nusselt number. It can see that the increment in Prandtl number reduces thermal conductivity which increases the local Nusselt number.

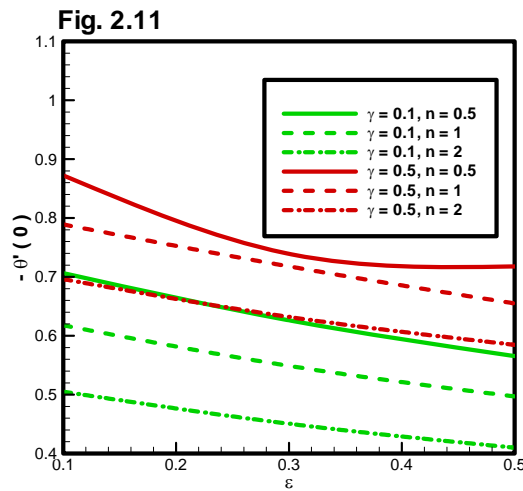


Fig. 2.11: Effects of physical parameters ϵ and γ on $-\theta'(0)$ for $n = 0.5, 1$ and 2 .

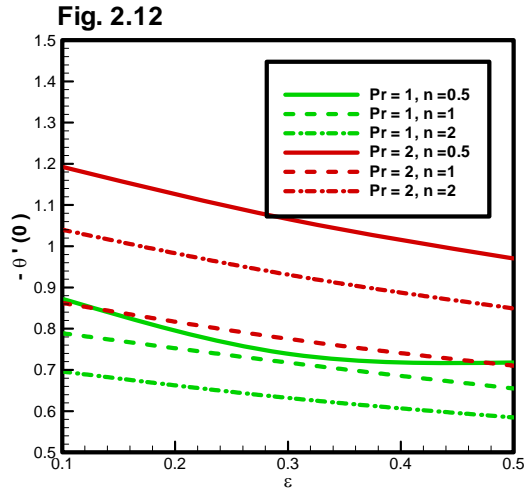


Fig. 2.12: Wall temperature gradient versus physical parameters Pr , ϵ and n .

The impacts thermophysical parameters ϵ , γ , Pr and n on Nusselt number is discussed in **Table 2.4**. It can be see from the table that fluid with constant thermal conductivity ($\epsilon = 0$) has larger local Nusselt number when compared with the fluid for variable thermal conductivity ($\epsilon = 0.5$). Also, γ and Pr enhances the Nusselt number.

Table 2.4: Effect of curvature parameter γ , thermal conductivity parameter ϵ , Prandtl number Pr and power law index n on local Nusselt number.

ϵ	n	Pr	γ	$-\theta'(0)$
0	0.5	1	0.5	0.9290
	0.1			0.8384
	2			0.7374
	1	1		0.8384
		2		1.1093
		3		1.3517
		1	0.1	0.6614
			0.6	0.8843
			1	1.0658
0.5	0.5	1	0.5	0.7178
	1			0.6549
	2			0.5846
	1	1		0.6549
		2		0.8491
		3		1.0307
		1	0.1	0.4971
			0.6	0.6945
			1	0.8512

2.4 Concluding remarks

Current chapter focuses on Sisko fluid flow with applied magnetic field. Thermal conductivity of fluid is considered temperature dependent. Solution is computed with shooting technique. It can be observed that

- Material parameter A and curvature parameter γ enhance fluid velocity while both power

law index n and magnetic field parameter M reduce it.

- By increasing thermal conductivity and curvature parameter γ fluid temperature rises while power law index n and Prandtl number Pr fall down temperature.
- Wall friction coefficient of power law fluid is much lesser than Sisko fluid while pseudo-plastic fluid has larger skin friction coefficient than both Newtonian and dilatant fluids.
- Magnetic field parameter M , Sisko fluid parameter A and curvature parameter γ increases skin friction coefficient absolutely.
- Local Nusselt number enlarges against curvature parameter γ and Prandtl number Pr .
- Nusselt number is larger of constant thermal conductivity as compare to variable thermal conductivity.

Chapter 3

Computational analysis of magnetohydrodynamic Sisko fluid flow over a stretching cylinder in the presence of viscous dissipation and temperature dependent thermal conductivity

In this chapter effects of viscous dissipation are included in flow analysis which is an extension of previous chapter. In practice, it is noticed that during the fluid motion viscosity some amount of kinetic energy is transformed into thermal energy i.e. dissipate energy. As this phenomenon processed because of viscosity, thus called viscous dissipation. Thus focus of current chapter is on MHD Sisko fluid flow over stretching surface under the influences of viscous dissipation and variable thermal conductivity. The variable similarity transforms are used on governing partial differential equations which non-dimensionalized the governing system. Attained equations are solved with the aid of Runge-Kutta method. Interesting aspects of flow velocity and temperature are computed and visualized via graphs for different parametric conditions. Influences of flow

parameters on wall shear stress and local Nusselt number are discussed briefly and concisely via figures and tables. The present results have good covenant with published results.

3.1 Development of problem

Consider the axisymmetric, steady state, electrically conducting, boundary layer flow of Sisko fluid over continuously stretching surface. Cylinder is stretched along axial direction with velocity $U(x) = cx$ for $c > 0$. A magnetic field of strength B_0 is imposed in radial direction. The effects of variable thermal conductivity and viscous dissipation are factored into analysis. After using Prandtl theory governing equations are transformed to

Fig. 3.1

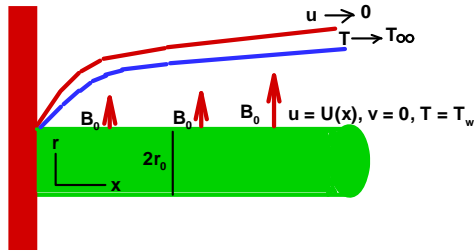


Fig. 3.1: Geometry of the fluid model.

$$\frac{\partial(ru)}{\partial x} + \frac{\partial(rv)}{\partial r} = 0, \quad (3.1)$$

$$u \frac{\partial u}{\partial x} + v \frac{\partial u}{\partial r} = \frac{a}{r\rho} \frac{\partial}{\partial r} \left(r \frac{\partial u}{\partial r} \right) - \frac{b}{r\rho} \left(-\frac{\partial u}{\partial r} \right)^n + \frac{nb}{\rho} \left(-\frac{\partial u}{\partial r} \right)^{n-1} \frac{\partial^2 u}{\partial r^2} - \frac{\sigma B_0^2}{\rho} u, \quad (3.2)$$

$$u \frac{\partial T}{\partial x} + v \frac{\partial T}{\partial r} = \frac{1}{r} \frac{\partial}{\partial r} \left(\alpha r \frac{\partial T}{\partial r} \right) + \frac{a}{\rho c_p} \left(-\frac{\partial u}{\partial r} \right)^2 + \frac{b}{\rho c_p} \left(-\frac{\partial u}{\partial r} \right)^{n+1}, \quad (3.3)$$

along with prescribed boundary conditions

$$\begin{aligned} u &= U(x), \quad v = 0 \text{ at } r = r_0 \text{ and } u \rightarrow 0 \text{ as } r \rightarrow \infty, \\ T &= T_w \text{ at } r = r_0 \text{ and } T \rightarrow T_\infty \text{ as } r \rightarrow \infty. \end{aligned} \quad (3.4)$$

In above differential system u and v are velocity components, a is high shear rate viscosity, b is power law region viscosity, n is power law index, σ is electrical conductivity while ρ denotes density of fluid. Temperature is denoted by T , T_w and T_∞ represent wall and ambient temperature respectively while c_p and $\alpha = \frac{\kappa(T)}{\rho c_p}$ are symbols of specific heat the thermal diffusivity.

The stream function Ψ of flow velocity is given below

$$u = \frac{1}{r} \frac{\partial \Psi}{\partial r}, \quad v = -\frac{1}{r} \frac{\partial \Psi}{\partial x}. \quad (3.5)$$

The suitable similarity transformations are defined as

$$\begin{aligned} \eta &= \frac{r^2 - r_0^2}{2xr_0} \text{Re}_b^{\frac{1}{n+1}}, \quad \Psi = xr_0 U \text{Re}_b^{\frac{-1}{n+1}} f(\eta), \\ \theta(\eta) &= \frac{T - T_\infty}{T_w - T_\infty}, \quad \alpha = \alpha_\infty (1 + \epsilon \theta), \end{aligned} \quad (3.6)$$

here ϵ and α_∞ represent thermal conductivity parameter and extreme thermal diffusivity while $\text{Re}_b = \frac{\rho x^n U^{2-n}}{b}$ called the Reynolds number.

The governing partial differential system is transformed into non-dimensional form by using above defined scaling variables. After employing these transforms, the continuity equation is satisfied while resting two equations are take the following form

$$\begin{aligned}
& A(1 + 2\gamma\eta)f''' + n(1 + 2\gamma\eta)^{\frac{n+1}{2}}(-f'')^{n-1}f''' - (n+1)\gamma(1 + 2\gamma\eta)^{\frac{n-1}{2}}(-f'')^n \\
& \quad + 2A\gamma f'' - f'^2 + \frac{2n}{n+1}ff'' - Mf' = 0,
\end{aligned} \tag{3.7}$$

$$\begin{aligned}
& (1 + 2\gamma\eta)(\theta'' + \epsilon(\theta\theta'' + \theta'^2)) + 2\gamma(1 + \epsilon\theta)\theta' + \frac{2n}{n+1}\text{Pr}f\theta' + \\
& A(1 + 2\gamma\eta)Ec\text{Pr}(-f'')^2 + Ec\text{Pr}(1 + 2\gamma\eta)^{\frac{n+1}{2}}(-f'')^{n+1} = 0,
\end{aligned} \tag{3.8}$$

and the boundary conditions reduce to

$$\begin{aligned}
f(0) &= 0, \quad f'(0) = 1, \quad \theta(0) = 1, \\
f'(\infty) &= 0, \quad \theta(\infty) = 0.
\end{aligned} \tag{3.9}$$

In above system, the symbols M , γ , A , Pr and Ec represent magnetic field parameter, curvature parameter, Sisko parameter, Prandtl number and Eckert number which are defined as

$$\begin{aligned}
\text{Re}_a &= \frac{\rho x U}{a}, \quad \gamma = \frac{x}{r_0} \text{Re}_b^{\frac{-1}{n+1}}, \quad M = \frac{\sigma x B_0^2}{\rho U}, \\
A &= \frac{\text{Re}_b^{\frac{2}{n+1}}}{\text{Re}_a}, \quad Ec = \frac{U^2}{c_p(T_w - T_\infty)}, \quad \text{Pr} = \frac{xU}{\alpha_\infty} \text{Re}_b^{\frac{-2}{1+n}}.
\end{aligned} \tag{3.10}$$

The fluid phenomenon in the vicinity of sheet surface is deliberated through wall friction and wall heat flux. These are defined as

$$C_{fx} = \frac{\tau_w}{\frac{1}{2}\rho U^2} \quad \text{and} \quad Nu_x = \frac{xq_w}{\kappa(T)(T_w - T_\infty)}. \tag{3.11}$$

In above formulas, surface friction coefficient and Nusselt number are denoted with C_{f_x} and Nu_x . Here τ_w and q_w denote surface friction and wall heat flux which are defined as

$$\tau_w = a\left(\frac{\partial u}{\partial r}\right)_{r=r_0} - b\left(-\frac{\partial u}{\partial r}\right)_{r=r_0}^n \text{ and } q_w = -\kappa(T)\left(\frac{\partial T}{\partial r}\right)_{r=r_0}. \quad (3.12)$$

Coefficient of wall friction and wall gradient are transferred into non-dimensional form given as

$$\frac{1}{2}C_{f_x} \text{Re}_b^{\frac{1}{n+1}} = Af''(0) - [-f''(0)]^n \text{ and } Nu_x \text{Re}_b^{\frac{-1}{n+1}} = -\theta'(0). \quad (3.13)$$

3.2 Numerical solution

As flow govern equations i.e. *Eqs.* (3.7)–(3.8) are highly nonlinear simultaneous set of ordinary differential equations. So, in order to find solution of these simultaneous equations along with boundary conditions (3.9), shooting technique in conjunction with fifth order Runge-Kutta integration scheme is employed. Both velocity and temperature profiles are discussed for different values of dimensionless parameters. Since fifth order Runge-Kutta technique tackles only initial value problems, so first *Eqs.* (3.7)–(3.8) are converted into set of first order differential system. Firstly above set of equations are re-written as

$$f''' = \frac{(n+1)\gamma(1+2\gamma\eta)^{\frac{n-1}{2}}(-f'')^n - 2A\gamma f'' + f'^2 - \frac{2n}{n+1}f f'' + Mf'}{A(1+2\gamma\eta) + n(1+2\gamma\eta)^{\frac{n+1}{2}}(-f'')^{n-1}}, \quad (3.14)$$

$$\begin{aligned} \theta'' = \frac{-1}{(1+2\gamma\eta)(1+\epsilon\theta)} & \left[\frac{2n}{n+1} \text{Pr} f\theta' + 2\gamma(1+\epsilon\theta)\theta' + \epsilon(1+2\gamma\eta)\theta'^2 \right. \\ & \left. + Ec \text{Pr}(A(1+2\gamma\eta)(-f'')^2 + (1+2\gamma\eta)^{\frac{n+1}{2}}(-f'')^{n+1}) \right]. \end{aligned} \quad (3.15)$$

New variables are defined in *Eq.* (3.16) are utilized to reduce first order differential equations

$$f = y_1, f' = y_2, f'' = y_3, f''' = y_3', \theta = y_4, \theta' = y_5 \text{ and } \theta'' = y_5'. \quad (3.16)$$

After inserting Eq. (3.16), into Eq. (3.14) – (3.15), new system of ordinary differential equations Eq. (3.17) – (3.21) is obtained

$$y_1' = y_2, \quad (3.17)$$

$$y_2' = y_3, \quad (3.18)$$

$$y_3' = \frac{(n+1)\gamma(1+2\gamma\eta)^{\frac{n-1}{2}}(-y_3)^n - 2A\gamma y_3 + y_2^2 - \frac{2n}{n+1}y_1 y_3 + M y_2}{A(1+2\gamma\eta) + n(1+2\gamma\eta)^{\frac{n+1}{2}}(-y_3)^{n-1}}, \quad (3.19)$$

$$y_4' = y_5, \quad (3.20)$$

$$y_5' = \frac{-1}{(1+2\gamma\eta)(1+\epsilon y_4)} \left[\frac{2n}{n+1} \text{Pr } y_1 y_5 + 2\gamma(1+\epsilon y_4)y_5 + \epsilon(1+2\gamma\eta)y_5^2 \right. \\ \left. + Ec \text{Pr}(A(1+2\gamma\eta)(-y_3)^2 + (1+2\gamma\eta)^{\frac{n+1}{2}}(-y_3)^{n+1}) \right], \quad (3.21)$$

together with the boundary conditions

$$y_1(0) = 0, y_2(0) = 1, y_2(\infty) = 0, y_4(0) = 1 \text{ and } y_4(\infty) = 0. \quad (3.22)$$

This system of equations is solved with shooting method, the following procedure is adopted:

1. Firstly best suited limit for η_∞ is chosen (η_∞ is 5 in this case).
2. Now choose appropriate initial guesses for $y_3(0)$ and $y_5(0)$.
3. In next step, ordinary differential system is solved by using Runge-Kutta Fehlberg scheme.
4. Finally, boundary residuals (absolute variations in given and calculated values of $y_2(\infty)$ and $y_4(\infty)$) are found. The solution will converge if boundary residuals are less than error tolerance which is considered 10^{-6} .

5. If values of boundary residuals are larger than error tolerance, then values of $y_3(0)$ and $y_5(0)$ are refined by Newton formula.

The procedure will continue unless the boundary residuals meet the desired criteria.

3.3 Results and discussion

In current investigation, the stretched flow of non-Newtonian Sisko fluid is examined under the impact of normally applied magnetic field. In addition, effects of viscous dissipation and variable thermal conductivity are also considered. Shooting technique is utilized to solve governing equations. The accuracy of solution is verified by comparing with existing literature. Wall friction factor versus power law index n are compared with reported data i.e. Hassanien et al. [42], Cortell [43], Liao [20], Andersson and Kumran [44] and Abel et al. [47] (see **Table 3.1**). It is observed that present results agree with previous upto desired significant digits. **Table 3.2** illustrates the comparison of Nusselt number i.e. $-\theta'(0)$ against alteration in Prandtl number Pr with previously published results i.e. Grubka and Bobba [41], Ishak et al. [23], Yih [19], Reddy [35] and Ali et al. [33]. This table shows that both results agreed upto significant number of digits.

Table 3.1: Comparison table of skin friction coefficient i.e. $|Af''(0) - (-f''(0))^n|$ for different values of power-law index n and considering $\gamma = 0, A = 0, M = 0$.

n	Hassanien et al. [42]	Cortell [43]	Liao [20]	Andersson and Kumaran [44]	Abel et al. [47]	Present Results
0.2				1.9287	1.943685	1.9200
0.4		1.2730		1.2715	1.272119	1.2716
0.5	1.16524			1.1605	1.167740	1.1640
0.6				1.0951	1.095166	1.0976
0.8	1.02883		1.0280	1.0284	1.028713	1.0282
1.0	1.0000	1.0000	1.0000	1.0000	1.000000	1.0000
1.2	0.98737			0.9874	0.987372	0.9888
1.4				0.9819	0.981884	0.9812
1.5	0.98090		0.9820	0.9806	0.980653	0.9805
1.6				0.9798	0.979827	0.9797
1.8	0.97971			0.9794	0.989469	0.9791
2.0		0.9797	0.9800	0.9800	0.979991	0.9801

Table 3.2: Comparison of $-\theta'(0)$ by varying Pr keeping $A = 0, M = 0, \gamma = 0, \epsilon = 0, Ec = 0, n = 1$.

Pr	Grubka and Bobba [41]	Ishak et al. [23]	Yih [19]	Reddy [35]	Ali et al. [33]	Present Results
0.71						0.8686
1.0	1	1	1	1	1.0001	1.0067
3.0	1.9237	1.9237	1.9237	1.9237	1.9230	1.9260
10.0	3.7207	3.7207	3.7207	3.7208	3.72028	3.7267

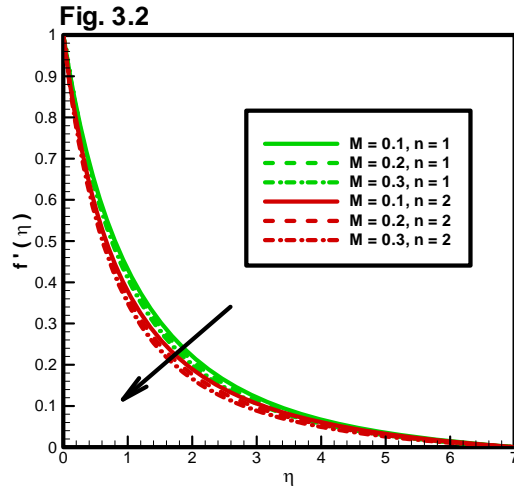


Fig. 3.2: Impacts of magnetic field parameter M and power law index n on velocity $f'(\eta)$.

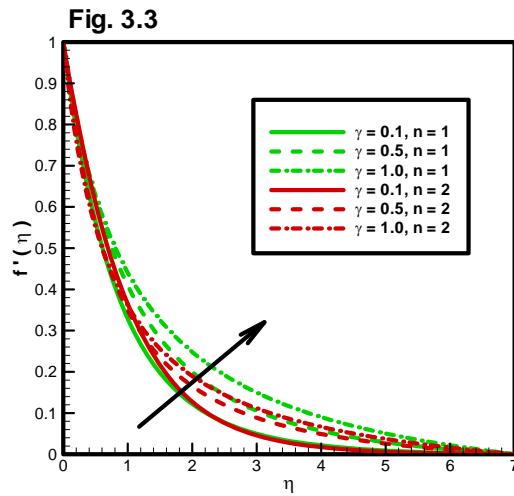


Fig. 3.3: Variations in velocity $f'(\eta)$ versus curvature parameter γ and power law index n .

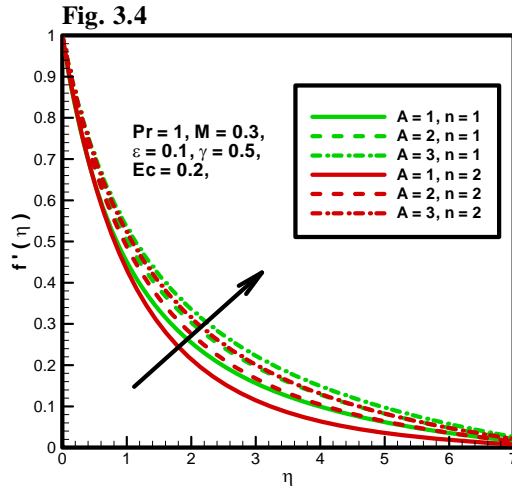


Fig. 3.4: Variations of $f'(\eta)$ for altering values of material parameter A and $n = 1, 2$.

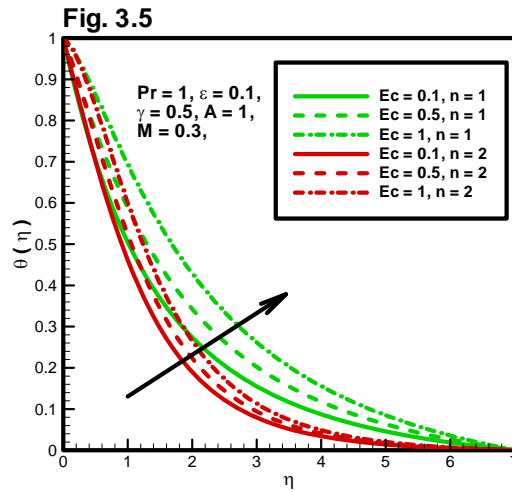


Fig. 3.5: Influence of Eckert number Ec on temperature profile $\theta(\eta)$ for power-law index $n = 1, 2$.

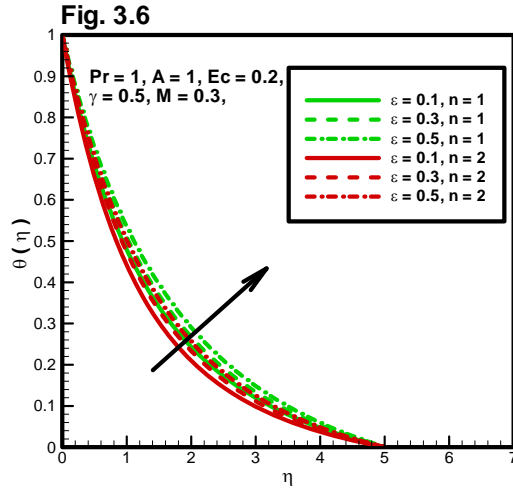


Fig. 3.6: Effects of thermal conductivity parameter ϵ and power-law index n on $\theta(\eta)$.

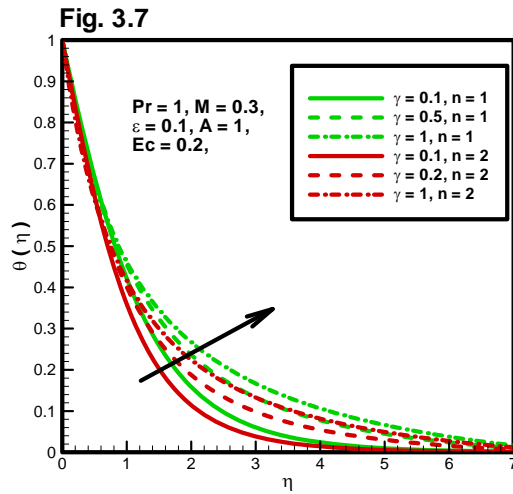


Fig. 3.7: Temperature profile $\theta(\eta)$ versus curvature parameter γ while keeping $n = 1, 2$.

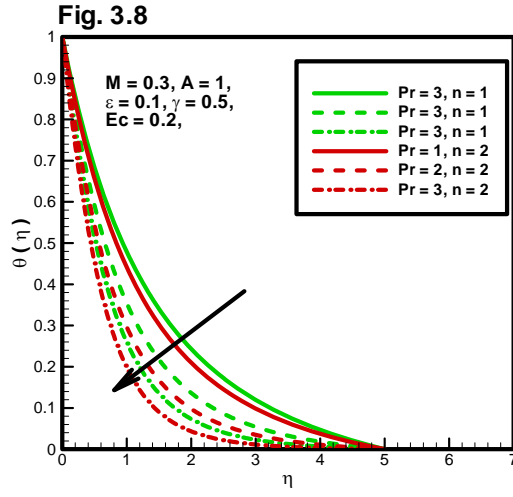


Fig. 3.8: Temperature profile $\theta(\eta)$ fluctuations versus Prandtl number Pr and $n = 1, 2$.

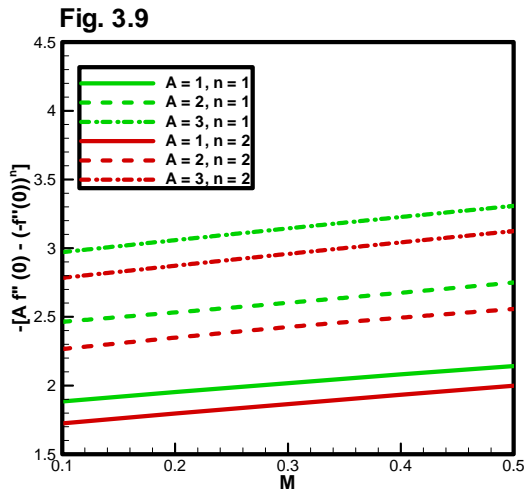


Fig. 3.9: Combined effects of Sisko parameter A as well as magnetic field parameter M on coefficient of skin friction by considering power law-index $n = 1, 2$.

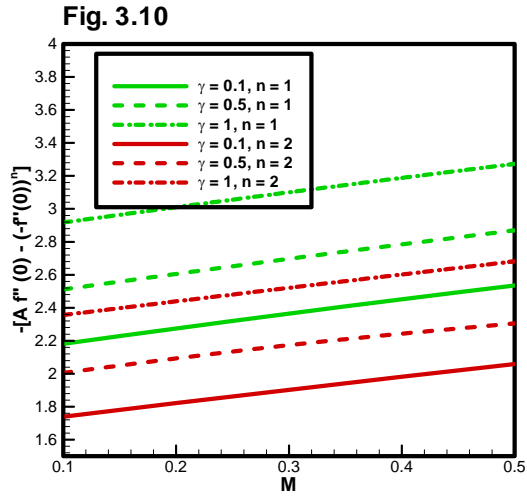


Fig. 3.10: Effects of magnetic field strength and curvature parameter γ on wall shear stress for power law-index $n = 1, 2$.

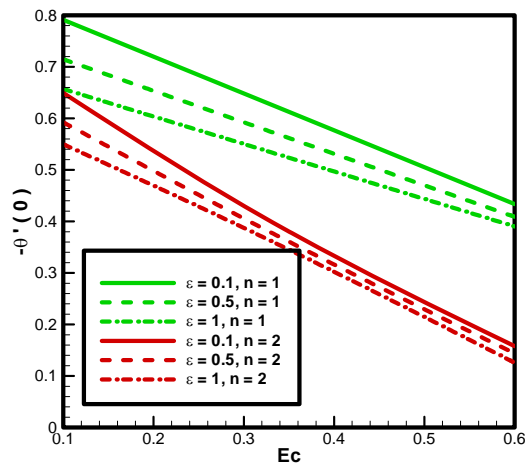


Fig. 3.11: Variations of Nusselt number versus Eckert number Ec , variable thermal conductivity parameter ϵ and power law-index $n = 1, 2$.

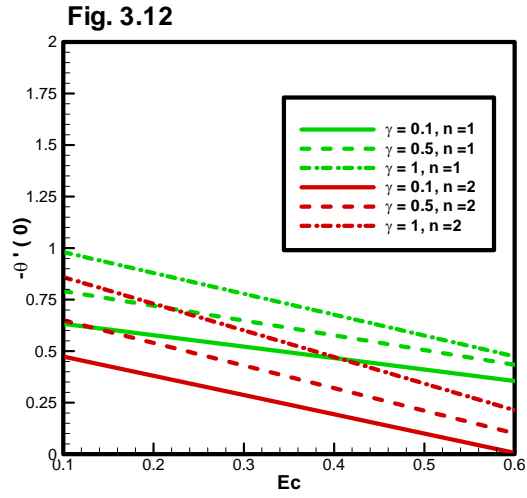


Fig. 3.12: Variations in wall heat transfer by altering curvature parameter γ , Eckert number Ec and $n = 1, 2$.

Table 3.3: Values of skin friction coefficient for different values of parameters γ, M and A for $n = 1, 2$.

γ	M	A	$(A + 1)f''(0)$	$Af''(0) - f''^2(0)$
0.1	0.3	0.2	-1.8221	-1.6455
0.			-2.0223	-1.9163
1.0			-2.2284	-2.1818
0.5	0.1		-2.4396	-2.4416
0.3	0.3		-1.9549	-1.8265
	0.5		-2.3716	-2.3528
	0.3	1	-2.8531	-2.8456
		2	-3.3594	-3.3201
		3	-1.8704	-1.7640

Table 3.4: Local Nusselt number against involving parameters γ , Ec and Pr for $n = 1, 2$.

γ	ϵ	Pr	Ec	$-\theta'(0)$	$-\theta'(0)$
				$n = 1$	$n = 2$
0.1	0.1	1	0.2	0.6327	0.4740
0.5				0.7914	0.6493
1.0				0.9804	0.8589
0.5	0.1			0.7914	0.6493
	0.3			0.7145	0.5922
	0.5			0.6569	0.5497
	0.1	1		0.7914	0.6493
		2		1.0428	0.7762
		3		1.2593	0.8986
		1	0.1	0.7914	0.6493
			0.3	0.6483	0.4301
			0.6	0.4336	0.1011

The variations in interested physical quantities are visualized through graphs and tables.

Fig. 3.2 exhibits the influence of magnetic field on velocity profile $f'(\eta)$. It is worth mentioning that the magnetic field strength decelerates the fluid momentum in boundary layer regime. Because magnetic field produces Lorentz force which resists fluid motion. Also, it is noticed that increment in power law index n leads to decrease in velocity $f'(\eta)$. **Fig. 3.3** displays the asymptotic curves of velocity profile against curvature parameter γ and power law index n . It is found that fluid motion experienced less resistance when curvature parameter enlarges which consequently enhances velocity. The presently computed results validated the above mentioned fact. **Fig. 3.4** displays the velocity curves by varying power law index n and Sisko parameter A . The figure shows that velocity profile $f'(\eta)$ enhances versus Sisko parameter A because larger values of A corresponds to fluid with low viscosity. Also, this figure reflects that the velocity profile decreases by varying power law index n .

Variations in temperature versus Eckert number Ec are deliberated via **Fig. 3.5** by fixing

power law index i.e. $n = 1, 2$. As Eckert number Ec accelerates the advective transport which consequently enhances the collision of particles, these collisions transformed kinetic energy into thermal energy, as a result, fluid temperature rises. Finally, it can be seen that temperature profile $\theta(\eta)$ decreases by increasing power-law index n . **Fig. 3.6** demonstrates the influence of thermal conductivity parameter ϵ on temperature profile $\theta(\eta)$. Enhancement in thermal conductivity boosted the capability of heat transference and hence fluid temperature. The curvature parameter γ effects on fluid temperature are depicted with the aid of **Fig. 3.7**. This graph shows that curvature parameter rises the fluid temperature. **Fig. 3.8** delineates the fluctuations in temperature profile for variations in Prandtl number Pr . It is observed that Prandtl number Pr decreases temperature profile $\theta(\eta)$.

Fig. 3.9 illustrates the magnetic field parameter M and Sisko parameter A on wall friction coefficient. Current graph describes that material parameter A increases the skin friction coefficient in absolute sense, it holds physically because larger values of material parameter A enhances boundary layer thickness. Also, magnetic field parameter M increases wall friction coefficient. Finally, this figure displays that wall friction coefficient has less values for $n = 2$ as compared to $n = 1$. **Fig. 3.10** represents graph of variations in coefficient of wall friction by altering fluid parameter γ and magnetic field parameter M . Since, Reynolds number and skin friction coefficient are in inverse relation as shown in *Eq. (3.13)*. Also, curvature parameter γ has inverse relation with Reynolds number, thus increase in curvature parameter γ , Reynolds number becomes low which alternatively enhances coefficient of wall friction.

Eckert number Ec and thermal conductivity parameter ϵ impacts on wall heat flux are displayed in **Fig. 3.11**. It is mentioned that both parameters decrease wall heat flux. Additionally, Nusselt number are decreased for power law index n . Deviations in surface heat flux i.e. $-\theta'(0)$ on altered values of Eckert number Ec and curvature parameter γ are shown by **Fig. 3.12**. This graph illustrates that Nusselt number declines versus Eckert number Ec while curvature parameter γ causes enhancement in wall heat flux.

The behavior of the governing parameters n, γ, A and M on coefficient of skin friction is analyzed via **Table 3.3**. This table shows that fluid parameters γ, A and M enlarge the skin friction coefficient absolutely for both cases i.e. $n = 1$ and 2 .

Table 3.4 reveals the influences of Prandtl number Pr , Eckert number Ec , thermal con-

ductivity parameter ϵ and curvature parameter γ on wall heat flux by keeping $n = 1, 2$. Wall heat flux is enhanced by varying Prandtl number Pr and curvature parameter γ while Eckert number Ec , thermal conductivity parameter ϵ and power law index n reduce wall temperature gradient.

3.4 Concluding remarks

In present chapter, the numerical simulations for MHD Sisko fluid are developed to explore the dynamics over stretching cylinder. Effects of temperature dependent thermal conductivity and viscous dissipation are taken into account. The modeled partial differential system is transformed into ordinary differential system by using scaling transforms which then solved numerically. The main outcomes of the current observation are:

- Both curvature parameter γ and Sisko parameter A accelerate fluid momentum while power law index n and magnetic field strength decelerate it.
- Prandtl number Pr and power law index n are responsible to decrease the temperature while it rise up against flow parameters Ec , γ and ϵ .
- The effects of all pertinent parameters i.e. M , A and γ on skin friction coefficient are qualitatively similar but Sisko parameter A has prominent effects in quantitative sense.
- Curvature parameter γ , Eckert number Ec and Prandtl number Pr augments the Nusselt number while thermal conductivity parameter ϵ and power law index n are responsible to reduce it.

Chapter 4

Combined effects of viscous dissipation and Joule heating on MHD Sisko nanofluid over a stretching cylinder

This chapter mathematically configures the physical situation focusing on MHD flow of Sisko nanofluid past over a stretching cylinder with cumulative effects of viscous dissipation and Joule heating. Nanofluid is a modern type of fluids which consists base fluid and nano-size particles. Different metals (copper, aluminum, silicon etc.) are used as nanoparticles. The basic purpose of including nanoparticles in fluids is to increase thermal conductivity of base fluid. Because it is found that mostly fluids (e.g. oil, ethylene glycol, water and engine oil) which are conventionally utilized in heat transfer have low heat conduction capacity. Also, movement of electrical conducting fluid produces heat. It is an important phenomenon known as Joule heating, it has many applications in different areas. The mathematical modelling of the considered physical problem produces nonlinear partial differential equations which are transfigured into non-dimensional form via suitable scaling group of transforms. Shooting technique is used to solve nonlinear set of flow govern equations. Comparison of numerical solution is made with the reported data to validate the model accuracy. Variations in velocity, temperature and

concentration are discussed under different parametric conditions. The numerically computed results are deliberated via graphs by selecting suitable values of the relevant physical parameters. Additionally to insight physical phenomenon in the vicinity of surface i.e. coefficients of wall friction, wall heat flux and wall mass flux are computed and explicated in both tabular and graphical manners.

4.1 Problem formulation

Let assume steady, axisymmetric, 2D flow of Sisko nanofluid passing through stretching cylinder. Cylinder surface is taken at $r = r_0$ and surface is stretching in x -direction with velocity $U(x) = cx$ where c is constant. Magnetic field of strength B_0 is utilized in normal direction i.e. r -direction. Effects of energy dissipation and Joule heating are assumed. The governing equations take the below-defined form (after imposing boundary layer theory)

Fig. 4.1

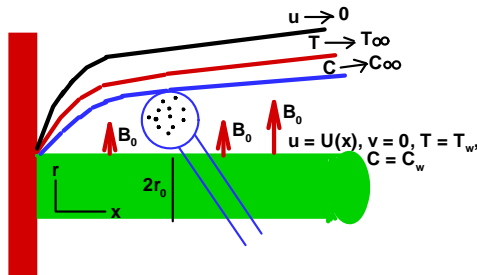


Fig. 4.1: Geometry of the problem.

$$\frac{\partial (ru)}{\partial x} + \frac{\partial (rv)}{\partial r} = 0, \quad (4.1)$$

$$u \frac{\partial u}{\partial x} + v \frac{\partial u}{\partial r} = \frac{a}{r\rho} \frac{\partial}{\partial r} \left(r \frac{\partial u}{\partial r} \right) - \frac{b}{r\rho} \left(-\frac{\partial u}{\partial r} \right)^n + \frac{nb}{\rho} \left(-\frac{\partial u}{\partial r} \right)^{n-1} \frac{\partial^2 u}{\partial r^2} - \frac{\sigma B_0^2}{\rho} u, \quad (4.2)$$

$$u \frac{\partial T}{\partial x} + v \frac{\partial T}{\partial r} = \frac{\alpha}{r} \frac{\partial}{\partial r} \left(r \frac{\partial T}{\partial r} \right) + \frac{\sigma B_0^2}{\rho c_p} u^2 + \frac{a}{\rho c_p} \left(-\frac{\partial u}{\partial r} \right)^2 + \frac{b}{\rho c_p} \left(-\frac{\partial u}{\partial r} \right)^{n+1} + \tau D_B \left(\frac{\partial C}{\partial r} \cdot \frac{\partial T}{\partial r} \right) + \frac{\tau D_T}{T_\infty} \left(\frac{\partial T}{\partial r} \right)^2, \quad (4.3)$$

$$u \frac{\partial C}{\partial x} + v \frac{\partial C}{\partial r} = \frac{D_B}{r} \frac{\partial}{\partial r} \left(r \frac{\partial C}{\partial r} \right) + \frac{D_T}{r T_\infty} \frac{\partial}{\partial r} \left(r \frac{\partial T}{\partial r} \right), \quad (4.4)$$

along with the boundary conditions

$$\begin{aligned} u &= U(x), \quad v = 0 \text{ at } r = r_0 \text{ and } u \rightarrow 0 \text{ as } r \rightarrow \infty, \\ T &= T_w \text{ at } r = r_0 \text{ and } T \rightarrow T_\infty \text{ as } r \rightarrow \infty, \\ C &= C_w \text{ at } r = r_0 \text{ and } C \rightarrow C_\infty \text{ as } r \rightarrow \infty. \end{aligned} \quad (4.5)$$

In *Eqs. (4.1)–(4.5)*, u and v denote the axial and radial velocity components respectively, a , b and n are Sisko fluid constants, σ denotes electrical conductivity, T denotes the temperature, C is nanoparticles concentration, c_p represents specific heat, D_B is Brownian motion diffusion coefficient, D_T is diffusion coefficient of thermophoresis and τ is the ratio of nanoparticle heat capacity to base fluid heat capacity. The temperature and volumetric fraction of nanoparticles at the surface of cylinder are denoted by T_w and C_w respectively while temperature and concentration away from the cylinder are symbolized by T_∞ and C_∞ .

The stream function of velocity is defined as

$$u = \frac{1}{r} \frac{\partial \Psi}{\partial r}, \quad v = -\frac{1}{r} \frac{\partial \Psi}{\partial x}. \quad (4.6)$$

To find similar solution of the governing equations i.e. *Eqs. (4.1) – (4.4)*, the following set of similarity variables is defined

$$\begin{aligned}\eta &= \frac{r^2 - r_0^2}{2xr_0} \text{Re}_b^{\frac{1}{n+1}}, \quad \Psi = xr_0U \text{Re}_b^{\frac{-1}{n+1}} f(\eta), \\ \theta(\eta) &= \frac{T - T_\infty}{T_w - T_\infty}, \quad \phi(\eta) = \frac{C - C_\infty}{C_w - C_\infty},\end{aligned}\tag{4.7}$$

where η denotes dimensionless length, f is dimensionless velocity, θ denotes dimensionless temperature, ϕ denotes the concentration of nanoparticles and Re_b denotes the Reynold number which is defined as $\text{Re}_b = \frac{\rho x^n U^{2-n}}{b}$.

After imposing the similarity transformations in *Eqs.* (4.1) – (4.4), the continuity equation vanishes while momentum, energy and nanoparticles concentration equations are modified to the following form

$$\begin{aligned}A(1 + 2\gamma\eta)f''' + n(1 + 2\gamma\eta)^{\frac{n+1}{2}}(-f'')^{n-1}f''' - (n+1)\gamma(1 + 2\gamma\eta)^{\frac{n-1}{2}}(-f'')^n \\ + 2A\gamma f'' - f'^2 + \frac{2n}{n+1}ff'' - Mf' = 0,\end{aligned}\tag{4.8}$$

$$\begin{aligned}(1 + 2\gamma\eta)\theta'' + 2\gamma\theta' + \frac{2n}{n+1}\text{Pr}f\theta' + M\text{EcPr}f'^2 + A(1 + 2\gamma\eta)\text{EcPr}(-f'')^2 \\ + \text{EcPr}(1 + 2\gamma\eta)^{\frac{n+1}{2}}(-f'')^{n+1} + (1 + 2\gamma\eta)(Nt\theta'^2 + Nb\theta'\phi') = 0,\end{aligned}\tag{4.9}$$

$$(1 + 2\gamma\eta)\phi'' + 2\gamma\phi' + \frac{2n}{n+1}Le\text{Pr}f\phi' + \frac{Nt}{Nb}(2\gamma\theta' + (1 + 2\gamma\eta)\theta'') = 0,\tag{4.10}$$

the boundary conditions in dimensionless form are

$$\begin{aligned}f(0) &= 0, \quad f'(0) = 1, \quad \theta(0) = 1, \quad \phi(0) = 1, \\ f'(\infty) &= 0, \quad \theta(\infty) = 0, \quad \phi(\infty) = 0.\end{aligned}\tag{4.11}$$

In the above system of simultaneous equations, γ represents the curvature parameter, A denotes the material parameter, M denotes magnetic field parameter, Pr is Prandtl number,

Ec , Nb and Nt represent Eckert number, Brownian motion parameter and thermophoresis parameter respectively while Le denotes Lewis number. They are defined below

$$\begin{aligned}\gamma &= \frac{x}{r_0} \text{Re}_b^{\frac{-1}{n+1}}, \quad M = \frac{\sigma x B_0^2}{\rho U}, \quad \text{Re}_a = \frac{\rho x U}{a}, \\ A &= \frac{\text{Re}_b^{\frac{2}{n+1}}}{\text{Re}_a}, \quad Ec = \frac{U^2}{c_p(T_w - T_\infty)}, \quad \text{Pr} = \frac{x U}{\alpha} \text{Re}_b^{\frac{-2}{1+n}}, \\ Nb &= \frac{\tau D_B(C_w - C_\infty)}{\nu}, \quad Nt = \frac{\tau D_T(T_w - T_\infty)}{T_\infty \nu}, \quad Le = \frac{\alpha}{D_B}.\end{aligned}\quad (4.12)$$

The physical quantities in the surface vicinity i.e. local wall friction coefficient C_{fx} , local wall heat flux coefficient Nu_x and local wall mass flux coefficient Sh_x are defined as

$$C_{fx} = \frac{\tau_w}{\frac{1}{2}\rho U^2}, \quad Nu_x = \frac{x q_w}{\kappa(T_w - T_\infty)} \quad \text{and} \quad Sh_x = \frac{x q_m}{D_B(C_w - C_\infty)}, \quad (4.13)$$

where τ_w is the stress at the surface, q_w and q_m are wall heat flux and mass flux. Mathematically, these quantities are given below

$$\tau_w = a\left(\frac{\partial u}{\partial r}\right)_{r=r_0} - b\left(-\frac{\partial u}{\partial r}\right)_{r=r_0}^n, \quad q_w = -\kappa\left(\frac{\partial T}{\partial r}\right)_{r=r_0} \quad \text{and} \quad q_m = -D_B\left(\frac{\partial C}{\partial r}\right)_{r=r_0}. \quad (4.14)$$

Using similarity transformations into *Eq.* (4.13)–(4.14), C_{fx} , Nu_x and Sh_x are transformed into following dimensionless form

$$\frac{1}{2}C_{fx} \text{Re}_b^{\frac{1}{n+1}} = Af''(0) - [-f''(0)]^n, \quad Nu_x \text{Re}_b^{\frac{-1}{n+1}} = -\theta'(0) \quad \text{and} \quad Sh_x \text{Re}_b^{\frac{-1}{n+1}} = -\phi'(0). \quad (4.15)$$

4.2 Numerical solution

The flow govern equations i.e. *Eqs.* (4.8) – (4.10) are nonlinear. So for computation of solution, shooting technique with Runge-Kutta fifth order integration scheme is employed and solution is investigated against variations in flow controlling parameters. As Runge-Kutta techniques only solve initial value problems, thus governing equations i.e. *Eqs.* (4.8) – (4.10) are reduced to first order. These equations are reorganized into following form

$$f''' = \frac{(n+1)\gamma(1+2\gamma\eta)^{\frac{n-1}{2}}(-f'')^n - 2A\gamma f'' + f'^2 - \frac{2n}{n+1}f f'' + Mf'}{A(1+2\gamma\eta) + n(1+2\gamma\eta)^{\frac{n+1}{2}}(-f'')^{n-1}}, \quad (4.16)$$

$$\theta'' = -\frac{1}{(1+2\gamma\eta)^{\frac{n+1}{2}}} \left[\frac{2n}{n+1} \text{Pr} f\theta' + 2\gamma\theta' + Ec \text{Pr} \{Mf'^2 + A(1+2\gamma\eta)(-f'')^2 + (1+2\gamma\eta)^{\frac{n+1}{2}}(-f'')^{n+1}\} + (1+2\gamma\eta)(Nt\theta'^2 + Nb\theta'\phi') \right], \quad (4.17)$$

$$\phi'' = -\frac{2\gamma\phi' + \frac{2n}{n+1}Le \text{Pr} f\phi' + \frac{Nt}{Nb}(2\gamma\theta' + (1+2\gamma\eta)\theta'')}{(1+2\gamma\eta)}. \quad (4.18)$$

Now above defined equations are transformed into first order differential system with the aid of below-defined variables

$$\begin{aligned} f &= y_1, f' = y_2, f'' = y_3, f''' = y_3', \theta = y_4, \theta' = y_5, \theta'' = y_5', \\ \phi &= y_6, \phi' = y_7 \text{ and } \phi'' = y_7'. \end{aligned} \quad (4.19)$$

After inserting *Eq.* (4.19) into *Eqs.* (4.16) – (4.18), they are transfigured into following differential system

$$y_1' = y_2, \quad (4.20)$$

$$y_2' = y_3, \quad (4.21)$$

$$y_3' = \frac{(n+1)\gamma(1+2\gamma\eta)^{\frac{n-1}{2}}(-y_3)^n - 2A\gamma y_3 + y_2^2 - \frac{2n}{n+1}y_1y_3 + My_2}{A(1+2\gamma\eta) + n(1+2\gamma\eta)^{\frac{n+1}{2}}(-y_3)^{n-1}}, \quad (4.22)$$

$$y_4' = y_5, \quad (4.23)$$

$$y_5' = -\frac{1}{(1+2\gamma\eta)} \left[\frac{2n}{n+1} \text{Pr } y_1y_5 + 2\gamma y_5 + Ec \text{Pr} \{My_2^2 + A(1+2\gamma\eta)(-y_3)^2 + (1+2\gamma\eta)^{\frac{n+1}{2}}(-y_3)^{n+1}\} + (1+2\gamma\eta)(Nty_5^2 + Nby_5y_7) \right], \quad (4.24)$$

$$y_6' = y_7, \quad (4.25)$$

$$y_7' = -\frac{\frac{2n}{n+1} \text{Pr } Ley_1y_7 + 2\gamma y_7 + \frac{Nt}{Nb}(2\gamma y_5 + (1+2\gamma\eta)y_5')}{(1+2\gamma\eta)}. \quad (4.26)$$

The subjected boundary conditions are reduce to

$$y_1(0) = 0, \quad y_2(0) = 1, \quad y_2(\infty) = 0, \quad y_4(0) = 1, \quad y_4(\infty) = 0, \quad (4.27)$$

$$y_6(0) = 1 \text{ and } y_6(\infty) = 0.$$

To solve above set of differential equations along with corresponding boundary conditions shooting method is implemented which consists the following steps:

1. Choose appropriate value for the limit η_∞ .
2. Select initial approximations for $y_3(0)$, $y_5(0)$ and $y_7(0)$.
3. Solved *Eqs.* (4.20) – (4.26) with the aid of Runge-Kutta method.
4. Solution convergence criteria is that absolute difference between given and calculated values of $y_2(\infty)$, $y_4(\infty)$, $y_6(\infty)$ are less than error tolerance i.e. 10^{-6} .
5. If these differences are greater than tolerance error, then guessed values of $y_3(0)$, $y_5(0)$ and $y_7(0)$ are refined by Newton method.

Process is repeated until the computed solution satisfies convergence criteria.

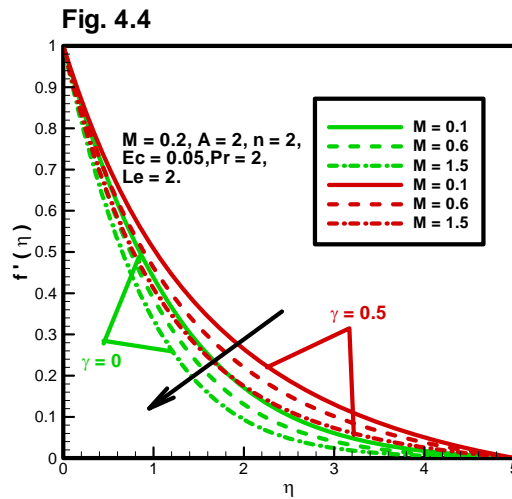
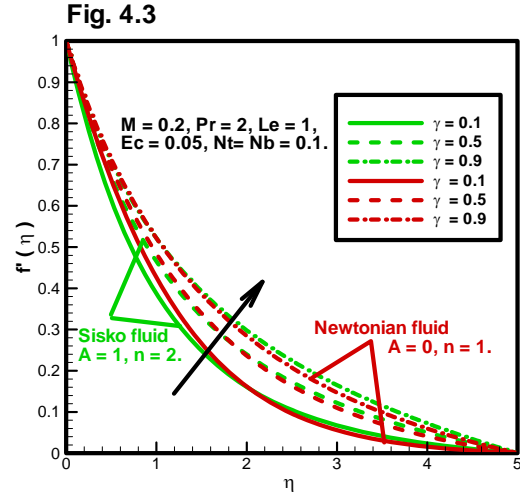
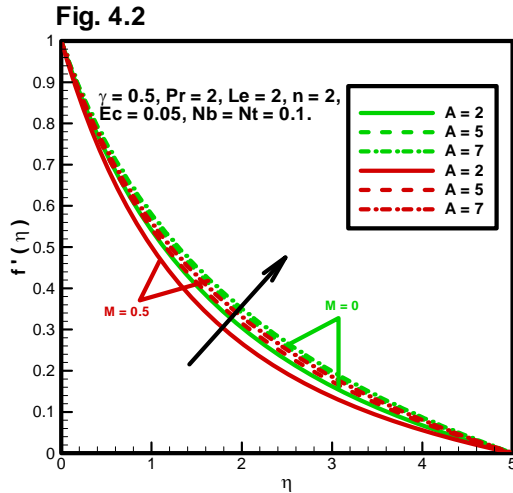
4.3 Results and discussion

To figure out physical problem more clearly, the numerical technique is implemented to solve governing differential equations, because it provides freedom to choose feasible values of governing parameters. In **Table 4.1**, a comparison of $-\theta'(0)$ values is established with previously reported data by varying Pr and putt resting parameters to zero. This table shows that computed results agree with previous data (see Khan and Pop [94], Wang [101] and Gorla and Sidawi [102]).

Table 4.1: Comparison table of $-\theta'(0)$ by altering Prandtl number Pr, when $M = \gamma = Ec = Nt = 0$, $Nb \rightarrow 0$ and $n = 1$.

Pr	Khan and Pop [94]	Wang [101]	Gorla and Sidawi [102]	Present Results
0.07	0.0663	0.0656	0.0656	0.0656
0.2	0.1691	0.1691	0.1691	0.1695
0.7	0.4539	0.4539	0.549	0.4539
2	0.9113	0.9114	0.9114	0.9114
7	1.8954	1.1854	1.1905	1.8954
20	3.3539	3.3539	3.3539	3.3538
70	6.4622	6.4622	6.4622	6.4621

1. Velocity profile

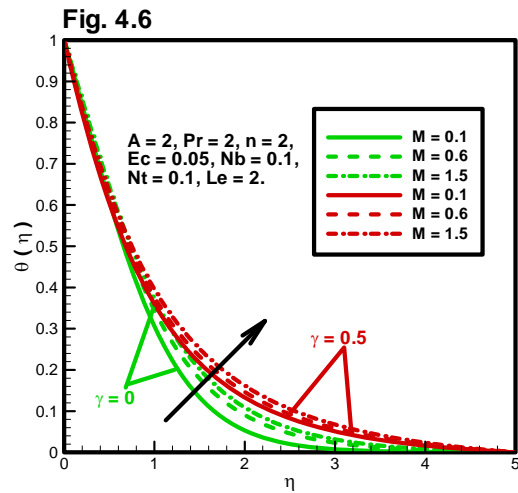
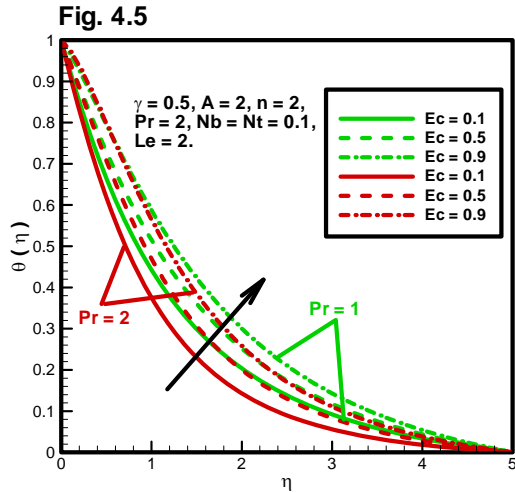


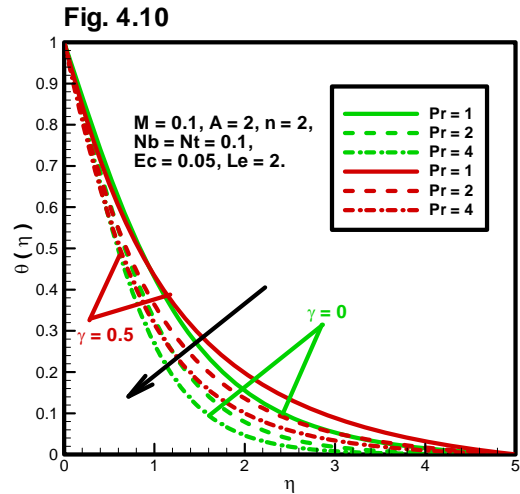
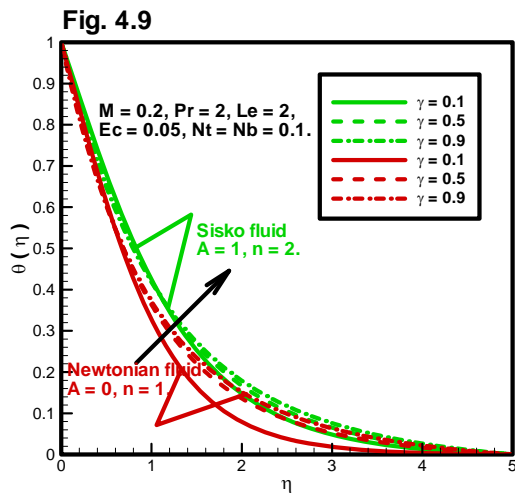
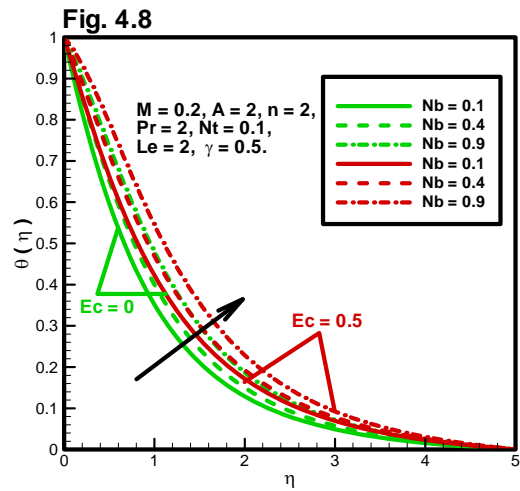
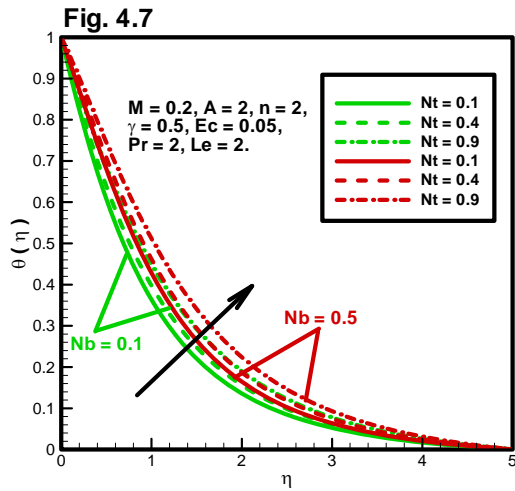
Figs. 4.2-4.4: Velocity profile variations against fluid momentum governing parameters A , γ , M and n .

Fig. 4.2 exhibits the behavior of fluid momentum versus Sisko parameter A on MHD Sisko fluid ($M = 0.5$) and Sisko fluid ($M = 0$). It is observed that Sisko fluid moves much faster than magnetohydrodynamic Sisko fluid. It could be noticed that material parameter A enhances fluid velocity but higher values of A have not create considerable disturbance in the fluid

movement i.e. change in velocity profile is small. A comparison of Sisko fluid velocity against the Newtonian fluid velocity is presented by fluctuating curvature parameter γ in **Fig. 4.3**. This figure shows that Sisko fluid have more acceleration than Newtonian fluid. Also, curvature parameter provides a substantial growth in the velocity for both Sisko and Newtonian fluids. In the vicinity of cylindrical surface curvature parameter has reverse effects on flow velocity. **Fig. 4.4** deliberates the variations in fluid movement for magnetic field parameter M and curvature parameter $\gamma = 0$ (stretching plate case) and $\gamma = 0.5$ (stretching cylinder case). From the figure, it can be analyzed that the motion of Sisko fluid on cylindrical surface is more rapid than plate surface. Additionally, this graph prevailed that magnetic field produces an appreciable resistance to fluid on both surfaces and hence reduces the fluid velocity.

2. Temperature profile



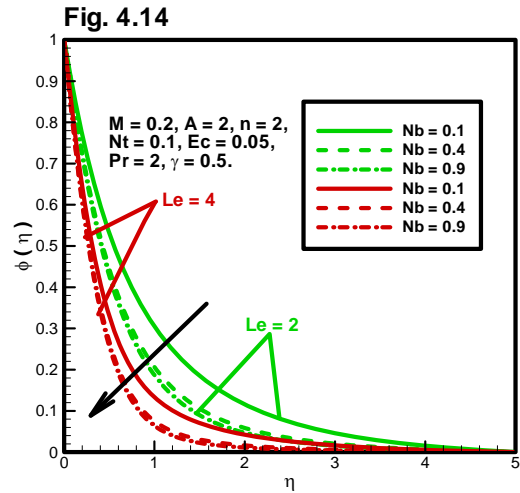
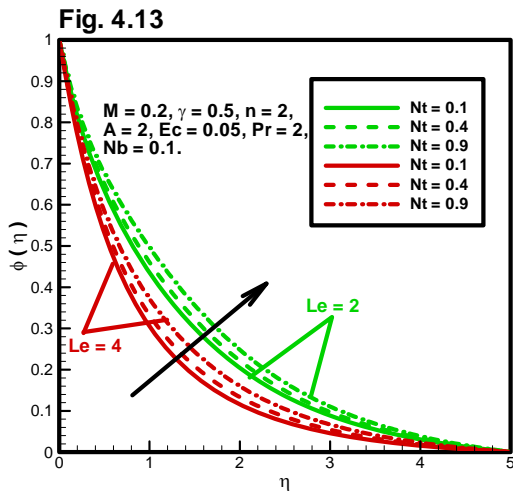
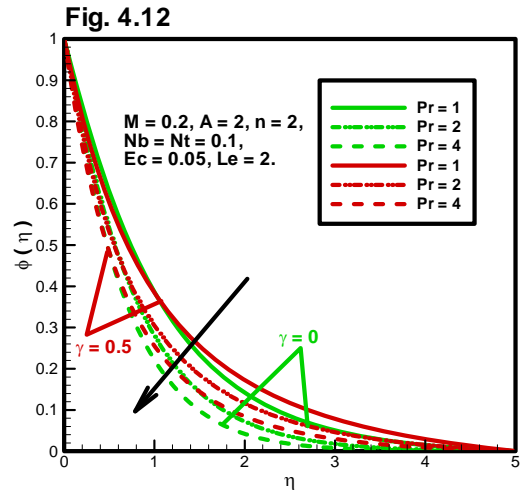
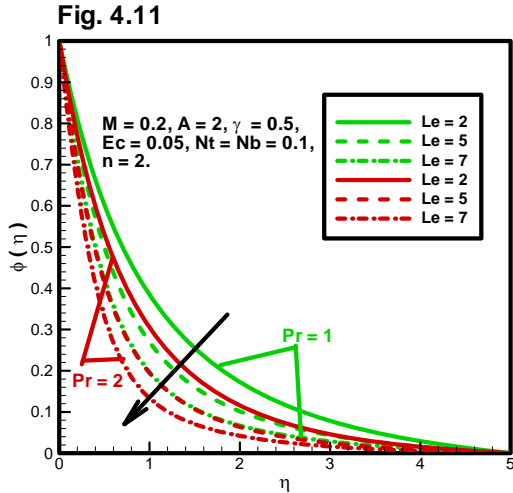


Figs. 4.5-4.10: Fluid temperature behavior against the heat flow responsible parameters $Ec, M, Pr, \gamma, Nb, Nt$ and n .

The temperature profile of non-Newtonian Sisko fluid is plotted in **Fig. 4.5** by altering Eckert number Ec and fixing Prandtl number $Pr = 1$ and 2 . This graph suggests that temperature declines versus Prandtl number. On the other hand, Eckert number Ec rises temperature more rapidly, because higher values of Eckert number correspond to accelerate the fluid particles which collide more frequently with each other and release heat which alternatively rises temperature. Impacts of Hartmann number M on temperature profile $\theta(\eta)$ are depicted via **Fig. 4.6** for curvature parameter $\gamma = 0$ (stretching plate case) and $\gamma = 0.5$ (stretching cylinder case).

This figure shows that the cylindrical surface is more hotter. Also, magnetic field parameter M increases the temperature, because applied magnetic field heats both surface and fluid particles. **Fig. 4.7** delineates the alteration in temperature versus thermophoresis parameter Nt for Brownian motion parameter ($Nb = 0.1, 0.5$). This figure shows that temperature is lower for $Nb = 0.1$ as compared to $Nb = 0.5$. Additionally, it is analyzed that thermophoresis parameter Nt rises the fluid temperature. Because thermophoresis phenomenon accelerates fluid and nanoparticles from hot region to cold region which alternatively escalates the temperature. **Fig. 4.8** shows temperature profile by altering Brownian motion parameter Nb and ($Ec = 0, 0.5$). This graph exhibits that effects of Eckert number Ec are noteworthy on temperature profile i.e. when effects of Eckert number are assumed, noticeable change in temperature is observed. Also, as Brownian motion tells the random movement of nanoparticles in the fluid, thus increasing Brownian motion parameter corresponds to collide particles more frequently. This collision of particles change kinetic energy into thermal energy. Hence it enhances the temperature. Curvature parameter γ impacts on temperature $\theta(\eta)$ are shown in **Fig. 4.9** for Newtonian and non-Newtonian fluids respectively. Curvature parameter enhances temperature profile versus both Newtonian and Sisko fluids (see **Fig. 4.9**). Also, current graph shows that Sisko fluid is much hotter than Newtonian fluid. The fluctuations is observed in Sisko nanofluid temperature against Prandtl number Pr as shown in **Fig. 4.10** by considering $\gamma = 0$ (stretching plate case) and $\gamma = 0.5$ (stretching cylinder case). One can see that the fluid temperature on cylindrical surface is more as compared to plate surface. In both cases fluid temperature falls down rapidly versus Prandtl number Pr . This holds physically because Prandtl number Pr inversely varies versus thermal conductivity i.e. capability of heat transfer.

3. Concentration profile

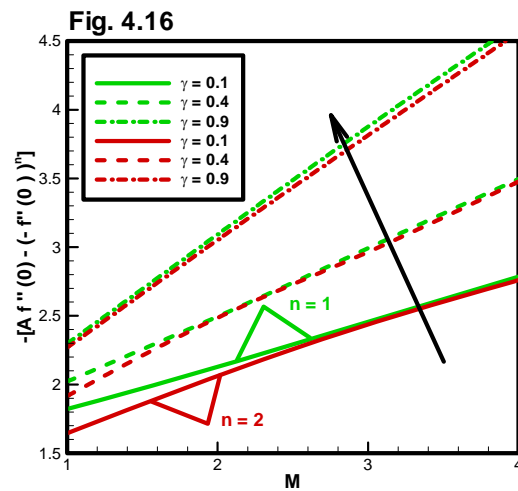
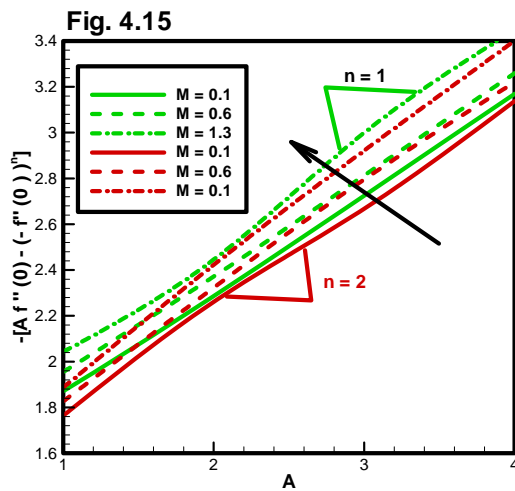


Figs. 4.11-4.14: Variations in concentration of nanoparticles on altering values of involved thermophysical parameters Nb, Nt, Le, Pr and n .

Fig. 4.11 portrays the impact of Lewis number Le on nanoparticles concentration profile $\phi(\eta)$ by assuming Prandtl number ($Pr = 1, 2$). The concentration of nanoparticles become low when Prandtl number increases. This graph illustrates that Lewis number Le declines the volumetric fraction of nanoparticles massively. It provides evidence to the fact that the Lewis

number varies inversely as mass diffusivity, hence Lewis number reduces mass diffusivity and concentration of nanoparticles. **Fig. 4.12** examines concentration profile $\phi(\eta)$ versus Prandtl number Pr while keeping $\gamma = 0$ (stretching plate case) and $\gamma = 0.5$ (stretching cylinder case). This figures exhibits that concentration of nanoparticles is higher in the case $\gamma = 0.5$ (stretching cylinder) as compared to $\gamma = 0$ (stretching plate case). Also, this figure deliberates that concentration profile $\phi(\eta)$ decreases considerably against Prandtl number Pr in both cases. **Fig. 4.13** reflects behavior of thermophoresis parameter Nt and Lewis number ($Le = 2, 4$) on concentration profile $\phi(\eta)$. It is observed from the concentration curves that nanoparticles concentration is very high in the case of Lewis number $Le = 2$. Additionally, this graph provides a valuable information that the thermophoresis parameter Nt increases concentration profile $\phi(\eta)$ in both cases. **Fig. 4.14** elaborates the impact of Brownian motion parameter Nb on the concentration profile $\phi(\eta)$ for Lewis number ($Le = 2, 4$). It can be deduces from the figure that Brownian motion parameter Nb decreases concentration profile $\phi(\eta)$ remarkably in quantitative sense. This result holds practically because Brownian motion enhances the random movement of nanoparticles i.e. they disperse nanoparticles in irregular way and hence concentration declines.

4. Wall friction factor (skin friction coefficient)



Figs. 4.15-4.16: Wall fraction factor versus physical parameters A , M , γ and n .

Fig. 4.15 deliberates magnetic field parameter M and Sisko parameter A effects on wall friction factor for power law index $n = 1, 2$. This graph exhibits that wall friction factor enlarges against larger values of both parameters while its values are declined verses power law index n . **Fig. 4.16** shows variations in wall friction factor against physical parameters A, γ and $n = 1, 2$. Current figure shows that curvature parameter escalates the factor of wall friction substantially in magnitude sense. Also, similar results can be observed for larger values of material parameter while wall friction factor slightly decreases against power law index.

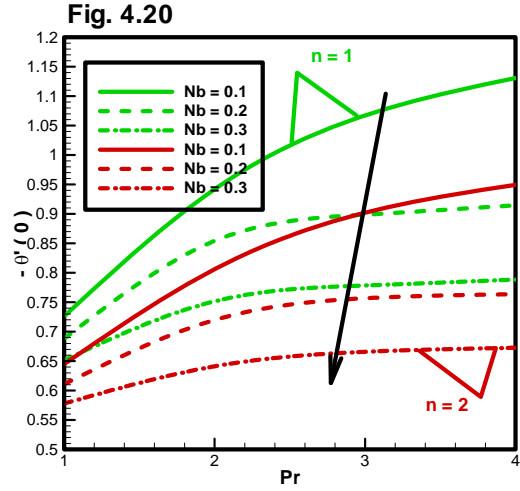
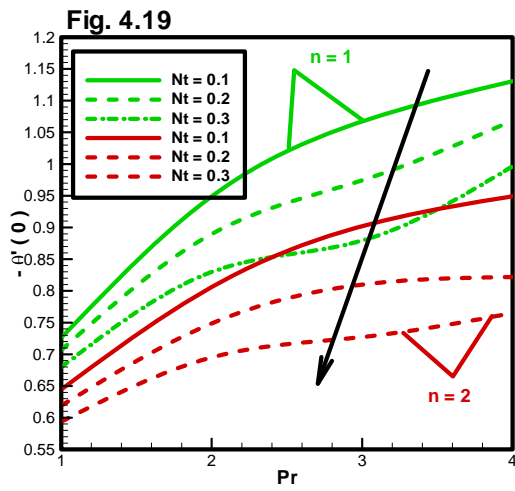
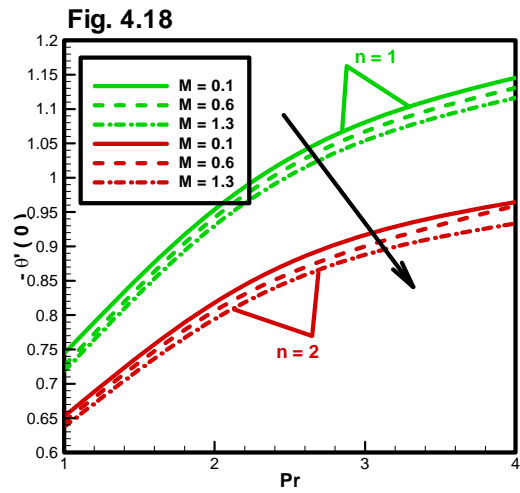
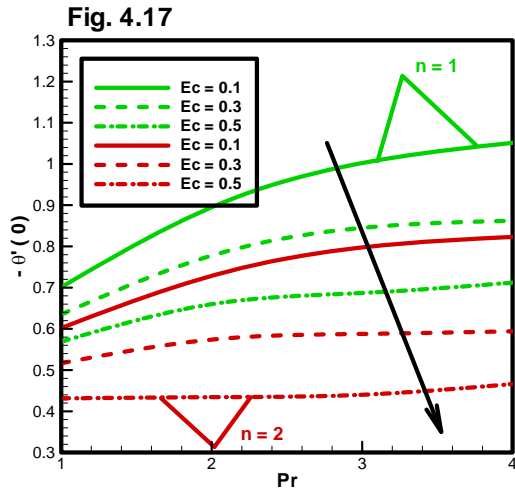
Table 4.2: Governing parameters γ, M and A effects on wall friction factor by keeping $n = 1$ and 2 .

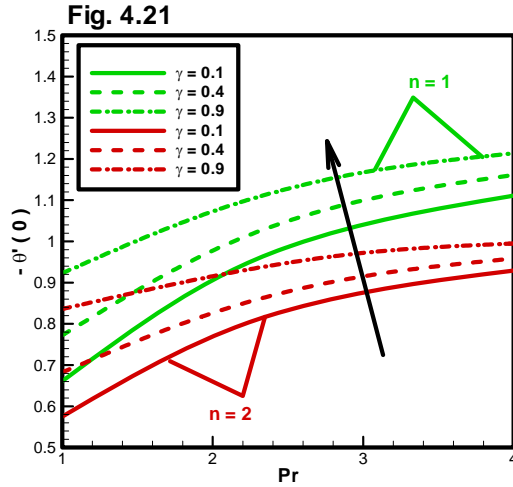
			$n = 1$	$n = 2$
γ	A	M	$(A + 1)f''(0)$	$Af''(0) - f''^2(0)$
0.1	1	0.2	-1.8221	-1.6455
0.4			-2.0223	-1.9163
0.7			-2.2284	-2.1818
1			-2.4496	-2.4318
0.3	1		-1.9549	-1.8265
	2		-2.3716	-2.3528
	3		-2.8531	-2.8454
	4		-3.3594	-3.3201
	1	0.1	-1.8704	-1.7640
		0.2	-1.9549	-1.8265
		0.3		-2.0374
		0.4		-2.1182

Table 4.2 shows wall friction coefficient against governing parameters A, M and γ on wall friction factor for $n = 1, 2$. This table shows that wall friction coefficient has larger values for $n = 1$. In addition, this table gives the information that larger values of all three parameter A, M and γ enhance the skin friction coefficient in absolute sense. But effects of material parameter are prominent on wall friction factor as compared to others effects i.e. skin friction

coefficient grows more rapidly against material parameter.

5. Wall heat flux (local Nusselt number)





Figs. 4.17-4.21: Influence of pertinent parameters on wall heat flux Ec , M , Pr , γ , Nb , Nt and n .

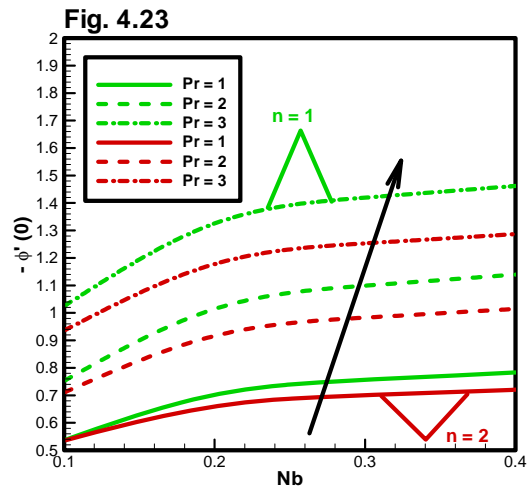
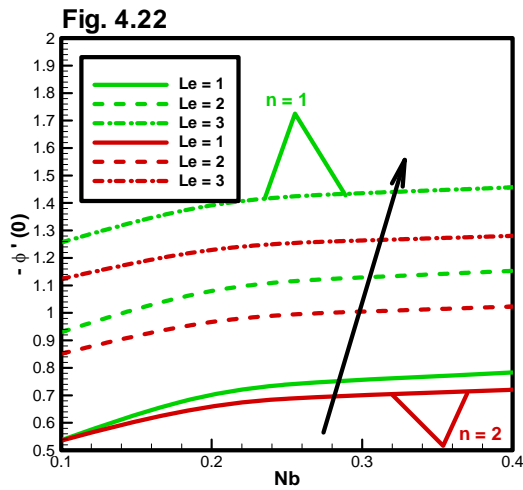
Figs. 4.17-4.21 depict the variations of wall heat flux by varying parameters Ec , M , Pr , γ , Nb , Nt and n . **Fig. 4.17** explains the behavior of wall heat flux coefficient versus Ec , Pr and n . This graph reveals that both Prandtl and Eckert numbers have reverse effects on local Nusselt number. Also, Eckert number affects Nusselt number more significantly rather than Prandtl number. The reason behind that Eckert number decreases enthalpy i.e. $T_w - T_\infty$, so it reduces heat transfer rate and hence Nusselt number. The behavior of $-\theta'(0)$ against magnetic field parameter M and Prandtl number Pr is illustrated in **Fig. 4.18** for power law index ($n = 1, 2$). This graph shows that Pr enlarges Nusselt number while magnetic field parameter M declines it. Also, one can see that the impact of magnetic parameter is not significant on heat transfer coefficient. **Fig. 4.19** displays the deviations in local Nusselt number for altering values of physical parameters n , Nt and Pr . Thermophoresis parameter inclines wall heat flux substantially which can be observed from the figure. Also, it can be deduced that wall heat flux diminishes for larger values of thermophoresis parameter. **Fig. 4.20** illustrates the behavior of thermophysical parameters Nb and Pr on $-\theta'(0)$ by selecting $n = 1, 2$. Brownian motion parameter Nb reduces the wall heat flux considerably. The combined impacts of Pr and γ on heat flux at surface are shown in **Fig. 4.21** by choosing power law index ($n = 1, 2$). This graph shows that local Nusselt number declines against power law index.

Table 4.3: Local surface heat flux by varying γ , Ec , M , Nt , Nb and Pr for $n = 1, 2$.

						$n = 1$	$n = 2$
γ	Ec	Pr	M	Nb	Nt	$-\theta'(0)$	$-\theta'(0)$
0.1	0.05	1	0.2	0.1	0.1	0.6520	0.5749
0.4						0.7646	0.6824
0.7						0.8792	0.7976
1						0.9900	0.9126
0.3	0.1					0.6898	0.6022
	0.3					0.5446	0.4313
	0.5					0.3992	0.2602
	0.7					0.2537	0.0891
	0.05	1				0.7262	0.6449
		2				0.9420	0.8061
		3				1.0672	0.9021
		4				1.1306	0.9492
		1	0.1			0.7443	0.6526
			0.2			0.7262	0.6449
			0.3			0.7183	0.6375
			0.4			0.7108	0.6303
			0.2	0.1		0.7262	0.6449
				0.3		0.6517	0.5780
				0.5		0.5827	0.5160
				0.7		0.5190	0.4588
				0.1	0.4	0.6461	0.5695
					0.5	0.6210	0.5458
					0.6	0.5966	0.5229
					0.7	0.5729	0.5001

Table 4.3 depicts the variations in Nusselt number by varying involved physical parameters γ , Ec , Pr , M , Nb , Nt and n . It is observed that physical parameters γ and Pr enlarge the Nusselt number while resting parameter i.e. Ec , M , Nb , n and Nt causes reduction in local Nusselt number. This table also discloses that the effects of Ec , Nb and Nt are prominent on coefficient of wall heat flux.

6. Wall mass flux (Local Sherwood number)



Figs. 4.22-4.23: Wall mass flux verses involving physical parameters Nb , Le , Pr and n .

The variations of physical parameters Nb , Pr , Le and n on $-\phi'(0)$ are illustrated in the **Figs. 4.22-4.23**. **Fig. 4.22** manifests the combined consequences of n , Nb and Le on local Sherwood number Sh_x . Both parameters Nb and Le accelerate the mass transfer but their effects on wall mass flux are not prominent which can be noticed from the figure. Also, power law index decrease local Sherwood number. The influences of Nb and Pr on wall mass flux i.e. $-\phi'(0)$ are shown by **Fig. 4.23** for power law index ($n = 1, 2$). This figure predicts that Prandtl number Pr enhances local Sherwood number.

Table 4.4: Local Sherwood number ($-\phi'(0)$) versus physical parameters Le , Nb , Nt and Pr for $n = 1, 2$.

				$n = 1$	$n = 2$
Pr	Le	Nb	Nt	$-\phi'(0)$	$-\phi'(0)$
1	1	0.1	0.1	0.5369	0.5353
2				0.7529	0.7105
3				1.0248	0.9362
4				1.3019	1.1745
1	1			0.5369	0.5353
	2			0.9298	0.8516
	3			1.2566	1.1235
	4			1.5317	1.3568
	1	0.1		0.5369	0.5353
		0.3		0.7564	0.7004
		0.5		0.7993	0.7325
		0.7		0.8170	0.7456
		0.1	0.4	0.1251	0.1192
			0.5	0.1592	0.1391
			0.6	0.2159	0.1478
			0.7	0.2353	0.1960

Variations in local Sherwood number against thermophysical parameters n , Le , Nb , Nt and Pr are presented in **Table 4.4**. This table explicates that the surface mass transfer enhances against progressing values of all involving parameters Le , Nb , Nt and Pr .

4.4 Concluding remarks

Present chapter communicates the speculative investigation of Sisko nanofluid over axially stretching surface. Also, viscous dissipation and Joule heating effects are factored into the

analysis. The computational solution of governing differential system is attained by employing well-known numerical approach shooting method. To insight problem in the physical sense, feasible values of controlled parameters are selected. The solutions of dimensionless velocity, temperature and concentration have asymptotic behavior (see graphs). The main outcomes of the problem are:

- The computed results revealed that curvature parameter γ and material parameter A both have qualitatively similar effects on dimensionless velocity $f'(\eta)$, but in quantitative sense material parameter A is significant impact on fluid movement while fluid acceleration retarded very rapidly versus magnetic field parameter M . Also, Sisko fluid moves faster than Newtonian fluid.
- A noticeable growth has been captured in wall friction factor against all three momentum controlling parameters (i.e. material parameter A , magnetic field parameter M and curvature parameter γ).
- Both Eckert number (viscous dissipation effect) and magnetic field parameter (Joule heating) substantially enlarge the temperature, a qualitatively similar consequences were observed against Brownian motion parameter Nb , thermophoresis parameter Nt and curvature parameter γ . But in quantifying sense, Eckert number has more prominent effects than resting parameters. On the other hand heat transfer trends verses Prandtl number Pr are different i.e. progressing values of Prandtl number corresponds to low temperature.
- Coefficient of wall heat flux enhances verses both Prandtl number Pr and curvature parameter γ while magnetic field parameter M , Eckert number Ec , thermophoresis parameter Nt and Brownian motion parameter Nb have opposite impacts.
- A relatively small growing behavior of nanoparticles concentration has been noticed for thermophoresis parameter Nt while impacts of Brownian motion parameter Nb , Prandtl number Pr and Lewis number Le lead to reduce concentration.
- Wall mass flux enhances by varying all controlling parameters Nb , Nt , Pr and Le .

Chapter 5

Computational and physical aspects of MHD Prandtl-Eyring fluid flow analysis over a stretching sheet

This chapter explores the applied magnetic field effects on Prandtl-Eyring fluid flow past a stretching surface. Prandtl-Eyring fluid model is capable of describing zero shear rate viscosity. Stretching of a sheet induces the flow (Couette flow). The mathematical formulation yields nonlinear partial differential equations, these equations are transfigured into ordinary differential equation by using scaling group of transformations. The resulting differential system is solved with the aid of Keller-Box method. Axial velocity is calculated and impacts of governing parameters are visualized inclusively on it through graphs. Wall friction factor is computed and sketched against variations in influential parameters. The present solution is certified by making comparison with existing literature. This comparison shows that computed results have good agreement with reported data.

5.1 Formulation of physical problem

Flow of viscoelastic fluid over two-dimensional surface is assumed, the surface is stretching in axial direction. A perpendicular magnetic field of strength B_0 is imposed on the fluid flow (see **Fig. 5.1**). The governing equations in usual notion are given below

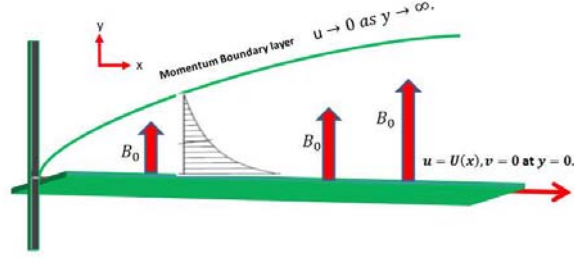


Fig. 5.1: Physical configuration of the problem.

$$\nabla \cdot \mathbf{V} = 0, \quad (5.1)$$

$$\rho \frac{D\mathbf{V}}{Dt} = \text{div } \mathbf{T} + \mathbf{J} \times \mathbf{B}, \quad (5.2)$$

where ∇ denotes differential operator, ρ is the fluid density, $\frac{D}{Dt}$ corresponds to material time derivative, $\mathbf{V} = (u, v, 0)$ is the velocity field, \mathbf{T} denotes Cauchy stress tensor and $\mathbf{B} = (0, B_0, 0)$ represents the magnetic field while $\mathbf{J} = \sigma(\mathbf{V} \times \mathbf{B})$ symbolized electric current density (in the absence of electric field). The mathematical quantities ∇ and $\frac{D}{Dt}$ are defined below

$$\nabla = \frac{\partial}{\partial x} \hat{e}_x + \frac{\partial}{\partial y} \hat{e}_y + \frac{\partial}{\partial z} \hat{e}_z, \quad (5.3)$$

$$\frac{D}{Dt} = \mathbf{V} \cdot \nabla, \quad (5.4)$$

since flow is steady so term $\frac{\partial}{\partial t}$ is neglected. Cauchy stress tensor is given as

$$\mathbf{T} = -p\mathbf{I} + \mathbf{S}, \quad (5.5)$$

where p depicts fluid pressure, the identity tensor is denoted by \mathbf{I} while \mathbf{S} is called extra stress tensor which is defined mathematically as

$$\mathbf{S} = \frac{A \operatorname{Si nh}^{-1}\left(\frac{\dot{\gamma}}{C}\right)}{\dot{\gamma}} \mathbf{A}_1, \quad (5.6)$$

where A and C are fluid parameters, $\mathbf{A}_1 = \nabla \mathbf{V} + (\nabla \mathbf{V})^t$ denotes first Rivlin-Ericksen tensor and $\dot{\gamma} = \sqrt{\frac{1}{2} \operatorname{tr}(\mathbf{A}_1^2)}$. Now expanding the inverse hyperbolic function in terms of Taylor series and neglecting higher order terms

$$\operatorname{Si nh}^{-1}\left(\frac{\dot{\gamma}}{C}\right) = \frac{\dot{\gamma}}{C} - \frac{\dot{\gamma}^3}{6C^3} + O\left(\left(\frac{\dot{\gamma}}{C}\right)^5\right). \quad (5.7)$$

By inserting Eq. (5.7) into Eq. (5.6)

$$\mathbf{S} = \left(\frac{A}{C} - \frac{A\dot{\gamma}^2}{6C^3}\right) \mathbf{A}_1. \quad (5.8)$$

Now compute first Rivlin-Ericksen tensor \mathbf{A}_1 and $\dot{\gamma}$

$$\mathbf{A}_1 = \begin{bmatrix} 2\frac{\partial u}{\partial x} & \frac{\partial v}{\partial x} + \frac{\partial u}{\partial y} & 0 \\ \frac{\partial v}{\partial x} + \frac{\partial u}{\partial y} & 2\frac{\partial v}{\partial y} & 0 \\ 0 & 0 & 0 \end{bmatrix}, \quad (5.9)$$

and

$$\dot{\gamma} = \sqrt{2\left(\frac{\partial u}{\partial x}\right)^2 + 2\left(\frac{\partial v}{\partial y}\right)^2 + \left(\frac{\partial v}{\partial x} + \frac{\partial u}{\partial y}\right)^2}. \quad (5.10)$$

Incorporating *Eqs.* (5.9) – (5.10) in *Eq.* (5.8), it takes the following form

$$\mathbf{S} = \left(\frac{A}{C} - \frac{A}{6C^3}\left(2\left(\frac{\partial u}{\partial x}\right)^2 + 2\left(\frac{\partial v}{\partial y}\right)^2 + \left(\frac{\partial v}{\partial x} + \frac{\partial u}{\partial y}\right)^2\right)\right) \begin{bmatrix} 2\frac{\partial u}{\partial x} & \frac{\partial v}{\partial x} + \frac{\partial u}{\partial y} & 0 \\ \frac{\partial v}{\partial x} + \frac{\partial u}{\partial y} & 2\frac{\partial v}{\partial y} & 0 \\ 0 & 0 & 0 \end{bmatrix}. \quad (5.11)$$

After inserting the concerned variables, continuity equation transmutes to

$$\frac{\partial u}{\partial x} + \frac{\partial v}{\partial y} = 0, \quad (5.12)$$

Now after simplification of $\mathbf{J} \times \mathbf{B}$, one can write

$$\mathbf{J} \times \mathbf{B} = \sigma(-B_0^2 u, 0, 0). \quad (5.13)$$

After incorporating \mathbf{T} , the linear momentum equation (in absence of pressure gradient) transfigured to

$$\rho \frac{D\mathbf{V}}{Dt} = \text{div } \mathbf{S} + \mathbf{J} \times \mathbf{B}, \quad (5.14)$$

Partial time derivative of flow field velocity is defined below (in components form)

$$\left(\frac{D\mathbf{V}}{Dt}\right)_x = \frac{Du}{Dt} = u \frac{\partial u}{\partial x} + v \frac{\partial u}{\partial y}, \quad (5.15)$$

$$\left(\frac{D\mathbf{V}}{Dt}\right)_y = \frac{Dv}{Dt} = u\frac{\partial v}{\partial x} + v\frac{\partial v}{\partial y}, \quad (5.16)$$

$$\left(\frac{D\mathbf{V}}{Dt}\right)_z = 0. \quad (5.17)$$

The divergence of stress tensor is defined below

$$\begin{aligned} (\operatorname{div} \mathbf{S})_x &= \frac{A}{C} \left(2\frac{\partial^2 u}{\partial x^2} + \frac{\partial^2 u}{\partial y^2} + \frac{\partial^2 v}{\partial x \partial y} \right) - \frac{A}{3C^3} \frac{\partial}{\partial x} \left\{ \left(2\left(\frac{\partial u}{\partial x}\right)^2 + 2\left(\frac{\partial v}{\partial y}\right)^2 + \left(\frac{\partial u}{\partial y} + \frac{\partial v}{\partial x}\right)^2 \right) \frac{\partial u}{\partial x} \right\} \\ &\quad - \frac{A}{6C^3} \frac{\partial}{\partial y} \left\{ \left(2\left(\frac{\partial u}{\partial x}\right)^2 + 2\left(\frac{\partial v}{\partial y}\right)^2 + \left(\frac{\partial u}{\partial y} + \frac{\partial v}{\partial x}\right)^2 \right) \left(\frac{\partial u}{\partial y} + \frac{\partial v}{\partial x} \right) \right\}, \end{aligned} \quad (5.18)$$

$$\begin{aligned} (\operatorname{div} \mathbf{S})_y &= \frac{A}{C} \left(\frac{\partial^2 v}{\partial x^2} + 2\frac{\partial^2 v}{\partial y^2} + \frac{\partial^2 u}{\partial x \partial y} \right) - \frac{A}{3C^3} \frac{\partial}{\partial y} \left\{ \left(2\left(\frac{\partial u}{\partial x}\right)^2 + 2\left(\frac{\partial v}{\partial y}\right)^2 + \left(\frac{\partial u}{\partial y} + \frac{\partial v}{\partial x}\right)^2 \right) \frac{\partial v}{\partial y} \right\} \\ &\quad - \frac{A}{6C^3} \frac{\partial}{\partial x} \left\{ \left(2\left(\frac{\partial u}{\partial x}\right)^2 + 2\left(\frac{\partial v}{\partial y}\right)^2 + \left(\frac{\partial u}{\partial y} + \frac{\partial v}{\partial x}\right)^2 \right) \left(\frac{\partial u}{\partial y} + \frac{\partial v}{\partial x} \right) \right\}, \end{aligned} \quad (5.19)$$

$$(\operatorname{div} \mathbf{S})_z = 0. \quad (5.20)$$

Inserting concerned expressions in the momentum equation becomes

$$\begin{aligned} u\frac{\partial u}{\partial x} + v\frac{\partial u}{\partial y} &= \frac{A}{\rho C} \left(2\frac{\partial^2 u}{\partial x^2} + \frac{\partial^2 u}{\partial y^2} + \frac{\partial^2 v}{\partial x \partial y} \right) - \frac{A}{3\rho C^3} \frac{\partial}{\partial x} \left\{ \left(2\left(\frac{\partial u}{\partial x}\right)^2 + 2\left(\frac{\partial v}{\partial y}\right)^2 + \left(\frac{\partial u}{\partial y} + \frac{\partial v}{\partial x}\right)^2 \right) \frac{\partial u}{\partial x} \right\} \\ &\quad - \frac{A}{6\rho C^3} \frac{\partial}{\partial y} \left\{ \left(2\left(\frac{\partial u}{\partial x}\right)^2 + 2\left(\frac{\partial v}{\partial y}\right)^2 + \left(\frac{\partial u}{\partial y} + \frac{\partial v}{\partial x}\right)^2 \right) \left(\frac{\partial u}{\partial y} + \frac{\partial v}{\partial x} \right) \right\} - \frac{\sigma B_0^2}{\rho} u, \end{aligned} \quad (5.21)$$

$$\begin{aligned} u\frac{\partial v}{\partial x} + v\frac{\partial v}{\partial y} &= \frac{A}{\rho C} \left(\frac{\partial^2 v}{\partial x^2} + \frac{\partial^2 v}{\partial y^2} \right) - \frac{A}{3\rho C^3} \frac{\partial}{\partial y} \left\{ \left(2\left(\frac{\partial u}{\partial x}\right)^2 + 2\left(\frac{\partial v}{\partial y}\right)^2 + \left(\frac{\partial u}{\partial y} + \frac{\partial v}{\partial x}\right)^2 \right) \frac{\partial v}{\partial y} \right\} \\ &\quad - \frac{A}{6\rho C^3} \frac{\partial}{\partial x} \left\{ \left(2\left(\frac{\partial u}{\partial x}\right)^2 + 2\left(\frac{\partial v}{\partial y}\right)^2 + \left(\frac{\partial u}{\partial y} + \frac{\partial v}{\partial x}\right)^2 \right) \left(\frac{\partial u}{\partial y} + \frac{\partial v}{\partial x} \right) \right\}, \end{aligned} \quad (5.22)$$

After employing boundary layer approximations in *Eqs.* (5.12), (5.21), (5.22), these equations deduced to

$$\frac{\partial u}{\partial x} + \frac{\partial v}{\partial y} = 0, \quad (5.23)$$

$$u \frac{\partial u}{\partial x} + v \frac{\partial u}{\partial y} = \frac{A}{\rho C} \frac{\partial^2 u}{\partial y^2} - \frac{A}{2\rho C^3} \left(\frac{\partial u}{\partial y} \right)^2 \frac{\partial^2 u}{\partial y^2} - \frac{\sigma B_0^2}{\rho} u, \quad (5.24)$$

along with the boundary conditions

$$u = U(x) = cx, \quad v = 0 \text{ at } y = 0 \text{ and } u \rightarrow 0 \text{ as } y \rightarrow \infty. \quad (5.25)$$

The stream function is chosen in the following form

$$u = \frac{\partial \Psi}{\partial y}, \quad v = -\frac{\partial \Psi}{\partial x}. \quad (5.26)$$

Below defined set of scaling transforms is utilized to transmute modelled partial differential system into dimensionless form

$$\eta = \sqrt{\frac{c}{\nu}} y, \quad \Psi = \sqrt{c\nu} x f(\eta), \quad (5.27)$$

Employing *Eq.* (5.27) into *Eqs.* (5.23) – (5.24), the continuity equation is satisfied while Navier-Stokes equations are transfigured to

$$\alpha f''' - \alpha \beta f''^2 f''' - f'^2 + f f'' - M f' = 0, \quad (5.28)$$

while the two-point conditions are reshaped to

$$f(0) = 0, f'(0) = 1, f'(\infty) = 0. \quad (5.29)$$

In Eq. (5.28), α and β denote the material parameters while Hartmann number is symbolized with M , these parameters are mathematically given as

$$\alpha = \frac{A}{\mu C}, \beta = \frac{c^3 x^2}{2C^2 \nu}, M = \frac{\sigma x B_0^2}{\rho U}. \quad (5.30)$$

Coefficient of skin friction is given below

$$C_{f_x} = \frac{\tau_w}{\frac{1}{2}\rho U^2}, \quad (5.31)$$

where C_{f_x} denotes the wall friction coefficient. In above relation, τ_w is the wall shear stress defined as

$$\tau_w = \frac{A}{C} \left(\frac{\partial u}{\partial y} \right)_{y=0} - \frac{A}{6C^3} \left(\frac{\partial u}{\partial y} \right)_{y=0}^3. \quad (5.32)$$

After incorporating the scaling transforms in Eqs. (5.31) – (5.32), coefficient of wall friction transformed into

$$\frac{1}{2} C_{f_x} \text{Re}_x^{\frac{1}{2}} = \alpha f''(0) - \frac{\alpha \beta}{3} [f''(0)]^3, \quad (5.33)$$

here Re_x denotes Reynolds number.

5.2 Keller-box method

Keller-box scheme is used to solve governing flow problem. This numerical scheme is unconditionally stable and its truncating error is of second order. Cebeci and Bradshaw [100] first time solve heat transfer problem by using Keller-box scheme. In the first step higher order differential system is re-designed into first order differential system. A set of new variables g and h is introduced

$$f' = g, \quad (5.34)$$

$$g' = h, \quad (5.35)$$

after inserting the new variables, *Eq.* (5.28) becomes

$$\alpha(1 - \beta h^2)h' + fh - g^2 - M^2g = 0. \quad (5.36)$$

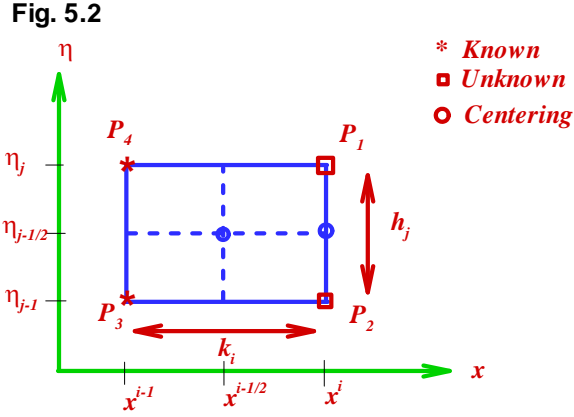


Fig. 5.2. Discretization of domain.

The $x - \eta$ plane is subdivided into meshes (see **Fig. 5.2**).

$$x^0 = 0, \quad x^i = x^{i-1} + k^i, \quad i = 1, 2, 3 \dots I, \quad (5.37)$$

$$\eta_0 = 0, \quad \eta_j = \eta_{j-1} + l_j, \quad j = 1, 2, 3 \dots J,$$

where k^i is the step-size in x -axis, on the other hand, h_j is difference between η values.

After that second order central difference scheme is utilized on involved derivatives. First, central difference scheme is utilized on *Eqs.* (5.34) – (5.35) at midpoint $(x^i, \eta_{j-1/2})$

$$\frac{f_j^i - f_{j-1}^i}{l_j} = \frac{g_j^i + g_{j-1}^i}{2}, \quad (5.38)$$

$$\frac{g_j^i - g_{j-1}^i}{l_j} = \frac{h_j^i + h_{j-1}^i}{2}. \quad (5.39)$$

But in *Eq.* (5.36), the involved derivative are approximated at mid-point $(x^{i-1/2}, \eta_{j-1/2})$, these equation takes the below-defined form

$$\alpha(h_j^i - h_{j-1}^i) - \frac{l_j}{2}\alpha\beta(h'h^2)_{j-1/2}^i + \frac{l_j}{2}f_{j-1/2}^i h_{j-1/2}^i - \frac{l_j}{2}(g_{j-1/2}^i)^2 - \frac{l_j}{2}Mg_{j-1/2}^i = L_{j-1/2}, \quad (5.40)$$

where

$$L_{j-1/2} = -\alpha(h_j^{i-1} - h_{j-1}^{i-1}) + \frac{l_j}{2}\alpha\beta(h'h^2)_{j-1/2}^{i-1} - \frac{l_j}{2}f_{j-1/2}^{i-1} h_{j-1/2}^{i-1} + \frac{l_j}{2}(g_{j-1/2}^{i-1})^2 + \frac{l_j}{2}Mg_{j-1/2}^{i-1}. \quad (5.41)$$

R.H.S of *Eq.* (5.41) i.e. $L_{j-1/2}$ comprises known quantities.

After using difference scheme, the boundary conditions are converted to

$$f_0^i = 0, \quad g_0^i = 1, \quad g_J^i = 0. \quad (5.42)$$

As above difference equations i.e. *Eqs.* (5.38) – (5.40) are highly nonlinear. The efficient numerical technique Newton's method is utilized to find solution.

$$\begin{aligned} f_j^{(k+1)} &= f_j^{(k)} + \delta f_j^{(k)}, \\ g_j^{(k+1)} &= g_j^{(k)} + \delta g_j^{(k)}, \\ h_j^{(k+1)} &= h_j^{(k)} + \delta h_j^{(k)}. \end{aligned} \quad (5.43)$$

Above defined expressions are incorporated into *Eqs.* (5.38) – (5.40), the above set of equations is converted into (after neglecting the second or higher terms in δ)

$$\delta f_j - \delta f_{j-1} - \frac{l_j}{2}(\delta g_j + \delta g_{j-1}) = (r_1)_j, \quad (5.44)$$

$$\delta g_j - \delta g_{j-1} - \frac{l_j}{2}(\delta h_j + \delta h_{j-1}) = (r_2)_j, \quad (5.45)$$

$$(a_1)_{j-1/2} \delta h_j + (a_2)_{j-1/2} \delta h_{j-1} + (a_3)_{j-1/2} \delta f_j + (a_4)_{j-1/2} \delta f_{j-1} \\ + (a_5)_{j-1/2} \delta g_j + (a_6)_{j-1/2} \delta g_{j-1} = (r_3)_j, \quad (5.46)$$

where

$$(a_1)_{j-1/2} = \alpha(1 - \frac{1}{2}\beta h_{j-1/2}^2) - \frac{l_j}{2}\alpha\beta(hh')_{j-1/2} + \frac{l_j f_{j-1/2}}{4}, \\ (a_2)_{j-1/2} = -\alpha(1 - \frac{1}{2}\beta h_{j-1/2}^2) - \frac{l_j}{2}\alpha\beta(hh')_{j-1/2} + \frac{l_j f_{j-1/2}}{4}, \\ (a_3)_{j-1/2} = \frac{l_j h_{j-1/2}}{4}, \quad (a_4)_{j-1/2} = (a_3)_{j-1/2}, \\ (a_5)_{j-1/2} = -\frac{l_j}{2}g_{j-1/2} - \frac{l_j M}{4}, \quad (a_6)_{j-1/2} = (a_5)_{j-1/2}, \quad (5.47)$$

$$(r_1)_j = -(f_j - f_{j-1}) + \frac{l_j}{2}(g_j + g_{j-1}),$$

$$(r_2)_j = -(g_j - g_{j-1}) + \frac{l_j}{2}(z_j + z_{j-1}),$$

$$(r_3)_j = -\alpha l_j h'_{j-1/2} + \frac{l_j}{2}[\alpha\beta(h'h^2)_{j-1/2} - f_{j-1/2}h_{j-1/2} + (g_{j-1/2})^2 + M g_{j-1/2}] + L_{j-1/2}, \quad (5.48)$$

while prescribed boundary conditions are altered to

$$\delta f_0 = 0, \quad \delta g_0 = 0, \quad \delta g_j = 0. \quad (5.49)$$

Since system of equations i.e. *Eqs.* (5.44) – (5.46) is linear. Firstly, these difference equations are converted into matrix form. The obtained matrix has block-tridiagonal structure given below

$$\begin{bmatrix} [A_1] & [C_1] & & & & & & & & \\ [B_2] & [A_2] & [C_2] & & & & & & & \\ & \ddots & \ddots & \ddots & & & & & & \\ & & & \ddots & \ddots & \ddots & & & & \\ & & & & [B_{j-1}] & [A_{j-1}] & [C_{j-1}] & & & \\ & & & & & [B_j] & [A_j] & [C_j] & & \end{bmatrix}
 \begin{bmatrix} [\delta_1] \\ [\delta_2] \\ \vdots \\ \vdots \\ [\delta_{j-1}] \\ [\delta_j] \end{bmatrix}
 =
 \begin{bmatrix} [r_1] \\ [r_2] \\ \vdots \\ \vdots \\ [r_{j-1}] \\ [r_j] \end{bmatrix},$$

$$[A][\delta] = [r], \quad (5.50)$$

the components of above-defined matrix system are given below

$$[A_j] = \begin{bmatrix} 0 & 1 & 0 \\ d & 0 & d \\ a_2 & a_3 & a_1 \end{bmatrix}, \quad [A_j] = \begin{bmatrix} d & 1 & 0 \\ -1 & 0 & d \\ (a_{\phi_j}) & (a_{3_j}) & (a_{1_j}) \end{bmatrix},$$

where $j = 2, 3, 4, \dots, J$.

$$[B_j] = \begin{bmatrix} 0 & -1 & 0 \\ 0 & 0 & d \\ 0 & (a_4)_j & (a_2)_j \end{bmatrix}, \quad [C_j] = \begin{bmatrix} d & 0 & 0 \\ 1 & 0 & 0 \\ (a_3)_j & 0 & 0 \end{bmatrix},$$

where $j = 2, 3, \dots, J$. where $j = 1, 2, \dots, J-1$.

$$[\delta_i] = \begin{bmatrix} \delta v_0 \\ \delta f_1 \\ \delta v_1 \end{bmatrix}, \quad [\delta_j] = \begin{bmatrix} \delta u_{j-1} \\ \delta f_j \\ \delta v_j \end{bmatrix},$$

where $j = 2, 3, \dots, J$.

$$\text{and } [r_j] = \begin{bmatrix} (r_1)_{j-1/2} \\ (r_2)_{j-1/2} \\ (r_3)_{j-1/2} \end{bmatrix} \quad \text{where } j = 1, 2, 3, \dots, J.$$

Well-known technique Thomas algorithm is employed to solve this block tridiagonal system. The solution will converge if $|\delta h_0|$ is less than error tolerance, on the other hand, if computed solution does not meet the criteria, then Newton method is utilized to refine the values of dependent variables. Computation process terminates if it meets convergence criteria.

5.3 Results and discussion

Current investigation configures the thermophysical features of stretched flow of MHD Prandtl-Eyring fluid. Keller-Bbox scheme is implemented to solve flow govern equation. The precision of applied method is validated through comparison with reported data (Akbar et al. [24] and Malik et al. [26], see **Table 5.1**). This table certifies that both solutions have good agreement.

Table 5.1: Comparative study of wall friction by varying Hartmann number M and considering fluid parameters $\alpha = 1$, $\beta = 0$.

M	Akbar et al. [24]	Malik et al. [26]	Present Results
0	-1	-1	-1
0.5	-1.11803	-1.11802	-1.1180
1.0	-1.41421	-1.41419	-1.4137
5.0	-2.44949	-2.44945	-2.4495
10	-3.31663	-3.31657	-3.3166
100	-10.04988	-10.04981	-10.0500
500	-22.38303	-22.38294	-22.3835
1000	-31.63859	-31.63851	-31.6391

Computed results are illustrated in graphical manners to understand the behaviour of physical quantities more clearly. Velocity and wall friction factor are depicted against variations in governing parameters via **Figs. 5.3-5.7**. **Table 5.2** is developed to delineate wall friction more accurately. The computed results are explained briefly and concisely.

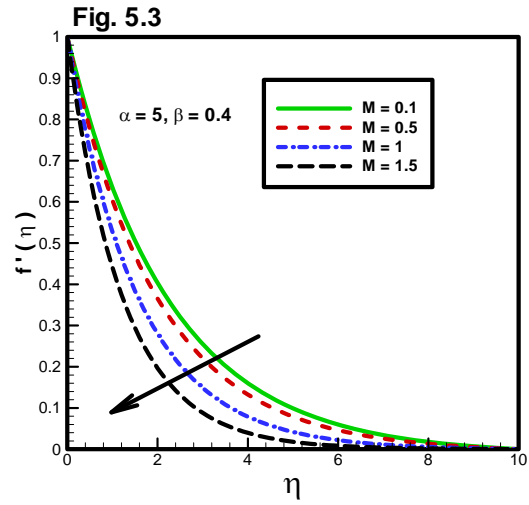


Fig. 5.3: Fluid velocity for Hartmann number M while keeping $\alpha = 5$, $\beta = 0.3$.

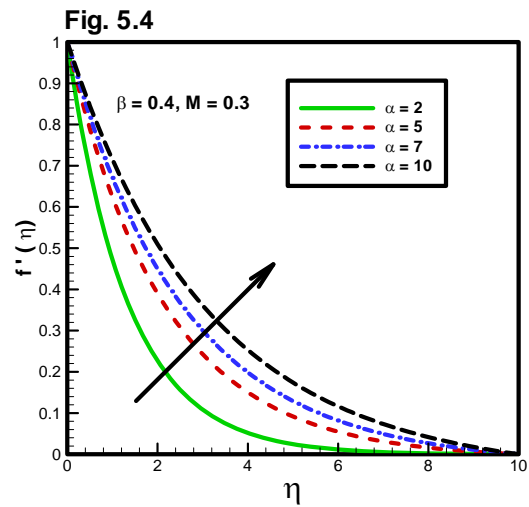


Fig. 5.4: Velocity profile versus variations in material parameter α while keeping $\beta = 0.4$ and $M = 0.3$.

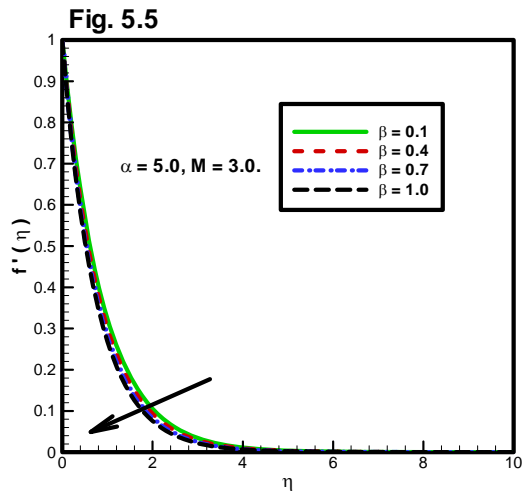


Fig. 5.5: Fluid parameter β influences on velocity profile by setting $\alpha = 5.0$ and $M = 3.0$.

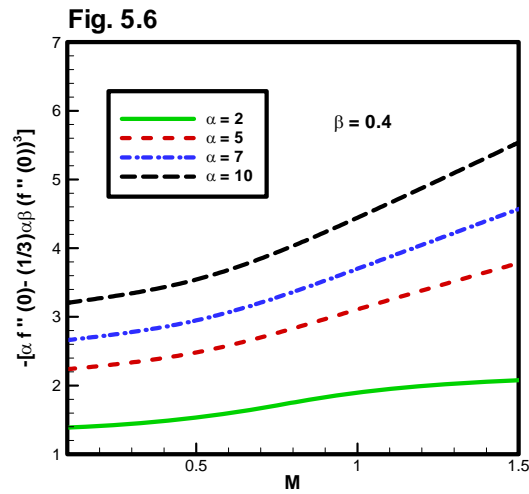


Fig. 5.6: Surface friction factor against deviations in Hartmann number M and fluid parameter α .

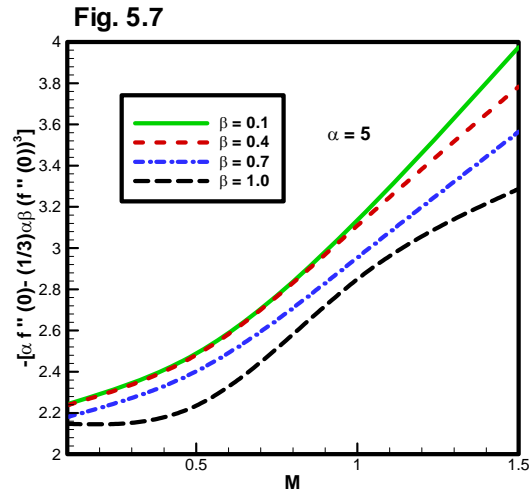


Fig. 5.7: Behaviour of surface friction factor against fluid parameter β and Hartmann number M .

Table 5.2: Coefficient of wall friction by varying fluid parameters α , β and Hartmann number M .

M	α	β	$\alpha f''(0) - \frac{\alpha\beta}{3}[f''(0)]^3$
0.1	5	0.4	-2.2375
0.5			-2.4815
1.0			-3.1092
1.5			-3.7833
0.3	2		-1.4020
	5		-2.2932
	7		-2.7350
	10		-3.2987
	5	0.1	-2.3274
		0.4	-2.2932
		0.7	-2.2574
		1.0	-2.2199

Behaviour of fluid velocity for different values of Hartmann number $M = 0.1, 0.5, 1, 1.5$ and retaining $\alpha = 5, \beta = 0.4$ is shown with the aid of **Fig. 5.3**. This figure demonstrates that the momentum transport is decelerated versus independent variable η , in addition, magnetic field strength is counterproductive to flow velocity. **Fig. 5.4** predicts impacts of fluid parameter α on velocity profile $f'(\eta)$ by keeping $M = 0.3, \beta = 0.4$. The fluid motion is accelerated against larger values of fluid parameter α because fluid parameter reduces the viscous effects. Consequently it accelerates the fluid motion. Variations in axial velocity $f'(\eta)$ versus alteration in fluid parameter β are deliberated in **Fig. 5.5**. In these computation, fixed values are assigned to other parameters i.e. $\alpha = 5, M = 3$. This figure shows that velocity curves are overlapping i.e. fluid parameter β deviates the fluid velocity very slightly. Also, this figure reports that the fluid velocity is decelerated against increment in fluid parameter β . This holds because momentum diffusivity has inverse relation with fluid parameter β .

Fig. 5.6 deliberates the attitude of wall shear stress against Hartmann number M and fluid

parameter α . One can notice that the wall friction curve for $\alpha = 2$ varies slowly versus Hartmann number M while surface friction coefficient rapidly increases against M for $\alpha = 5, 7$ and 10 . Finally, this figure spectacles skin friction enlarge against larger values of both parameters. The behaviour of concerned physical quantity against Hartmann number M and fluid parameter β is displayed via **Fig. 5.7**. This graph perceived that the fluid parameter β slightly decrease the skin friction factor while rapid escalations is observed in wall friction against Hartmann number M . Finally, this figure tells us that the surface friction reduces by increasing fluid parameter β .

The variations in local wall shear stress is exhibited in **Table 5.2** by altering parameters α , β and M . The friction of wall enhances against α and M while its opposite behaviour is captured versus fluid parameter β .

5.4 Conclusions

A speculative investigation is configured to elaborate the effects of magnetic field on stretched flow of Prandtl-Eyring fluid. The governing mathematical system is tackled with Keller-box scheme. The computed results are reported through graphs and tables by varying governing parameters α , β and M . The major outcomes inferred from current analysis are listed below:

- Fluid momentum appreciably grows versus fluid parameter α while it decays against fluid parameter β .
- Magnetic field strength produces deceleration in fluid velocity.
- Magnetic field has prominent effects on local wall shear as compared to effects of fluid parameters α and β . Additionally, both parameters α and M enlarge the wall friction while fluid parameter β reduces it.

Chapter 6

Application of generalized Fourier heat conduction law on MHD viscoinelastic fluid flow over stretching surface

Current chapter extends last chapter work by including heat transfer analysis. As heat transfer plays sensible role in the quality of industrial products. For instance controlling the heat transfer during the processes like polymer extrusion, glass fiber production and cooling/heating in heat exchangers or chambers etc. is a crucial factor regarding quality products. Also, in this chapter Christov-Cattaneo heat flux model is used. Here Oldroyd upper convective derivative is used (instead of partial time derivative) for heat flux. The current flow configuration spotlights the thermophysical aspects of MHD viscoinelastic fluid flow over stretching surface. Fluid momentum problem is mathematically formulated by using constitutive law of Prandtl-Eyring model. Also, non-Fourier heat flux law is considered to investigate the heat transfer in fluid flow. The governing problem consists nonlinear partial differential equations with prescribed boundary conditions. In order to facilitate the computation process, the governing problem is transmuted into dimensionless form via appropriate group of similarity transforms. Numerical technique (shooting method) is employed to solve dimensionless boundary value problem. Ex-

pressions for dimensionless velocity and temperature are found and investigated under different parametric conditions. The important features of fluid flow near the wall i.e. wall friction factor and wall heat flux are deliberated by altering the pertinent parameters. The impact of governing parameters is highlighted through graphical as well as tabular manner against focused physical quantities (velocity, temperature, wall friction factor and wall heat flux). A comparison with reported literature is presented to validate calculated results. This comparison shows that computed solutions agrees reported data which led to confidence the present computations.

6.1 Physical configuration of problem

Let assume boundary layer flow of MHD Prandtl-Eyring fluid past a stretching sheet. The flow is induced due to stretching of sheet in axial direction (x -axis) with stretching rate $U(x) = cx$. The magnetic field of strength B_0 is applied in perpendicular direction (y -axis). Incorporating above defined assumptions, the governing equations are transfigured into form (by restricting the problem in boundary layer region)

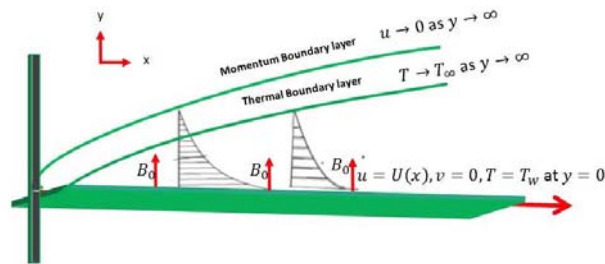


Fig. 6.1: Geometry of the problem.

$$\frac{\partial u}{\partial x} + \frac{\partial v}{\partial y} = 0, \quad (6.1)$$

$$u \frac{\partial u}{\partial x} + v \frac{\partial u}{\partial y} = \frac{A}{\rho C} \frac{\partial^2 u}{\partial y^2} - \frac{A}{2\rho C^3} \left(\frac{\partial u}{\partial y}\right)^2 \frac{\partial^2 u}{\partial y^2} - \frac{\sigma B_0^2}{\rho} u, \quad (6.2)$$

the prescribed boundary conditions are

$$u = U(x), \quad v = 0 \text{ at } y = 0 \text{ and } u \rightarrow 0 \text{ as } y \rightarrow \infty. \quad (6.3)$$

Here u, v denote axial and radial components of velocity, ρ is fluid density, σ is electrical conductivity and A, C symbolized the fluid parameters.

For heat transfer analysis, the first thermodynamic law is used. The mathematical equation of this law is defined as

$$\rho c_p (\mathbf{V} \cdot \nabla T) = -\nabla \cdot \mathbf{q}. \quad (6.4)$$

In this expression, T is temperature, c_p is specific heat and \mathbf{q} called heat flux. To find heat flux \mathbf{q} usually researchers utilized classical Fourier law, but here Christov-Cattaneo heat flux model is used. This law is defined below

$$\mathbf{q} + \lambda (\mathbf{V} \cdot \nabla \mathbf{q} - \mathbf{q} \cdot \nabla \mathbf{V} + (\nabla \cdot \mathbf{V}) \mathbf{q}) = -\kappa(T) \nabla T, \quad (6.5)$$

here, λ denotes the thermal relaxation parameter, the expression of classical Fourier law can be deduced from the above defined equation by letting $\lambda = 0$. Also, $\kappa(T)$ i.e. thermal conductivity is taken temperature dependent defined as $\kappa(T) = \kappa_\infty (1 + \epsilon \frac{T - T_\infty}{T_w - T_\infty})$ here ϵ displays variable thermal conductivity parameter while κ_∞ is ambient thermal conductivity. By

eliminating \mathbf{q} from Eq. (6.4) and Eq. (6.5) and after inserting all concerned expressions, the thermodynamics law converted into

$$u \frac{\partial T}{\partial x} + v \frac{\partial T}{\partial y} + \lambda \left(u \frac{\partial u}{\partial x} + v \frac{\partial u}{\partial y} \right) \frac{\partial T}{\partial x} + \left(u \frac{\partial v}{\partial y} + v \frac{\partial v}{\partial y} \right) \frac{\partial T}{\partial y} + 2uv \frac{\partial^2 T}{\partial x \partial y} + u^2 \frac{\partial^2 T}{\partial x^2} + v^2 \frac{\partial^2 T}{\partial y^2} = \frac{1}{\rho c_p} \frac{\partial}{\partial y} \left(\kappa(T) \frac{\partial T}{\partial y} \right), \quad (6.6)$$

along with temperature boundary conditions

$$T = T_w \text{ at } y = 0 \text{ and } T \rightarrow T_\infty \text{ as } y \rightarrow \infty. \quad (6.7)$$

Here T_w and T_∞ correspond to wall temperature and free stream temperature respectively.

The stream function for flow velocity is defined below

$$u = \frac{\partial \Psi}{\partial y}, \quad v = -\frac{\partial \Psi}{\partial x}. \quad (6.8)$$

The below-defined scaling group of similarity variables are utilized to transfer modelled partial differential system into ordinary differential system

$$\eta = \sqrt{\frac{c}{\nu}} y, \quad \Psi = \sqrt{c\nu x} f(\eta), \quad \theta = \frac{T - T_\infty}{T_w - T_\infty}. \quad (6.9)$$

After imposing the above defined similarity variables in Eqs. (6.1), (6.2), (6.6), the continuity equation satisfies identically while both momentum and thermal energy equations are transformed into following form

$$\alpha f''' - \alpha \beta f''^2 f''' - f'^2 + f f'' - M f' = 0, \quad (6.10)$$

$$(1 + \epsilon\theta)\theta'' + \epsilon\theta'^2 + \text{Pr} f\theta' - \text{Pr}\gamma(ff'\theta' + f^2\theta'') = 0, \quad (6.11)$$

subject to the prescribed two-point conditions

$$\begin{aligned} f(0) &= 0, \quad f'(0) = 1, \quad f'(\infty) \rightarrow 0, \\ \theta(0) &= 1, \quad \theta(\infty) \rightarrow 0. \end{aligned} \quad (6.12)$$

The dimensionless variables α and β called the Prandtl-Eyring fluid parameters, M is the Hartmann number, Pr denotes Prandtl number while thermal relaxation parameter is represented with γ . These are mathematically defined as

$$\alpha = \frac{A}{\mu C}, \quad \beta = \frac{c^3 x^2}{2C^2 \nu}, \quad M = \frac{\sigma x B_0^2}{\rho U}, \quad \text{Pr} = \frac{\nu}{\alpha}, \quad \gamma = \lambda c. \quad (6.13)$$

To explore the physical phenomenon near the wall i.e. surface friction factor and surface heat flux coefficients are computed. These are given below

$$C_{f_x} = \frac{\tau_w}{\frac{1}{2}\rho U^2} \quad \text{and} \quad Nu_x = \frac{xq_w}{\kappa(T)(T_w - T_\infty)}, \quad (6.14)$$

where C_{f_x} and Nu_x exhibit wall friction coefficient and local Nusselt number respectively while τ_w and q_w show surface shear stress and heat flux respectively. The last two variables are defined as

$$\tau_w = \frac{A}{C} \left(\frac{\partial u}{\partial y} \right)_{y=0} - \frac{A}{6C^3} \left(\frac{\partial u}{\partial y} \right)_{y=0}^3 \quad \text{and} \quad q_w = -\kappa(T) \left(\frac{\partial T}{\partial y} \right)_{y=0}. \quad (6.15)$$

Non-dimensional form of wall friction factor and wall heat flux is achieved by inserting similarity variables into *Eqs.* (6.14) – (6.15)

$$\frac{1}{2}C_{f_x} \text{Re}_x^{\frac{1}{2}} = \alpha f''(0) - \frac{\alpha\beta}{3}[f''(0)]^3 \text{ and } Nu_x \text{Re}_x^{-\frac{1}{2}} = -\theta'(0), \quad (6.16)$$

Here Re_x is the mathematical symbol of Reynolds number.

6.2 Computational algorithm

As the modelled equations (Eqs. (6.10) – (6.11)) of under consideration problem are highly nonlinear coupled equations, thus numerical technique (shooting method) is employed to find more realistic and compatible solution. Initially, these higher order equations are shifted to first order, so these equations are re-arranged as

$$f''' = \frac{f'^2 - ff'' + Mf'}{\alpha(1 - \beta f''^2)}, \quad (6.17)$$

$$\theta'' = -\frac{\text{Pr}(f\theta' - \gamma ff'\theta') + \epsilon\theta'^2}{(1 + \epsilon\theta) - \text{Pr}\gamma f^2}. \quad (6.18)$$

The below defined group of variables is inserted in the above system

$$f = z_1, \quad f' = z_2, \quad f'' = z_3, \quad f''' = z'_3, \quad \theta = z_4, \quad \theta' = z_5 \text{ and } \theta'' = z'_5. \quad (6.19)$$

After inserting the new variables, the flow problem takes the following form

$$\left(\begin{array}{c} z'_1 = z_2, \\ z'_2 = z_3, \\ z'_3 = \frac{z_2^2 - z_1 z_3 + M z_2}{\alpha(1 - \beta z_3^2)}, \\ z'_4 = z_5 \\ z'_5 = -\frac{\text{Pr}(z_1 z_5 - \gamma z_1 z_2 z_5) + \epsilon z_5^2}{(1 + \epsilon z_4) - \text{Pr}\gamma z_1^2}, \end{array} \right)$$

along with two-point conditions

$$z_1(0) = 0, z_2(0) = 1, z_2(\infty) = 0, z_4(0) = 1 \text{ and } z_4(\infty) = 0.$$

First missing initial conditions $z_3(0)$ and $z_5(0)$ are added instead of $z_2(\infty)$ and $z_4(\infty)$, this step transmuted the BVP into IVP. Now, Runge-Kutta scheme is employed to tackle resulting problem for suitable value of η_∞ . After considering some random values of η_∞ , it is found that the results are accurate in the range $\eta \in [0, 7]$ for feasible values of governing parameters.

6.3 Results and discussion

6.3.1 Validation of present results

Principal objective of this chapter is investigation of heat transfer with generalized Fourier heat flux model of MHD Prandtl-Eyring fluid flow past a stretching sheet. Mathematical modelled system is solved with fifth order Runge-Kutta scheme. To authenticate the present computations, comparison is established with reported literature (Akbar et al. [24], Malik et al. [26] and Previous chapter results) via **Table 6.1**. It is absolutely clear that calculated values have close agreement with previous literature which leads to faith on current numerical procedure.

Table 6.1: Comparative analysis of skin friction coefficient by varying Hartmann number M and considering $\alpha = 1, \beta = \epsilon = \gamma = 0$.

M	Akbar et al. [24]	Malik et al. [26]	Previous chapter results	Present Results
0	-1	-1	-1	-1
0.5	-1.11803	-1.11802	-1.1180	-1.1201
1.0	-1.41421	-1.41419	-1.4137	-1.4142
5.0	-2.44949	-2.44945	-2.4495	-2.4495
10	-3.31663	-3.31657	-3.3166	-3.3166
100	-10.04988	-10.04981	-10.0500	-10.0500
500	-22.38303	-22.38294	-22.3835	-22.3890
1000	-31.63859	-31.63851	-31.6391	-31.6392

6.3.2 Velocity profile

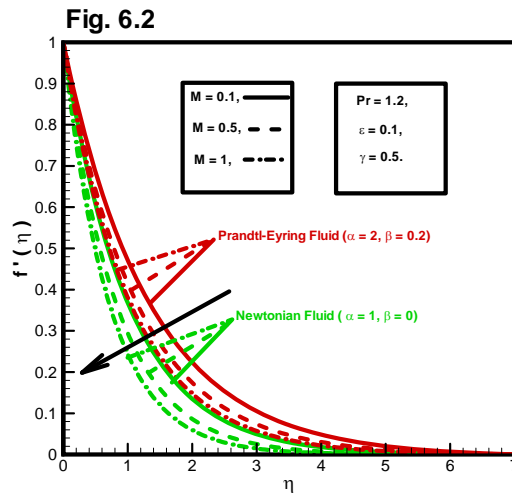


Fig. 6.2: Impact of Hartmann number on Newtonian and non-Newtonian fluid velocity.

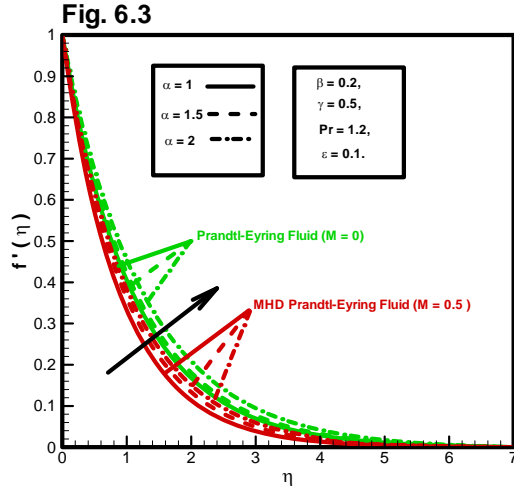


Fig. 6.3: Variations in velocity profile against fluid parameter α .

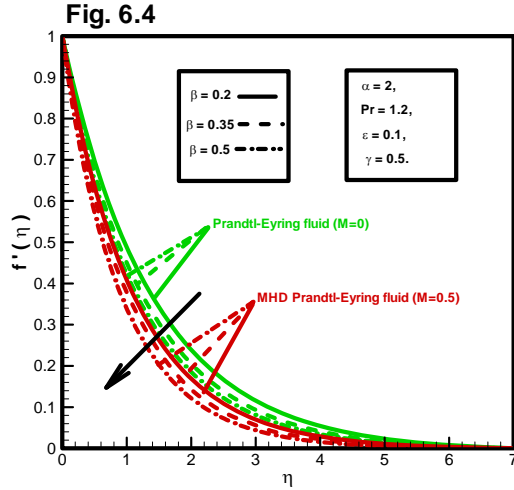


Fig. 6.4: Velocity curves under the impact of fluid parameter β .

Figs. 6.2-6.4 illuminate fluctuations in velocity profile under different parametric conditions. A contrast of fluid momentum for Prandtl-Eyring and Newtonian fluids against Hartmann number is communicated through **Fig. 6.2**. A substantial enhancement in velocity is

noticed for Prandtl-Eyring fluid versus Newtonian fluid for all values of Hartmann number. Also, both fluids have similar respond against Hartmann number i.e. their linear momentums decline against proceeding values of Hartmann number. This physically implies that Hartmann number is responsible to generate Lorentz force (an opposing force). Effects of fluid parameter α on dynamics of non-Newtonian fluid (by letting $M = 0.0$ and 0.5) has been captured with the aid of **Fig. 6.3**. This graph anticipates that magnetic field strength does not provide favorable situation for fluid movement. Additionally, this graph infers that fluid velocity grows rapidly verses fluid parameter α . It sounds practicable because fluid parameter α lessen the viscosity and alternatively fluid moves rapidly. **Fig. 6.4** discloses the consequences of fluid parameter β on Prandtl-Eyring fluid velocity (by letting $M = 0.0$ and 0.5). Fluid parameter β has capability to decelerate velocity (it can be observed from figure).

6.3.3 Temperature profile

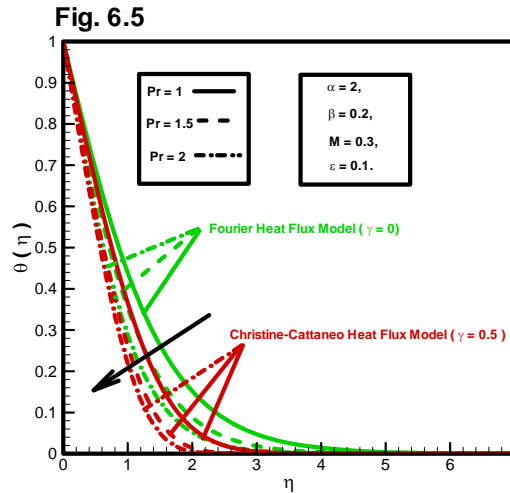


Fig. 6.5: Temperature profile by varying Prandtl number.

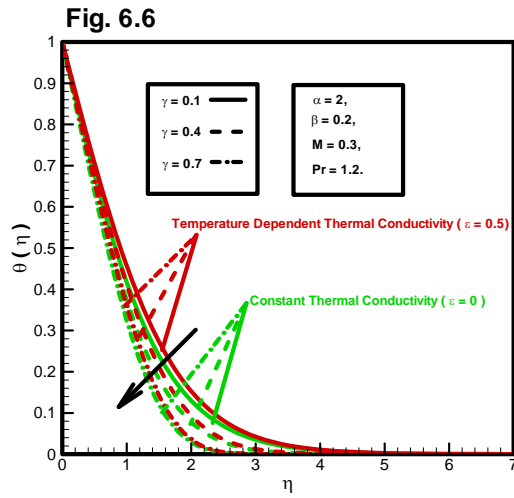


Fig. 6.6: Thermal relaxation parameter effects on temperature.

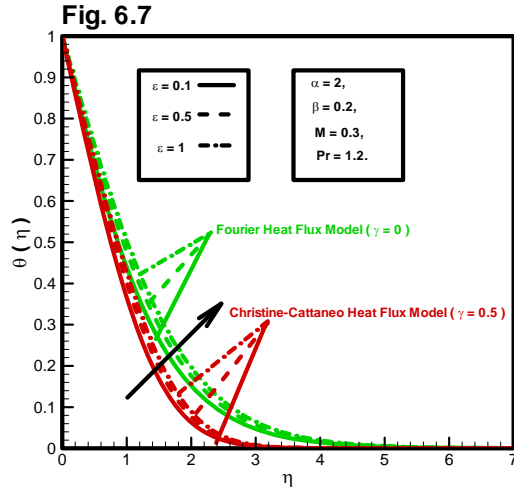


Fig. 6.7: Effects of thermal conductivity on temperature field.

In **Fig. 6.5**, a comparison between Fourier heat flux law and Christov-Cattaneo heat flux law has been established for different values of Prandtl number. Fluid temperature is larger in case of Fourier heat flux model (see graph). Finally, this graph reveals that expeditious fall

down in temperature is noticed against Prandtl number. This result holds in practice because high Prandtl number corresponds to fluid having low thermal conductivity. An speculative investigation of thermal relaxation parameter γ effects on thermal dynamics of fluid has been delineated through **Fig. 6.6** (by assuming $\epsilon = 0.0$ and 0.5). This figure predicts that the fluids with high thermal conductivity are more hotter. Also, temperature exhibit declining behaviour against thermal relaxation parameter. It justifies the fact that for large relaxation time fluid molecules take more time to transport thermal energy which alternatively reduces the temperature. This Christov-Cattaneo heat flux model reduces to Fourier model for thermal relaxation parameter $\gamma = 0$. An important aptitude of thermodynamics i.e. thermal conductivity effects on temperature is interpreted via **Fig. 6.7**. This figure predicts that thermal conductivity enhances the temperature quickly. It strengthen the fact that thermal conductivity is capacity of heat conductance. Thus liquids with higher thermal conductivity transport the heat rapidly and vice versa.

6.3.4 Wall friction factor and wall heat flux

Table 6.2: Influence of governing parameters (M , α , β , γ , ϵ and Pr) on wall friction factor and wall heat flux

M	α	β	γ	ϵ	Pr	$ \alpha f''(0) - \frac{\alpha\beta}{3}[f'''(0)]^3 $	$-\theta'(0)$
0.1	2.0	0.2	0.5	0.1	1.2	1.5052	0.7615
0.5						1.6921	0.7339
1.0						1.8536	0.7091
0.3	1.0					1.2212	0.6829
	1.5					1.4189	0.7218
	2.0					1.5507	0.7487
	2.0	0.1				1.6029	0.7507
		0.3				1.5809	0.7465
		0.5				1.5556	0.7416
		0.2	0.1				0.7004
			0.5				0.7183
			1.0				0.7428
			0.5	0.1			0.7428
				0.5			0.6977
				1.0			0.6540
				0.1	1.0		0.6584
					1.5		0.7893
					2.0		0.9278

Table 6.2 emphasizes the alteration of internal friction between fluid and solid wall verses momentum controlling parameters (M , α and β). It can be noticed that the magnetic field intensity boosts the internal friction because it aligned the fluid particles. Qualitatively similar outcomes are observed for internal friction against fluid parameter α but fluid parameter β decreases the internal friction slightly. This table also provides the behaviour of wall heat flux

by varying flow parameters (M , α , β , γ , ϵ and Pr). One can see that the both fluid parameters (α , β) enhance temperature gradient (in magnitude sense) but magnetic field provides resistance to flow heat through surface. Also, it can be noticed that both thermal relaxation parameter as well as Prandtl number enhance wall temperature gradient while effects of thermal conductivity parameter are found to be reversed.

6.4 Enumerated key findings

Current communication endeavours the heat transfer analysis of MHD Prandtl-Eyring fluid flow past a stretching surface manifested with the Christov-Cattaneo heat flux model. The problem is formulated under boundary layer assumptions and solved numerically with shooting technique. Salient features of current investigation are catalogued below:

- Prandtl-Eyring fluid moves faster than both Newtonian fluid and MHD Prandtl-Eyring fluid.
- Strength of magnetic field defiances the movement of fluid. Additionally, both fluid parameters have oppugnant effects on fluid momentum.
- Temperature for Christov-Cattaneo heat flux model is less for Fourier heat flux model i.e. high estimations in the thermal relaxation parameter are responsible for fall down in temperature.
- Prandtl number and thermal conductivity parameter influenced temperature significantly but qualitively opposite behaviour has been noticed.
- Both fluid parameter α and Hartmann number M reinforce internal friction while Prandtl-Eyring parameter β reduces it.
- Absolute heat transfer coefficient grows against both fluid parameters (α , β), thermal relaxation parameter and Prandtl number while opposing behaviour is observed for magnetic field parameter and thermal conductivity parameter.

Chapter 7

Thermal energy change in Christov-Cattaneo heat flux model for MHD fluid flow over variable thickened sheet with Hall current effects: A computational study

Present chapter carry out the speculative investigation on MHD viscous fluid flow over variable stretching sheet with Hall current phenomenon. Hall current phenomenon is prominent when intensity of applied magnetic field is strong or density of fluid is low. It is due to the fact that electron carries the induced current and moves faster than ions. This phenomenon generates an isotropic conductivity which is known as Hall current. The occurrence of Hall current demands the modification of Ohm's law, also consequences of this phenomenon enhance the order of flow govern differential equations. Hall current has many practical applications e.g. Hall accelerators, Hall sensors and turbine etc. Christov-Cattaneo heat flux law is utilized for heat transfer analysis. Present configuration produces partial differential equations with nonlinearity of higher order. The modelled partial differential system is switched into ordinary differential system with the aid of an appropriate similarity transforms. The resulting similarity

equations are solved with Runge-Kutta method. The expressions for axial velocity, transverse velocity and temperature are numerically computed and effects of controlling parameters on them are visualized with the help of graphs. To insight flow behaviour in the neighbour region of sheet surface, local wall friction factors and local heat flux are calculated. Flow govern parameters impacts on these quantities are elaborated through tabular representations. A suitable correlation of current results with previously reported data (in limiting case) is presented for the validation of computed results.

7.1 Problem development

Consider the incompressible electrically conducting flow of Newtonian fluid passing over a stretching sheet with variable thickness. The sheet is stretched along the axial direction i.e. x -axis with stretching rate $U(x) = U_0(x+b)^n$, here U_0 is reference velocity, b is relative stretching parameter while n denotes velocity exponent parameter. The y -axis is taken perpendicular to the stretching surface. The sheet is non-flat and its surface is taken at $y = A(x+b)^{\frac{1-n}{2}}$ where A is stretching coefficient and its values are assumed small to avoid pressure gradient along the sheet. Applied magnetic field of strength $B_0(x)$ is taken in y -direction. The low magnetic Reynolds number is assumed (i.e. induced magnetic field is negligible). Hall current effects are considered in flow distribution, since Hall currents generates the cross flow, so flow becomes three dimensional. Also, quantities are assumed constant along z -axis and last assumption is true for surface of infinite extent.

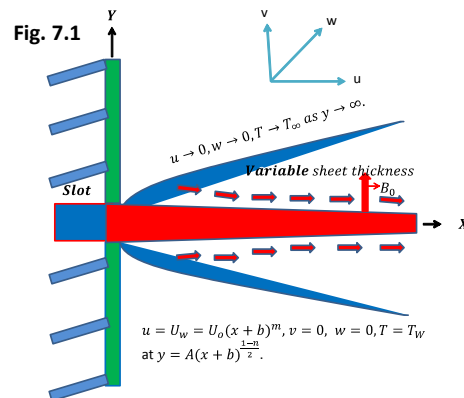


Fig. 7.1: Physical description of the problem.

Modified Ohm's law is defined below (by adding Hall current effects)

$$\mathbf{J} = \sigma(\mathbf{E} + \mathbf{V} \times \mathbf{B} - \frac{1}{en_e} \mathbf{J} \times \mathbf{B} + \frac{1}{en_e} \nabla p_e). \quad (7.1)$$

Here $\mathbf{J} = (J_x, J_y, J_z)$ denotes current density, σ denotes electrical conductivity, $\mathbf{V} = (u, v, w)$ is velocity, \mathbf{E} denotes the electric field, p_e called electronic pressure and $\mathbf{B} = (0, B(x), 0)$ denotes magnetic field. The flow is considered in the absence of electric field and pressure gradient ($\mathbf{E} = \mathbf{0}$ and $\nabla p_e = 0$). Since sheet is considered non-conducting so $J_y = 0$, thus, after imposing the aforementioned conditions, the above defined physical law transformed to

$$J_x = \frac{\sigma B^2(x)}{1+m^2}(mu - w), \quad J_z = \frac{\sigma B^2(x)}{1+m^2}(u + mw), \quad (7.2)$$

where $m = \frac{\sigma B(x)}{en_e}$ is the Hall parameter. Now, the governing mass and momentum equations along with boundary layer approximations are given below (see Parsad et al. [36])

$$\frac{\partial u}{\partial x} + \frac{\partial v}{\partial y} = 0, \quad (7.3)$$

$$u \frac{\partial u}{\partial x} + v \frac{\partial u}{\partial y} = \nu \frac{\partial^2 u}{\partial y^2} - \frac{\sigma B^2(x)}{\rho(1+m^2)}(u + mw), \quad (7.4)$$

$$u \frac{\partial w}{\partial x} + v \frac{\partial w}{\partial y} = \nu \frac{\partial^2 w}{\partial y^2} + \frac{\sigma B^2(x)}{\rho(1+m^2)}(mu - w), \quad (7.5)$$

along with appropriate boundary conditions

$$\begin{aligned} u &= U(x), \quad v = 0, \quad w = 0, \quad \text{at } y = A(x+b)^{\frac{1-n}{2}}, \\ u &\rightarrow 0, \quad w \rightarrow 0, \quad \text{at } y \rightarrow \infty. \end{aligned} \quad (7.6)$$

The heat equation of steady viscous flow is defined as

$$\rho c_p \mathbf{V} \cdot \nabla T = -\nabla \cdot \mathbf{q}, \quad (7.7)$$

here ρ is density, c_p called specific heat, T and \mathbf{q} denote temperature and heat flux. Here, the temperature equation is defined in terms of Christov-Cattaneo heat flux law which is defined below

$$\mathbf{q} + \lambda(\mathbf{V} \cdot \nabla \mathbf{q} - \mathbf{q} \cdot \nabla \mathbf{V} + (\nabla \cdot \mathbf{V})\mathbf{q}) = -\kappa \nabla T. \quad (7.8)$$

In Eq. (7.8), κ is thermal conductivity, λ is the thermal relaxation parameter, if $\lambda = 0$ then above defined thermodynamic law is converted into classical Fourier law. In present analysis, incompressible flow is considered, so $\nabla \cdot \mathbf{V} = 0$. After, inserting this assumption in above defined heat equation (Eq. (7.8)), it becomes

$$\mathbf{q} + \lambda(\mathbf{V} \cdot \nabla \mathbf{q} - \mathbf{q} \cdot \nabla \mathbf{V}) = -\kappa \nabla T. \quad (7.9)$$

Eliminating \mathbf{q} from Eq. (7.7) and Eq. (7.9), the heat equation for viscous fluid flow takes the form

$$\begin{aligned} u \frac{\partial T}{\partial x} + v \frac{\partial T}{\partial y} &= \alpha \frac{\partial^2 T}{\partial y^2} - \lambda \left(\left(u \frac{\partial u}{\partial x} + v \frac{\partial u}{\partial y} \right) \frac{\partial T}{\partial x} + \left(u \frac{\partial v}{\partial x} + v \frac{\partial v}{\partial y} \right) \frac{\partial T}{\partial y} + 2uv \frac{\partial^2 T}{\partial x \partial y} \right. \\ &\quad \left. + u^2 \frac{\partial^2 T}{\partial x^2} + v^2 \frac{\partial^2 T}{\partial y^2} \right), \end{aligned} \quad (7.10)$$

prescribed two-point conditions for fluid temperature are

$$T = T_w \text{ at } y = A(x+b)^{\frac{1-n}{2}} \text{ and } T \rightarrow T_\infty \text{ as } y \rightarrow \infty. \quad (7.11)$$

The expressions $\alpha = \frac{\kappa}{\rho c_p}$, T_w and T_∞ defined in Eq. (7.11) correspond to thermal diffusivity, surface temperature and ambient temperature respectively.

Stream function is given below

$$u = \frac{\partial \Psi}{\partial y}, \quad v = -\frac{\partial \Psi}{\partial x}. \quad (7.12)$$

The following transformations are utilized to transfigured flow govern system into non-dimensional form (see Parsad et al. [36], Salahuddin et al. [83], Malik et al. [84], Fang et al. [103] and Khader and Megahed [104])

$$\begin{aligned} \eta &= y \sqrt{\frac{n+1}{2}} \frac{U_0}{\nu} (x+b)^{\frac{n-1}{2}}, \quad \Psi = F(\eta) \sqrt{\frac{2}{n+1}} U_0 \nu (x+b)^{\frac{n+1}{2}}, \\ w &= U(x) H(\eta), \quad \Theta = \frac{T - T_\infty}{T_w - T_\infty}. \end{aligned} \quad (7.13)$$

With the aid of Eq. (7.12) and Eq. (7.13), the velocity components along x and y directions can be written as

$$u = U(x) F'(\eta) \quad \text{and} \quad v = -\sqrt{\frac{n+1}{2}} \nu U_0 (x+b)^{\frac{n-1}{2}} \times [F(\eta) + \eta F'(\eta) (\frac{n-1}{n+1})]. \quad (7.14)$$

Inserting the above defined similarity variables i.e. Eqs. (7.13) – (7.14) into modelled governing partial differential equations i.e. Eq. (7.3), Eq. (7.4), Eq. (7.5) and Eq. (7.10). The mass conservation equation is identically satisfied, on the other hand velocity and temperature equations become

$$F''' + FF'' - \frac{2n}{n+1} F'^2 - \frac{2M}{(1+n)(1+m^2)} (F' + mH) = 0, \quad (7.15)$$

$$H'' + FH' - \frac{2n}{n+1}F'H + \frac{2M}{(1+n)(1+m^2)}(mF' - H) = 0, \quad (7.16)$$

$$\Theta'' + \text{Pr} F\Theta' + \text{Pr} \gamma \left(\frac{n-3}{2}FF'\Theta' - \frac{n+1}{2}F^2\Theta'' \right) = 0, \quad (7.17)$$

while prescribed boundary conditions are reshaped to

$$\begin{aligned} F(\alpha) &= \alpha \frac{1-n}{1+n}, \quad F'(\alpha) = 1, \quad H(\alpha) = 0, \quad \Theta(\alpha) = 1, \\ F'(\infty) &= 0, \quad H(\infty) = 0, \quad \Theta(\infty) = 0. \end{aligned} \quad (7.18)$$

Here $\alpha = A\sqrt{\frac{n+1}{2}\frac{U_0}{\nu}}$ exhibits the wall thickness parameter while $\eta = \alpha = A\sqrt{\frac{n+1}{2}\frac{U_0}{\nu}}$ corresponds to surface of sheet. In order to facilitate the computing process, the following suitable transformations are inserted into above defined boundary value problem (see Parsad et al. [36])

$$f(\chi) = F(\eta - \alpha), \quad h(\chi) = H(\eta - \alpha), \quad \theta(\chi) = \Theta(\eta - \alpha). \quad (7.19)$$

After employing the recently defined variables in *Eqs.* (7.15)–(7.17), the modified governing equations take the following form

$$f''' + ff'' - \frac{2n}{n+1}f'^2 - \frac{2M}{(1+n)(1+m^2)}(f' + mh) = 0, \quad (7.20)$$

$$h'' + fh' - \frac{2n}{n+1}f'h + \frac{2M}{(1+n)(1+m^2)}(mf' - h) = 0, \quad (7.21)$$

$$\theta'' + \text{Pr} f\theta' + \text{Pr} \gamma \left(\frac{n-3}{2}ff'\theta' - \frac{n+1}{2}f^2\theta'' \right) = 0, \quad (7.22)$$

while given boundary conditions are converted to

$$\begin{aligned}
f(0) &= \alpha \frac{1-n}{1+n}, \quad f'(0) = 1, \quad h(0) = 0, \quad \theta(0) = 1, \\
f'(\infty) &= 0, \quad h(\infty) = 0, \quad \theta(\infty) = 0.
\end{aligned} \tag{7.23}$$

In above non-linear set of differential equations prime denotes the derivative w.r.t χ . Also, the dimensionless variables (magnetic field parameter M , Prandtl number Pr and thermal relaxation parameter γ) are given below

$$M = \frac{2\sigma(x+b)^n B_0^2}{\rho U(x)}, \quad \text{Pr} = \frac{\nu}{\alpha} \quad \text{and} \quad \gamma = \lambda U_0(x+b)^{n-1}. \tag{7.24}$$

The coefficients of horizontal and transverse wall frictions as well as wall heat flux are computed to insight problem near the sheet surface. The mathematical expressions of these quantities are given below

$$C_{fx} = \frac{\tau_{w_x}}{\frac{1}{2}\rho U^2}, \quad C_{fz} = \frac{\tau_{w_z}}{\frac{1}{2}\rho U^2} \quad \text{and} \quad Nu_x = \frac{xq_w}{\kappa(T_w - T_\infty)}, \tag{7.25}$$

where τ_{w_x} , τ_{w_z} and q_w represent wall shear stresses and heat flux respectively, these are defined below

$$\tau_{w_x} = \mu \left(\frac{\partial u}{\partial y} \right)_{y=A(x+b)^{1-\frac{n}{2}}}, \quad \tau_{w_z} = \mu \left(\frac{\partial w}{\partial y} \right)_{y=A(x+b)^{1-\frac{n}{2}}}, \quad q_w = -\kappa \left(\frac{\partial T}{\partial y} \right)_{y=A(x+b)^{1-\frac{n}{2}}}. \tag{7.26}$$

After inserting similar variables, the above defined expressions take the form

$$\frac{1}{2}C_{fx} \text{Re}_x^{\frac{1}{2}} = \sqrt{\frac{n+1}{2}} f''(0), \quad \frac{1}{2}C_{fz} \text{Re}_x^{\frac{1}{2}} = \sqrt{\frac{n+1}{2}} h'(0), \quad Nu_x \text{Re}_x^{\frac{-1}{2}} = -\sqrt{\frac{n+1}{2}} \theta'(0), \tag{7.27}$$

here Re_x displays the Reynolds number and it is defined as $\text{Re}_x = \frac{(x+b)U(x)}{\nu}$.

7.2 Numerical solution

The governing equations i.e. *Eqs.* (7.20) – (7.22) are highly nonlinear in nature, a numerical approach shooting is employed to compute solution. According to solution procedure, primarily higher order system is transferred to first order differential system. For this aim re-write them in the following form

$$f''' = \frac{2n}{n+1}f'^2 - ff'' + \frac{2M}{(1+n)(1+m^2)}(f' + mh), \quad (7.28)$$

$$h'' = \frac{2n}{n+1}f'h - fh' - \frac{2M}{(1+n)(1+m^2)}(mf' - h), \quad (7.29)$$

$$\theta'' = \frac{-\text{Pr} f\theta' - \text{Pr} \gamma \left(\frac{n-3}{2} ff'\theta'\right)}{1 - \frac{n+1}{2} \text{Pr} \gamma f^2}. \quad (7.30)$$

The following defined variables are applied to above mentioned equations

$$f = z_1, f' = z_2, f'' = z_3, f''' = z'_3, h = z_4, h' = z_5, h'' = z'_5, \theta = z_6, \theta' = z_7 \text{ and } \theta'' = z'_7. \quad (7.31)$$

The transformed system is given below

$$\begin{aligned} z'_1 &= z_2, z'_2 = z_3, \\ z'_3 &= \frac{2n}{n+1}z_2^2 - z_1z_3 + \frac{2M}{(1+n)(1+m^2)}(z_2 + mz_4), \\ z'_4 &= z_5, z'_5 = \frac{2n}{n+1}z_2z_4 - z_1z_5 - \frac{2M}{(1+n)(1+m^2)}(mz_2 - z_4), \\ z'_6 &= z_7, z'_7 = \frac{-\text{Pr} z_1z_7 - \frac{n-3}{2} \text{Pr} \gamma z_1z_2z_7}{1 - \frac{n+1}{2} \text{Pr} \gamma z_1^2}, \end{aligned} \quad (7.32)$$

along with prescribed conditions

$$\begin{aligned}
z_1(0) &= \alpha \frac{1-n}{1+n}, \quad z_2(0) = 1, \quad z_4(0) = 0 \quad \text{and} \quad z_6(0) = 1, \\
z_2(\infty) &= 0, \quad z_4(\infty) = 0 \quad \text{and} \quad z_6(\infty) = 0.
\end{aligned}
\tag{7.33}$$

Now above differential system is solved with Runge-Kutta-Fehlberg technique after adding initial conditions $z_3(0) = \alpha_1$, $z_5(0) = \alpha_2$ and $z_7(0) = \alpha_3$ (as an alternative of $z_2(\infty) = 0$, $z_4(\infty) = 0$ and $z_6(\infty) = 0$). The solution is computed for different values of χ_∞ and found that solution is accurate in the region $0 \leq \chi \leq 4$ for suitable values of flow govern parameters.

7.3 Results and discussion

7.3.1 Validity of computed results

Present communication is an speculative investigation of the problem addressing Hall current effects on magnetohydrodynamic flow of viscous fluid along with non-Fourier heat flux theory over variable stretching sheet. Shooting technique is employed to solve governing system. The validity of calculated solution is checked by comparing results with previously reported data (Fang et al. [103] and Khadar and Megahed [104]). This table ensures the accuracy of presently computed results and leads to confidence on the adapted method.

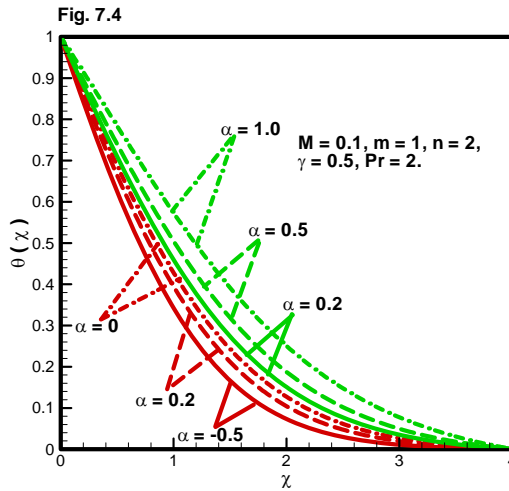
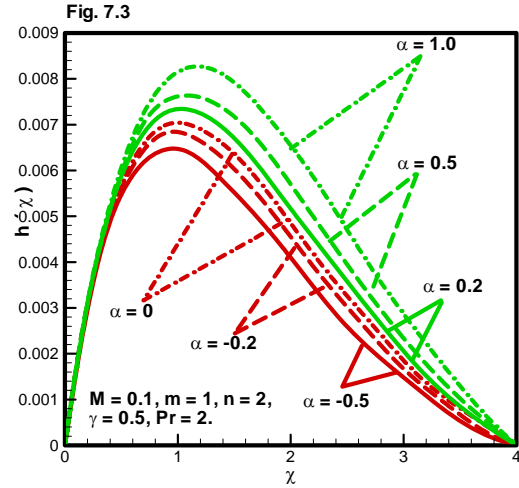
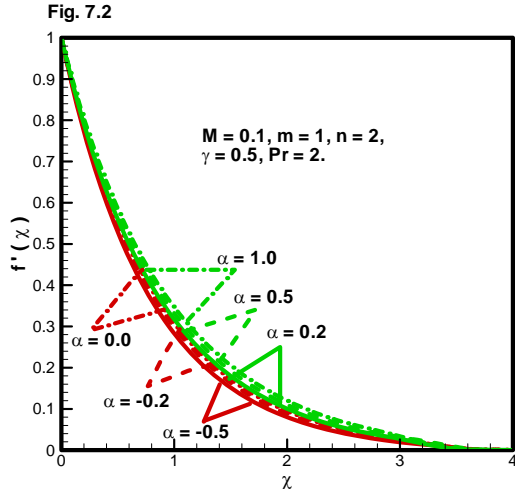
Table 7.1: Comparative analysis of wall friction factor $-f''(0)$ against wall thickness parameter α and non-linearity parameter n but $M = \gamma = 0$.

	$\alpha = 0.5$			$\alpha = 0.25$		
n	Fang et al.	Khader and	Present Results	Fang et al.	Khadar and	Present Results
	[103]	Megahed [104]		[103]	Megahed [104]	
10.0	1.0603	1.0603	1.0605	1.1433	1.1433	1.1437
9.0	1.0589	1.0588	1.0591	1.1401	1.1404	1.1408
7.0	1.0550	1.0551	1.0552	1.1323	1.1322	1.1327
5.0	1.0486	1.0486	1.0486	1.1186	1.1186	1.1190
3.0	1.0359	1.0358	1.0359	1.0905	1.0904	1.0909
2.0	1.0234	1.0234	1.0234			
1.0	1.0000	1.0000	1.0000	1.0000	1.0000	1.0005
0.5	0.9798	0.9798	0.9801	0.9338	0.9337	0.9341
0	0.9576	0.9577	0.9577	0.7843	0.7843	0.7843
-1/3	1.0000	1.000	1.0000	0.5000	0.5000	0.5000
-0.5	1.1667	1.1666	1.1667	0.0833	0.0833	0.0833

7.3.2 Effects of wall thickness parameter

Figs. 7.2-7.4 exhibit the physical aspects of wall thickness parameter α on axial velocity, normal velocity and temperature. Qualitatively identical manners have been captured in all three physical quantities against variations in wall thickness parameter while fluid energy affected dominantly in quantifying sense. Since $n > 1$ corresponds to mass injection in axial direction, thus higher values of wall thickness parameter α leads to reduce wall shear stress and hence consequentially axial velocity $f'(\chi)$ is accelerated. Also, one can see that the enhancement in wall thickness leads to accelerate the fluid motion in normal direction i.e. higher values of α corresponds to increase in normal velocity component $h(\chi)$. The variable thickness of wall i.e. increasing values of α motivates the transferal of heat from the surface, it accelerates the

convection of fluid and hence temperature.

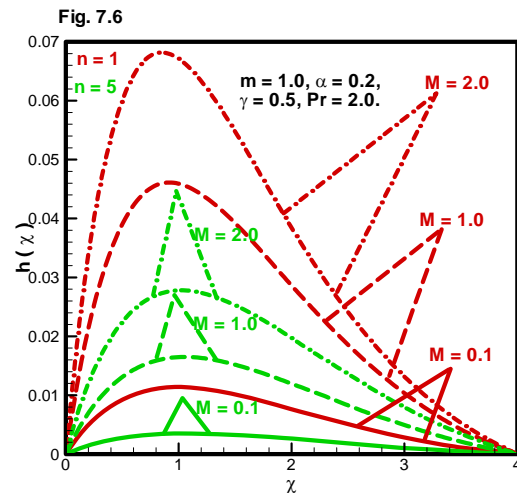
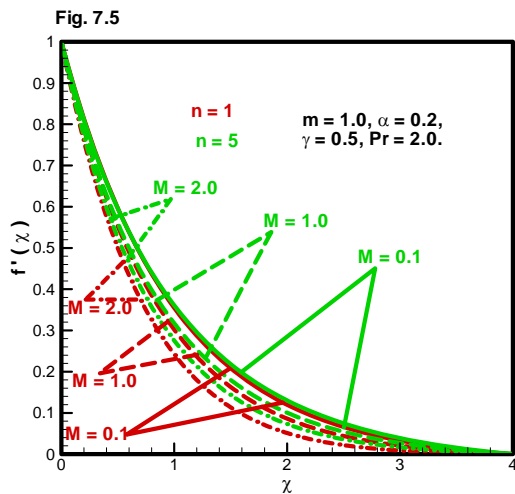


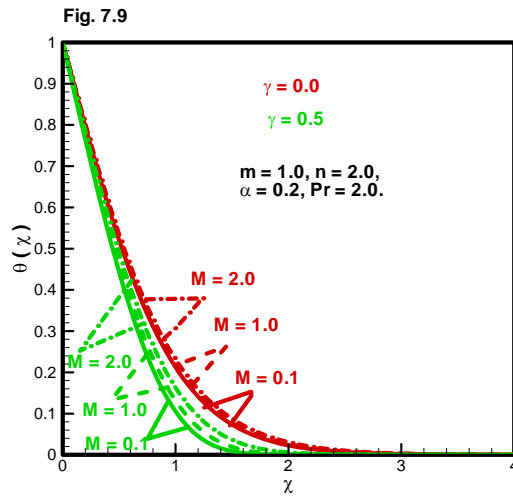
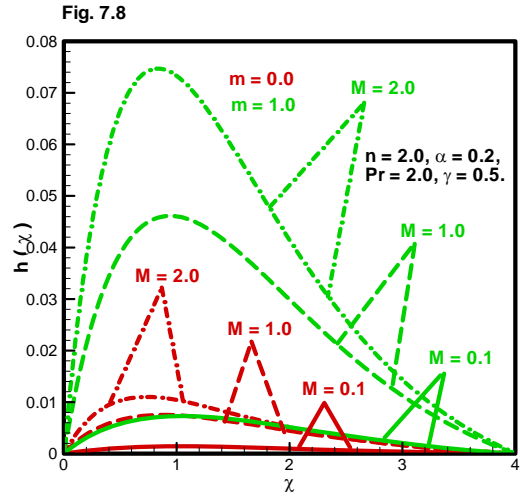
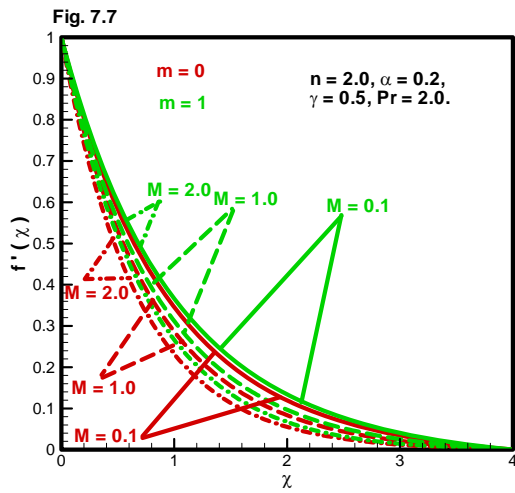
Figs. 7.2-7.4: Influence of variable stretching parameter α on horizontal velocity profile, transverse velocity profile and temperature profile.

7.3.3 Effects of Hartmann number

Figs. 7.5-7.6 communicate the Hartmann number effects on horizontal and transverse velocity components over flat sheet ($n = 1$) and non-flat sheet ($n = 5$). The non-flatness of the sheet

is responsible to grow the horizontal velocity while oppugnant impact on transverse velocity is encapsulated. Additionally, these graphs explicate that the both velocity components display similar patterns against Hartmann number i.e. both velocity profiles have decreasing manner. It holds physically because strength of magnetic field produces Lorentz force (an opposing force), thus higher values of Hartmann number corresponds to enhance Lorentz force which consequentially decelerates the velocity. **Figs. 7.7-7.8** explain the influences of Hartmann number in the absence of Hall current for $m = 0, = 1$. It can be noticed that presence of Hall current leads to enlarge the both velocity components while decreasing behavior of horizontal and transverse velocities has been noticed against Hartmann number. **Fig. 7.9** exposes the Hartmann number consequences on temperature for classical Fourier law ($\gamma = 0$) and Christov-Cattaneo heat flux model ($\gamma = 0.5$). The variations in Hartmann number produce the homogeneous results for both cases in qualitative manner while effects on Christov-Cattaneo heat flux are prominent in quantifying sense. Because when electrical conducting fluid particles are passed through magnetic field, they strike with ions and release thermal energy. Thus, strength of magnetic field generates heating in the fluid and this sequentially rises the temperature.



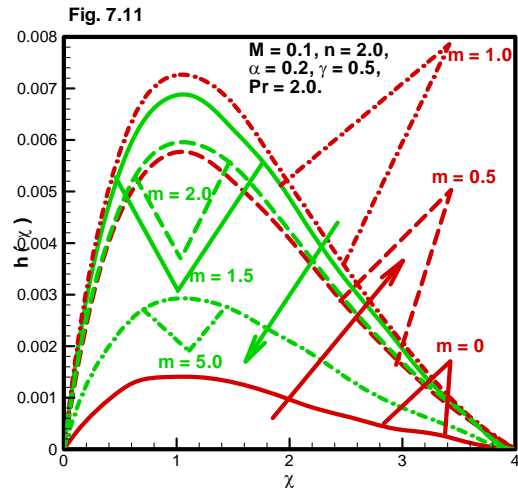
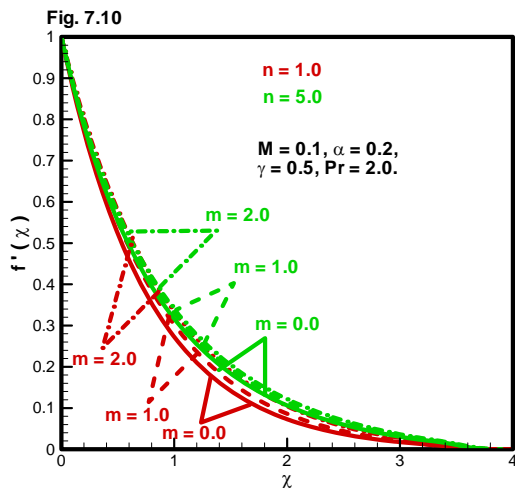


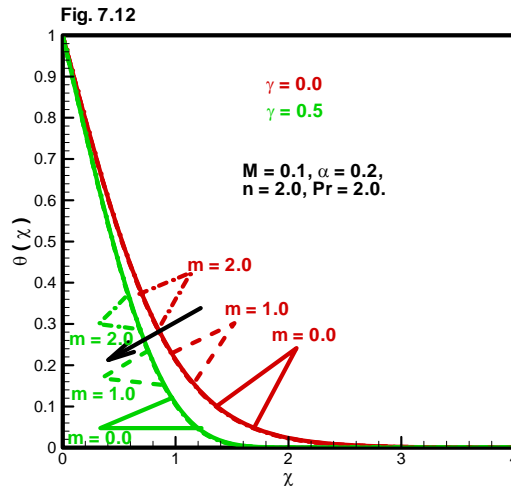
Figs. 7.5-7.9: Effects of Hartmann number on horizontal velocity, transverse velocity and temperature profile.

7.3.4 Effects of Hall parameter

Fig. 7.10 focuses on the comparative analysis of horizontal velocity over flat ($n = 1$) and non-flat ($n = 5$) stretching sheet by varying Hall parameter. This graph illustrates that the fluid movement is more rapid on non-flat sheet as compared to flat sheet. Also, the influence of Hall parameter leads to accelerate the fluid motion but in magnitude sense this acceleration is not significant. Because increasing values of Hall parameter corresponds to reduce in damping

magnetic force on axial velocity which alternatively accelerates axial velocity. **Fig. 7.11** conveys the interesting facts about the Hall parameter effects on transverse velocity component, it can be seen that when Hall parameter values advances from 0 to 1 the normal acceleration is positive while reverse behaviour has been recorded when its values are taken greater than 1. It holds because larger values of Hall parameter correspond to reduce the damping factor and hence it causes reduction in transverse velocity. **Fig. 7.12** prevails the Hall parameter on effects on fluid temperature for both cases i.e. Fourier heat flux model ($\gamma = 0$) and Christov-Cattaneo heat flux model ($\gamma = 0.5$). The temperature profile reduces against increasing values of Hall parameter but this falls down in temperature is inconsequential. Finally, this graph predicts that fluid temperature is high in case of Fourier heat flux model.



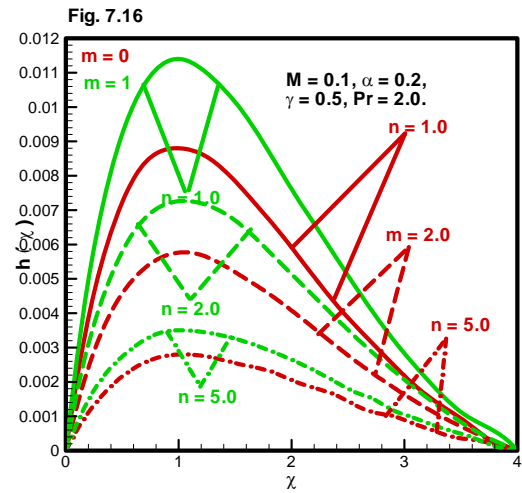
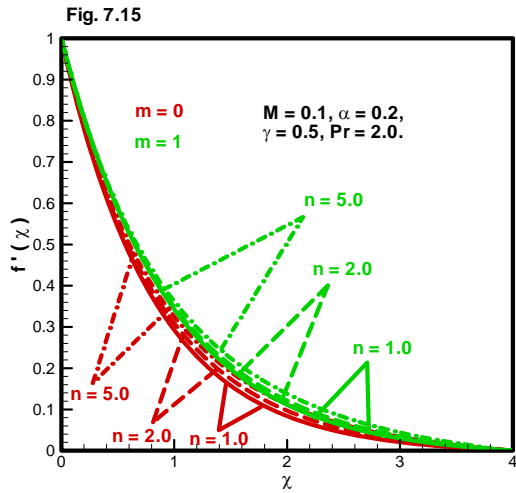
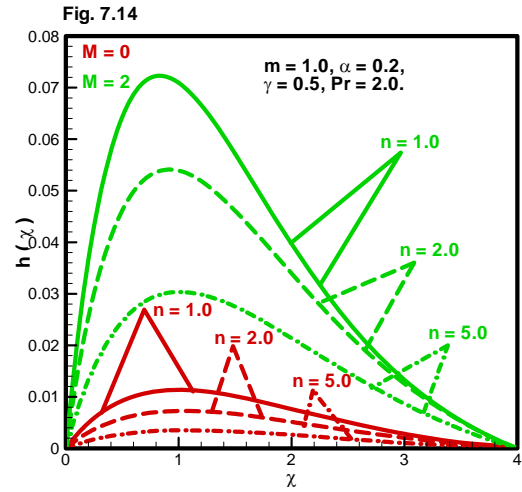
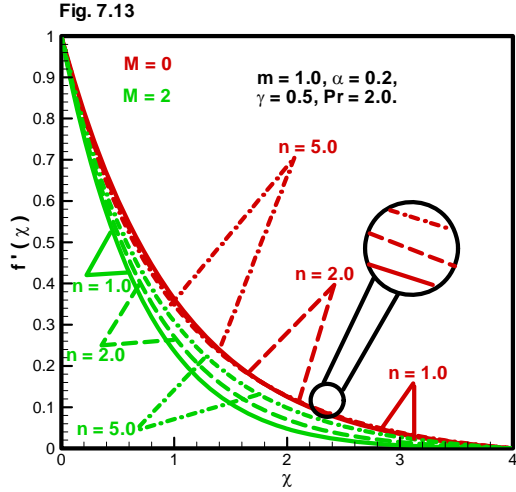


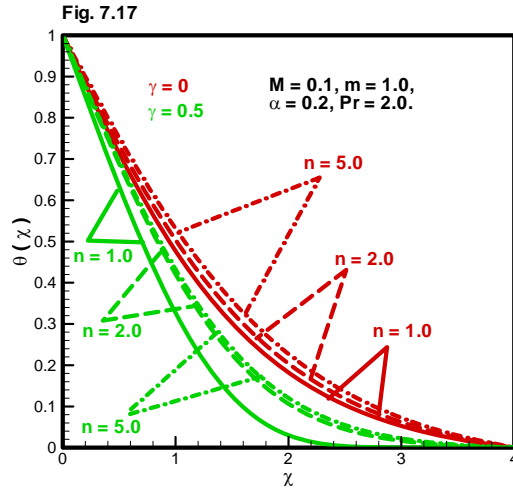
Figs. 7.10-7.12: Impact of Hall parameter on horizontal velocity profile, transverse velocity profile and temperature profile.

7.3.5 Effects of nonlinearity parameter

Figs. 7.13-7.14 are adorned to investigate the behaviour of horizontal and transverse velocities by varying non-linearity parameter n for $M = 0$ (viscous flow) and $M = 0.2$ (magnetohydrodynamic flow). The effects of nonlinearity parameter are found to be insignificant on both velocity components in viscous flow while magnetohydrodynamic flow is strongly influenced by it. As $n > 1$ corresponds to mass injection in axial direction, thus large values of this leads to reduce the wall shear stress remarkably. Hence fluid momentum is accelerated very rapidly in axial direction (see **Fig. 7.13**). On the other hand, **Fig. 7.14** exhibits decreasing manner of transverse velocity component versus non-linearity parameter for both fluids. The consequences of non-linearity parameter on both velocity components is described in **Figs. 7.15-7.16** for $m = 0$ and $m = 1$. These graphs suggest that the presence of Hall current enhances the fluid velocity in both directions while opponent attitude is captured in axial and normal velocity components against nonlinearity parameter. **Fig. 7.17** depicts temperature profile versus non-linearity parameter for $\gamma = 0$ and $\gamma = 0.5$. Increment in nonlinearity parameter correspond to non-flatness of sheet, as non-flatness provides favorable environment to heat transfer, so fluid temperature amplifies significantly against nonlinearity parameter(it can be encapsulated in

this figure).

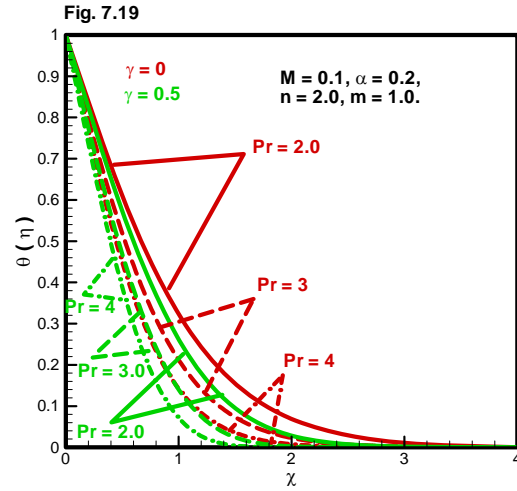
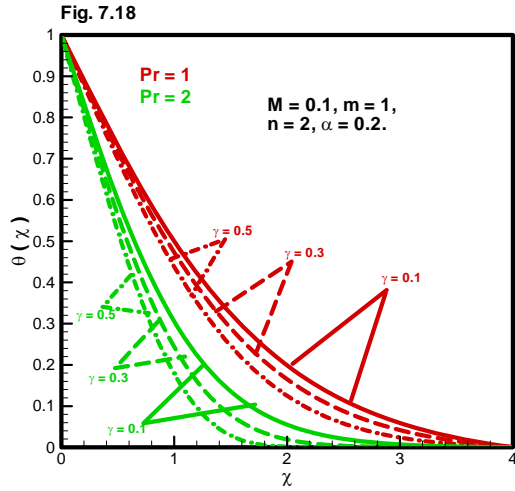




Figs. 7.13-7.17: The impacts of nonlinearity index on horizontal velocity, transverse velocity and temperature.

7.3.6 Effects of thermal relaxation parameter and Prandtl number

Fig. 7.18 shows the temperature profile versus variations in thermal relaxation parameter and keeping $Pr = 1, 2$. This graph explicates that fluid temperature substantially reduces versus Prandtl number. Also, thermal relaxation parameter is responsible to decline thermal energy in substantial amount. Physically, it is true because increasing values of γ corresponds to enhance in relaxation time i.e. fluid particles take more time to transfigure thermal energy, the consequences of this phenomenon reduces temperature in large amount. Prandtl number effects on fluid temperature is analyzed over non-flat sheet by **Fig. 7.19** for $\gamma = 0$ and $\gamma = 0.5$. The fluid temperature declines against Prandtl number, because fluid with high Prandtl number have low thermal conductivity (capability of heat transfer).



Figs. 7.18-7.19: Fluid temperature variations versus thermal relaxation parameter and Prandtl number.

7.3.7 Radial and transverse friction factors and local Nusselt number

The inclusive picture of physical quantities $-f''(0)$, $-h'(0)$ and $-\theta'(0)$ is elaborated via **Tables 7.2-7.5**.

Table 7.2 interprets the attitude of wall friction factors and wall heat flux coefficients towards different values of M , m , n , γ and Pr while keeping wall thickness parameter $\alpha = 0$ (constant stretching) and $\alpha = 0.2$ (variable stretching). This table infers that contributions of wall thickness parameter reduce the radial wall friction and wall heat flux coefficients while transverse component of friction remained unaffected. Furthermore, axial and normal wall friction factors advances to higher values (in magnitude sense) against Hartmann number while behaviour of local Nusselt number is opposite against it. The influence of Hall parameter enhances heat flux in quantifying sense while wall friction factors display dual behaviour (they increase for $m \leq 1$ and decreases for $m > 1$). The nonlinearity parameter enlarges the horizontal skin friction coefficient and local Nusselt number while transverse wall friction shows opposing behaviour. Prandtl number and thermal relaxation parameter increase the Nusselt number.

Table 7.2: Numerical values of $-f''(0)$, $-h'(0)$ and $-\theta'(0)$ by varying M , m , n , γ and Pr while keeping α fixed i.e. $\alpha = 0, 0.2$.

					$\alpha = 0.0$			$\alpha = 0.2$		
M	m	n	γ	Pr	$-f''(0)$	$-h'(0)$	$-\theta'(0)$	$-f''(0)$	$-h'(0)$	$-\theta'(0)$
0.1	1.0	2.0	0.3	1.0	1.1195	0.0182	0.6450	1.0878	0.0182	0.5908
1.0					1.2560	0.1558	0.6120	1.2230	0.1558	0.5570
2.0					1.4012	0.2697	0.5758	1.3689	0.2697	0.5238
0.1	0.5				1.1283	0.0144	0.6428	1.0965	0.0144	0.5888
	1.0				1.1195	0.0182	0.6450	1.0878	0.0182	0.5908
	2.0				1.1106	0.0147	0.6472	1.0789	0.0147	0.5930
	5.0				1.1057	0.0071	0.6484	1.0740	0.0071	0.5942
	10.0				1.1049	0.0037	0.6487	1.0731	0.0037	0.5944
	1.0	1.0			1.0287	0.0290	0.6088	1.0287	0.0290	0.6088
		2.0			1.1195	0.0182	0.6450	1.0878	0.0182	0.6108
		5.0			1.2044	0.0086	0.7906	1.1432	0.0086	0.6201
		2.0	0.1				0.6023			0.5680
			0.3				0.6450			0.5908
			0.5				0.6991			0.6322
			0.3	1.0			0.6450			0.5908
				2.0			1.0410			0.9234
				3.0			1.2048			1.1753

Table 7.3 delivers the quantitative analysis of physical phenomena near the sheet surface by varying involving parameters M , α , n , γ and Pr and considering Hall parameter $m = 0$ and $m = 5.0$. This table presents that in the absence of Hall parameter transverse wall friction is negligible. Also, effects of Hall current are opposite on horizontal wall friction and wall heat flux. In addition, both Hartmann number and nonlinearity parameter accelerate the magnitude of axial wall friction factor but opposite results are found in case of wall thickness parameter

on it. Hartmann number and wall thickness parameter increase transverse component of wall friction while it reduces due to nonlinearity parameter. The homogeneous results are recorded for local Nusselt number by increasing Prandtl number and thermal relaxation parameter.

Table 7.3: Numerical values of $-f''(0)$, $-h'(0)$ and $-\theta'(0)$ by varying M , α , n , γ and Pr while keeping m fixed i.e. $m = 0, 5.0$.

					$m = 0.0$			$m = 5.0$		
M	α	n	γ	Pr	$-f''(0)$	$-h'(0)$	$-\theta'(0)$	$-f''(0)$	$-h'(0)$	$-\theta'(0)$
0.1	0.2	2.0	0.3	1.0	1.1022	1.5353×10^{-25}	0.5874	1.0740	0.0071	0.5942
1.0					1.3405	3.9563×10^{-31}	0.5362	1.0865	0.0720	0.5905
2.0					1.5649	9.2869×10^{-24}	0.4977	1.1043	0.1376	0.5845
0.1	-0.5				1.2179	2.7432×10^{-26}	0.8010	1.1895	0.0060	0.8083
	-0.2				1.1668	6.2361×10^{-22}	0.7007	1.1385	0.0064	0.7079
	0.0				1.1340	3.5042×10^{-23}	0.6414	1.1057	0.0067	0.6484
	0.2				1.1022	1.5335×10^{-25}	0.5874	1.0740	0.0071	0.5942
	0.5				1.0563	7.9282×10^{-19}	0.5147	1.0283	0.0073	0.5212
	0.2	1.0			1.0519	8.0031×10^{-26}	0.6046	1.0062	0.0114	0.6131
		2.0			1.1022	1.5353×10^{-25}	0.5874	1.0740	0.0071	0.5942
		5.0			1.1500	9.6847×10^{-25}	0.6174	1.1369	0.0033	0.6227
		2.0	0.1				0.5555			0.5606
			0.3				0.5874			0.5942
			0.5				0.6255			0.6367
			0.3	1.0			0.5874			0.5942
				2.0			0.9188			0.9278
				3.0			1.1706			1.1572

Table 7.4 presents comparative analysis of wall friction factors and local Nusselt number for $n = 1$ (constant stretching) and $n = 5$ (variable stretching) by varying controlling parameter. The nonlinear stretching parameter has tendency to increase the friction of wall in both

directions as well as heat flux. Additionally, Hartmann number is capable to enhance both wall friction factors while it reduces wall heat flux. The influence of wall thickness parameter is exactly oppugnant to Hartmann number effects i.e. it reduces the friction of surface in both directions while enhances the heat flux. The behaviour of all three physical quantities is dual against Hall parameter i.e. they increase for $m \leq 1$ and reduces for $m > 1$. Nusselt number quantitatively enlarges versus both thermal relaxation parameter and Prandtl number.

Table 7.4: Numerical values of $-f''(0)$, $-\theta'(0)$ and $-h'(0)$ by varying M , α , m , γ and Pr while keeping n fixed i.e. $n = 1.0, 5.0$.

					$n = 1.0$			$n = 5.0$		
M	m	α	Pr	γ	$-f''(0)$	$-h'(0)$	$-\theta'(0)$	$-f''(0)$	$-h'(0)$	$-\theta'(0)$
0.1	1.0	0.2	1.0	0.3	1.0287	0.0290	0.6088	1.1432	0.0082	0.6201
1.0					1.2476	0.2261	0.5668	1.2062	0.0799	0.5939
2.0					1.2936	0.2601	0.5583	1.2764	0.1480	0.5655
0.1	1.0				1.0287	0.0290	0.6088	1.1432	0.0082	0.6201
	2.0				1.0142	0.0236	0.6116	1.1391	0.0069	0.6218
	5.0				1.0062	0.0146	0.6131	1.1369	0.0033	0.6227
	10.0				1.0048	0.0059	0.6134	1.1363	0.0003	0.6229
	2.0	-0.2					-	1.2694	0.0089	1.1013
		0.0					-	1.2044	0.0085	0.7906
		0.2					-	1.1432	0.0082	0.6201
		0.5					-	1.0584	0.0081	0.4312
		0.2	1.0				0.6088			0.6201
			2.0				0.9542			1.1470
			3.0				1.2271			1.3085
			1.0	0.1			0.5975			0.5508
				0.3			0.6088			0.6201
				0.5			0.6237			0.7339

Table 7.5 shows contrast of local Nusselt number for classical Fourier's law ($\gamma = 0$) and

Christov-Cattaneo heat flux model ($\gamma = 0.5$) by varying pertinent flow parameters. This table emphasizes that thermal relaxation parameter significantly enhances the heat flux i.e. local Nusselt number has larger magnitude in case of Christov-Cattaneo heat flux model. The behaviour of Nusselt number is enhancing verses Hartmann number while both nonlinearity parameter and wall thickness parameter are responsible for reduction in Nusselt number, also Nusselt number reflects dual nature for Hall parameter.

Table 7.5: Numerical values of $-\theta'(0)$ by varying M , α , n , m and Pr while keeping γ fixed i.e. $\gamma = 0, 0.5$.

					$\gamma = 0.0$	$\gamma = 0.5$
α	m	n	M	Pr	$-\theta'(0)$	$-\theta'(0)$
-0.5	1.0	2.0	0.1	1.0	0.6913	0.9069
-0.2					0.6263	0.7745
0.0					0.5846	0.6991
0.2					0.5444	0.6322
0.5					0.4867	0.5454
0.2	0.5				0.5430	0.6295
	1.0				0.5444	0.6322
	2.0				0.5456	0.6351
	5.0				0.5466	0.6367
	10.0				0.5467	0.6370
	1.0	1.0			0.5929	0.6237
		2.0			0.5444	0.6322
		5.0			0.4976	0.7335
		2.0	0.1		0.5444	0.6322
			1.0		0.5217	0.5878
			2.0		0.5003	0.5455
			0.1	1.0	0.5444	0.6322
				2.0	0.8079	0.8373
				5.0	1.3349	-
				7.0	1.5191	-

7.4 Enumerated key results

In this chapter, a theoretical model is presented to disclose Hall current phenomenon on MHD viscous fluid flow along with Christov-Cattaneo model over variable stretching sheet. The formulated mathematical system is solved with shooting technique. Numerical results are obtained versus controlling parameters i.e. Hartmann number, nonlinearity parameter, Hall parameter, wall thickness parameter, thermal relaxation parameter and Prandtl number. The principal outcomes of current study are highlighted below:

- Fluid velocities sustained an appreciable resistance of strong magnetic field while strength of magnetic field is quite beneficial for fluid temperature. Both wall friction factors grows verses Hartmann number while temperature gradient is reduces against it.
- Hall parameter exerts the opposing force on transverse velocity while it slightly accelerates the axial velocity and declines temperature insignificantly. Coefficients of skin friction and wall heat flux exhibit dual nature verses Hall parameter.
- An increase in wall thickness parameter provoked both velocities and temperature while its significance induces the reduction in wall friction factor and surface heat flux.
- Nonlinearly stretching surface bestowed the favorable situation to fluid movement in axial direction and heat transfer while transverse velocity shows deceleration over it. Additionally, it enhances the axial friction factor and wall heat flux while it has reverse effects on transverse wall friction factor.
- An enhancement in thermal relaxation leads to cooling of fluid while wall heat flux accelerates against it.
- Prandtl number has tendency to depreciate temperature while it enhances wall heat flux.

Chapter 8

On the movement of gravity-driven swimming microorganisms in viscous nanofluid flow

This chapter interprets the thermophysical features of bioconvection flow of gyrotactic swimming microorganisms through viscous nanofluid in the boundary layer regime. Bioconvection occurred because microorganisms are slight denser than base fluid and since they swim in upward direction which causes hydrodynamic instability. The microorganisms are self-propelled which enlarges the fluid density by swimming in a specific direction in the fluid due to gravity, light, or chemical attraction. This kind of problems has been encountered in many biomicrosystems e.g. enzyme biosensor, chip-size micro-devices for evaluating nanoparticle toxicity, the critical functional alveolarcapillary interface of the human lung to evaluate toxic and inflammatory responses of the lung to silica nanoparticles etc. So, the major concern of present chapter is to narrate the properties of gravity-driven swimming microorganisms in MHD viscous nanofluid flow past a stretching surface by taking Joule heating effects into account. The constitutive set of partial differential equations are non-dimensionalized through suitable similarity transformations. The governing non-dimensional partial differential equations are solved with finite element method. The influence of involving parameters on interesting physical quantities are deliberated through graphs.

8.1 Configuration of physical problem

Let assume 2D, steady, incompressible viscous nanofluid flow past through stretching sheet in the presence of gyrotactic swimming microorganisms. The coordinate system is chosen such as x – axis is axial direction while y – axis is normal direction. The sheet is stretching in x –direction with stretching rate $U_0 \frac{cy}{L}$ (here U_0 knows as reference velocity, c is a constant and L is the characteristic length). Magnetic field of strength B_0 is experienced in normal direction. Both electric field as well as induced magnetic fields are neglected. Since, magnetic field is applied to fluid particles they behave like conductor, so Joule heating effects are taken into account. Temperature, nanoparticle volume fraction and motile microorganisms density are kept constant at wall and their magnitudes are T_w , C_w and n_w respectively. Also, away from the sheet the magnitude of these quantities is represented with T_∞ , C_∞ and n_∞ respectively. Also, it is assumed that the presence of nanoparticle does not affects the movement of swimming microorganisms. Further, it is assumed that suspension of nanoparticles is dilute because bioconvection occurred in dilute suspension otherwise large concentration of nanoparticles enhances the base-fluid viscosity which ultimately suppress the bioconvection. Under the Boussinesq approximation, the governing boundary layer equations of mass, momentum, energy, nanoparticle concentration and motile microorganisms concentration are given below (see Refs. [105 – 107])

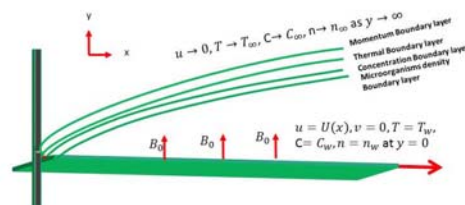


Fig. (8.1): Geometry of the problem.

$$\frac{\partial \bar{u}}{\partial \bar{x}} + \frac{\partial \bar{v}}{\partial \bar{y}} = 0, \quad (8.1)$$

$$\begin{aligned} \bar{u} \frac{\partial \bar{u}}{\partial \bar{x}} + \bar{v} \frac{\partial \bar{u}}{\partial \bar{y}} &= \nu_f \frac{\partial^2 \bar{u}}{\partial \bar{y}^2} + g\beta(1 - C_\infty)(\bar{T} - T_\infty) - \frac{g(\rho_p - \rho_f)}{\rho_f}(\bar{C} - C_\infty) \\ &\quad - \frac{g\gamma(\rho_m - \rho_f)}{\rho_f}(\bar{n} - n_\infty) - \frac{\sigma B_0^2}{\rho_f} \bar{u}, \end{aligned} \quad (8.2)$$

$$\bar{u} \frac{\partial \bar{T}}{\partial \bar{x}} + \bar{v} \frac{\partial \bar{T}}{\partial \bar{y}} = \alpha \frac{\partial^2 \bar{T}}{\partial \bar{y}^2} + \tau(D_B \frac{\partial \bar{C}}{\partial \bar{y}} \cdot \frac{\partial \bar{T}}{\partial \bar{y}} + \frac{D_T}{T_\infty} (\frac{\partial \bar{T}}{\partial \bar{y}})^2) + \frac{\sigma B_0^2}{(\rho c_p)_f} u^2, \quad (8.3)$$

$$\bar{u} \frac{\partial \bar{C}}{\partial \bar{x}} + \bar{v} \frac{\partial \bar{C}}{\partial \bar{y}} = D_B \frac{\partial^2 \bar{C}}{\partial \bar{y}^2} + \frac{D_T}{T_\infty} \frac{\partial^2 \bar{T}}{\partial \bar{y}^2}, \quad (8.4)$$

$$\bar{u} \frac{\partial \bar{n}}{\partial \bar{x}} + \bar{v} \frac{\partial \bar{n}}{\partial \bar{y}} + \frac{bW_c}{(C_w - C_\infty)} \frac{\partial}{\partial \bar{y}} (\bar{n} \frac{\partial \bar{C}}{\partial \bar{y}}) = D_m \frac{\partial^2 \bar{n}}{\partial \bar{y}^2}, \quad (8.5)$$

subjected to boundary conditions

$$\begin{aligned} \bar{u} &= U_0 \frac{c\bar{x}}{L}, \quad \bar{v} = 0, \quad \bar{T} = T_w, \quad \bar{C} = C_w \text{ and } \bar{n} = n_w \text{ at } \bar{y} = 0, \\ \bar{u} &\rightarrow 0, \quad \bar{T} \rightarrow T_\infty, \quad \bar{C} \rightarrow C_\infty \text{ and } \bar{n} \rightarrow n_\infty \text{ at } \bar{y} \rightarrow \infty. \end{aligned} \quad (8.6)$$

In the above set of equations, (\bar{x}, \bar{y}) are cartesian coordinates, (\bar{u}, \bar{v}) are velocity components along (\bar{x}, \bar{y}) , \bar{T} , \bar{C} and \bar{n} are temperature, nanoparticle concentration and density of motile microorganisms respectively, ν_f denotes kinematic viscosity, g called gravitational acceleration, ρ_f , ρ_p and ρ_m are densities of base-fluid, nanoparticle and motile microorganisms respectively. Here α called thermal diffusivity, $\tau = \frac{(\rho c_p)_p}{(\rho c_p)_f}$ is the ratio between nanoparticle and fluid heat capacities, D_B , D_T and D_m are diffusion coefficients of Brownian motion, thermophoresis and motile microorganisms respectively. Also, γ represents the average volume of microorganisms cells, b exhibits coefficient of chemical reaction and W_c is maximum speed of swimming cell.

The governing mathematical system is converted into non-dimensional form with the aid of below defined variables

$$\begin{aligned}
x &= \frac{\bar{x}}{L}, \quad y = \frac{\bar{y}}{L} \text{Re}^{\frac{1}{2}}, \quad u = \frac{\bar{u}}{U_0}, \quad v = \frac{\bar{v}}{U_0} \text{Re}^{\frac{1}{2}}, \quad T = \frac{\bar{T} - T_\infty}{T_w - T_\infty}, \\
C &= \frac{\bar{C} - C_\infty}{C_w - C_\infty} \quad \text{and} \quad n = \frac{\bar{n} - n_\infty}{n_w - n_\infty}.
\end{aligned} \tag{8.7}$$

After incorporating the above defined variables in governing boundary layer equations (Eqs. (8.1) – (8.5)), these are converted into following form

$$\frac{\partial u}{\partial x} + \frac{\partial v}{\partial y} = 0, \tag{8.8}$$

$$u \frac{\partial u}{\partial x} + v \frac{\partial u}{\partial y} = \frac{\partial^2 u}{\partial y^2} + \frac{Gr}{\text{Re}^2} (T - NrC - Rbn) - Mu, \tag{8.9}$$

$$\text{Pr} \left(u \frac{\partial T}{\partial x} + v \frac{\partial T}{\partial y} \right) = \frac{\partial^2 T}{\partial y^2} + \text{Pr} (Nb \frac{\partial C}{\partial y} \cdot \frac{\partial T}{\partial y} + Nt \left(\frac{\partial T}{\partial y} \right)^2 + MEcu^2), \tag{8.10}$$

$$\text{Pr} \text{Le} \left(u \frac{\partial C}{\partial x} + v \frac{\partial C}{\partial y} \right) = \frac{\partial^2 C}{\partial y^2} + \frac{Nt}{Nb} \frac{\partial^2 T}{\partial y^2}, \tag{8.11}$$

$$\text{Pr} \text{Lb} \left(u \frac{\partial n}{\partial x} + v \frac{\partial n}{\partial y} \right) + \text{Pe} \left(\sigma \frac{\partial^2 C}{\partial y^2} + \frac{\partial}{\partial y} \left(n \frac{\partial C}{\partial y} \right) \right) = \frac{\partial^2 n}{\partial y^2}, \tag{8.12}$$

along with the boundary conditions

$$\begin{aligned}
u &= cx, \quad v = 0, \quad T = 1, \quad C = 1 \quad \text{and} \quad n = 1 \quad \text{at} \quad y = 0, \\
u &\rightarrow 0, \quad T \rightarrow 0, \quad C \rightarrow 0 \quad \text{and} \quad n \rightarrow 0 \quad \text{as} \quad y \rightarrow \infty.
\end{aligned} \tag{8.13}$$

Here (x, y) are non-dimensional cartesian coordinates, u, v, T, C and n are non dimensional axial and normal velocity components, temperature, nanoparticles concentration and concentration of microorganisms respectively. Also, $M = \frac{\sigma x B^2}{U \rho}$ is the Hartmann number, $\frac{Gr}{\text{Re}^2} = \frac{g \beta (1 - C_\infty) (T_w - T_\infty) x^3 / \nu^2}{U^2 x^2 / \nu^2}$ represents local Richardson number, $Nr = \frac{(\rho_p - \rho_f) (C_w - C_\infty)}{\rho_f \beta (1 - C_\infty) (T_w - T_\infty)}$ is the buoyancy ratio parameter, $Rb = \frac{\gamma (\rho_m - \rho_\infty) (n_w - n_\infty)}{\rho_f \beta (1 - C_\infty) (T_w - T_\infty)}$ is the bioconvection Rayleigh number, $\text{Pr} = \frac{\nu}{\alpha}$ is the Prandtl number, $Nb = \frac{\tau D_B (C_w - C_\infty)}{\nu}$ is the Brownian motion parameter,

$Nt = \frac{\tau D_T (T_w - T_\infty)}{T_\infty \nu}$ is the thermophoresis parameter, $Ec = \frac{U^2}{C_p (T_w - T_\infty)}$ is the local Eckert number, $Le = \frac{\alpha}{D_B}$ and $Lb = \frac{\alpha}{D_m}$ are the traditional Lewis number and the bioconvection Lewis number respectively, $Pe = \frac{bWc}{D_m}$ is the bioconvection Peclet number and $\sigma = \frac{n_\infty}{(n_w - n_\infty)}$ is the microorganisms concentration difference parameter.

Coefficients of skin friction, wall heat and mass fluxes and motile microorganisms density at wall are defined as

$$C_{fx} = \frac{L\bar{\tau}_w}{\frac{1}{2}\rho U_0^2}, \quad Nu_x = \frac{L\bar{q}_w}{\kappa(T_w - T_\infty)}, \quad Sh_x = \frac{L\bar{q}_m}{D_B(C_w - C_\infty)} \quad \text{and} \quad Nn_x = \frac{L\bar{q}_n}{D_m(n_w - n_\infty)}, \quad (8.14)$$

here $\bar{\tau}_w$, \bar{q}_w , \bar{q}_m and \bar{q}_n symbolized the wall shear stress, wall heat and mass fluxes and wall flux of microorganisms density respectively which are given below

$$\bar{\tau}_w = \mu \left(\frac{\partial \bar{u}}{\partial y} \right)_{y=0}, \quad \bar{q}_w = -\kappa \left(\frac{\partial \bar{T}}{\partial y} \right)_{y=0}, \quad \bar{q}_m = -D_B \left(\frac{\partial \bar{C}}{\partial y} \right)_{y=0} \quad \text{and} \quad \bar{q}_n = -D_m \left(\frac{\partial \bar{n}}{\partial y} \right)_{y=0}. \quad (8.15)$$

After using the non-dimensional variables in *Eqs.* (8.14) – (8.15), we get

$$\frac{1}{2}C_{fx} \text{Re}^{\frac{1}{2}} = \left(\frac{\partial u}{\partial y} \right)_{y=0}, \quad Nu_x \text{Re}^{\frac{1}{2}} = -\left(\frac{\partial T}{\partial y} \right)_{y=0}, \quad Sh_x \text{Re}^{\frac{1}{2}} = -\left(\frac{\partial C}{\partial y} \right)_{y=0} \quad \text{and} \quad Nn_x \text{Re}^{\frac{1}{2}} = -\left(\frac{\partial n}{\partial y} \right)_{y=0}. \quad (8.16)$$

8.2 Finite element method

The governing system i.e. (*Eqs.* (8.8) – (8.12)) along with boundary condition (8.13) is highly nonlinear in nature. To compute the numerical solutions for this system, a numerical technique finite element is utilized. According to this method, firstly governing system is converted into variational or weak form. For this governing equations (*Eqs.* (8.9) – (8.12)) are integrated along y-axis

$$\begin{aligned}
R1 = & \int_0^\infty u \frac{\partial u}{\partial x} \Psi(y) dy + \int_0^\infty v \frac{\partial u}{\partial y} \Psi(y) dy + \int_0^\infty \frac{\partial u}{\partial y} \frac{d\Psi(y)}{dy} dy - \\
& \frac{Gr}{Re^2} \int_0^\infty [T - NrC - R_b n] \Psi(y) dy + \int_0^\infty Mu \Psi(y) dy, \tag{8.17}
\end{aligned}$$

$$\begin{aligned}
R2 = & \Pr \int_0^\infty u \frac{\partial T}{\partial x} \Psi(y) dy + \Pr \int_0^\infty v \frac{\partial T}{\partial y} \Psi(y) dy + \int_0^\infty \frac{\partial T}{\partial y} \frac{d\Psi(y)}{dy} dy - \\
& \Pr \int_0^\infty [Nb \frac{\partial T}{\partial y} \cdot \frac{\partial C}{\partial y} + Nt (\frac{\partial T}{\partial y})^2 + MEcu^2] \Psi(y) dy, \tag{8.18}
\end{aligned}$$

$$\begin{aligned}
R3 = & \Pr Le \int_0^\infty u \frac{\partial C}{\partial x} \Psi(y) dy + \Pr Le \int_0^\infty v \frac{\partial C}{\partial y} \Psi(y) dy + \int_0^\infty \frac{\partial C}{\partial y} \frac{d\Psi(y)}{dy} dy + \\
& \frac{Nt}{Nb} \int_0^\infty \frac{\partial T}{\partial y} \frac{d\Psi(y)}{dy} dy, \tag{8.19}
\end{aligned}$$

$$\begin{aligned}
R4 = & \Pr Lb \int_0^\infty u \frac{\partial n}{\partial x} \Psi(y) dy + \Pr Lb \int_0^\infty v \frac{\partial n}{\partial y} \Psi(y) dy + \int_0^\infty \frac{\partial n}{\partial y} \frac{d\Psi(y)}{dy} dy + Pe\sigma \int_0^\infty \frac{\partial C}{\partial y} \frac{d\Psi(y)}{dy} dy \\
& + Pe \int_0^\infty (n \frac{\partial C}{\partial y}) \frac{d\Psi(y)}{dy} dy. \tag{8.20}
\end{aligned}$$

The integrals can be decomposed into sum of sub-integrals (i.e. domain of integration is subdivided into finite number of elements)

$$\begin{aligned}
R1 = & \sum_{e=1}^N [\int_e u \frac{\partial u}{\partial x} \Psi(y) dy + \int_e v \frac{\partial u}{\partial y} \Psi(y) dy + \int_e \frac{\partial u}{\partial y} \frac{d\Psi(y)}{dy} dy \\
& - \frac{Gr}{Re^2} \int_e (T - NrC - R_b n) \Psi(y) dy + M \int_e u \Psi(y) dy, \tag{8.21}
\end{aligned}$$

$$\begin{aligned}
R2 = & \sum_{e=1}^N [\Pr \int_e u \frac{\partial T}{\partial x} \Psi(y) dy + \Pr \int_e v \frac{\partial T}{\partial y} \Psi(y) dy + \int_e \frac{\partial T}{\partial y} \frac{d\Psi(y)}{dy} dy \\
& - \Pr \int_e [Nb \frac{\partial T}{\partial y} \cdot \frac{\partial C}{\partial y} + Nt (\frac{\partial T}{\partial y})^2 + MEcu^2] \Psi(y) dy], \tag{8.22}
\end{aligned}$$

$$\begin{aligned}
R3 = & \sum_{e=1}^N [\text{Pr } Le \int_e u \frac{\partial C}{\partial x} \Psi(y) dy + \text{Pr } Le \int_e v \frac{\partial C}{\partial y} \Psi(y) dy + \int_e \frac{\partial C}{\partial y} \frac{d\Psi(y)}{dy} dy \\
& + \frac{Nt}{Nb} \int_e \frac{\partial T}{\partial y} \frac{d\Psi(y)}{dy} dy], \tag{8.23}
\end{aligned}$$

$$\begin{aligned}
R4 = & \sum_{e=1}^N [\text{Pr } Lb \int_0^\infty u \frac{\partial n}{\partial x} \Psi(y) dy + \text{Pr } Lb \int_0^\infty v \frac{\partial n}{\partial y} \Psi(y) dy + \int_0^\infty \frac{\partial n}{\partial y} \frac{d\Psi(y)}{dy} dy \\
& + Pe\sigma \int_0^\infty \frac{\partial C}{\partial y} \frac{d\Psi(y)}{dy} dy + Pe \int_e (n \frac{\partial C}{\partial y}) \frac{d\Psi(y)}{dy} dy], \tag{8.24}
\end{aligned}$$

here $\Psi(y)$ is the global testing function.

Now, the global coordinate (i.e. y) is transformed into local coordinate (i.e. s) by using following relations

$$y = y_l + (s + 1)(y_r - y_l)/2 \text{ and } dy = [(y_r - y_l)/2]ds = Jds, \tag{8.25}$$

where y_l and y_r are the left and right endpoints of element.

In local coordinates the residuals take the below-defined form

$$\begin{aligned}
R1 = & \sum_{e=1}^N [\int_{-1}^1 u \frac{\partial u}{\partial x} \Psi(s) J ds + \int_{-1}^1 v \frac{\partial u}{\partial y} \Psi(s) J ds + \int_{-1}^1 \frac{\partial u}{\partial y} \frac{d\Psi(s)}{ds} ds - \\
& \frac{Gr}{Re^2} \int_{-1}^1 (T - NrC - R_b n) \Psi(s) J ds + M \int_{-1}^1 u \Psi(s) J ds], \tag{8.26}
\end{aligned}$$

$$\begin{aligned}
R2 = & \sum_{e=1}^N [\text{Pr} \int_{-1}^1 u \frac{\partial T}{\partial x} \Psi(s) J ds + \text{Pr} \int_{-1}^1 v \frac{\partial T}{\partial s} \Psi(s) ds + \int_{-1}^1 \frac{\partial T}{\partial s} \frac{d\Psi(s)}{ds} \frac{ds}{J} - \\
& \text{Pr } Nb \int_{-1}^1 \frac{\partial T}{\partial s} \cdot \frac{\partial C}{\partial s} \Psi(s) \frac{ds}{J} - \text{Pr } Nt \int_{-1}^1 (\frac{\partial T}{\partial s})^2 \Psi(s) \frac{ds}{J} - \text{Pr } MEc \int_{-1}^1 u^2 \Psi(s) J ds], \tag{8.27}
\end{aligned}$$

$$\begin{aligned}
R3 = & \sum_{e=1}^N [\text{Pr} L e \int_{-1}^1 u \frac{\partial C}{\partial x} \Psi(s) J ds + \text{Pr} L e \int_{-1}^1 v \frac{\partial C}{\partial s} \Psi(s) ds + \int_{-1}^1 \frac{\partial C}{\partial s} \frac{d\Psi(s)}{ds} \frac{ds}{J} \\
& + \frac{Nt}{Nb} \int_{-1}^1 \frac{\partial T}{\partial s} \frac{d\Psi(s)}{ds} \frac{ds}{J}], \tag{8.28}
\end{aligned}$$

$$\begin{aligned}
R4 = & \sum_{e=1}^N [\text{Pr} L b \int_{-1}^1 u \frac{\partial n}{\partial x} \Psi(s) J ds + \text{Pr} L b \int_{-1}^1 v \frac{\partial n}{\partial s} \Psi(s) ds + \int_{-1}^1 \frac{\partial n}{\partial s} \frac{d\Psi(s)}{ds} \frac{ds}{J} \\
& + P e \sigma \int_{-1}^1 \frac{\partial C}{\partial s} \frac{d\Psi(s)}{ds} \frac{ds}{J} + P e \int_{-1}^1 (n \frac{\partial C}{\partial s}) \frac{d\Psi(s)}{ds} \frac{ds}{J}]. \tag{8.29}
\end{aligned}$$

To solve the integrals in above set of residuals, the interested physical quantities are defined in the form of interpolation polynomials

$$\begin{aligned}
u &= \sum_{e=1}^n U_n(x) \Psi_n(s), \quad v = \sum_{e=1}^n V_n(x) \Psi_n(s), \quad T = \sum_{e=1}^n T_n(x) \Psi_n(s), \\
C &= \sum_{e=1}^n C_n(x) \Psi_n(s), \quad n = \sum_{e=1}^n N_n(x) \Psi_n(s). \tag{8.30}
\end{aligned}$$

By using the above set of variables, the residuals is converted into following form

$$\begin{aligned}
R1_m = & \sum_{e=1}^N [\int_{-1}^1 (\sum_{n=1}^{n_e} U_n \Psi_n(s)) (\sum_{l=1}^{n_e} \frac{dU_l}{dx} \Psi_l(s)) \Psi_m(s) J ds + \int_{-1}^1 (\sum_{n=1}^{n_e} V_n \Psi_n(s)) (\sum_{l=1}^{n_e} U_l \frac{d\Psi_l(s)}{ds}) \Psi_m(s) ds \\
& + \int_{-1}^1 (\sum_{n=1}^{n_e} U_n \frac{d\Psi_n(s)}{ds}) \frac{d\Psi_m(s)}{ds} \frac{ds}{J} - \frac{Gr}{\text{Re}^2} \int_{-1}^1 (\sum_{n=1}^{n_e} T_n \Psi_n(s) - Nr \sum_{n=1}^{n_e} C_n \Psi_n(s) - \\
& R_b \sum_{n=1}^{n_e} N_n \Psi_n(s)) \Psi_m(s) J dS - M \int_{-1}^1 \sum_{n=1}^{n_e} U_n \Psi_n(s) \Psi_m(s) J dS], \tag{8.31}
\end{aligned}$$

$$\begin{aligned}
R2_m = & \sum_{e=1}^N \{ \int_{-1}^1 \Pr(\sum_{n=1}^{n_e} U_n \Psi_n(s)) (\sum_{l=1}^{n_e} \frac{dT_l}{dx} \Psi_l(s)) \Psi_m(s) J ds + \int_{-1}^1 (\sum_{n=1}^{n_e} V_n \Psi_n(s)) (\sum_{l=1}^{n_e} T_l \frac{d\Psi_l(s)}{ds}) \Psi_m(s) ds \} \\
& + \int_{-1}^1 (\sum_{n=1}^{n_e} T_n \frac{d\Psi_n(s)}{ds}) \frac{d\Psi_m(s)}{ds} \frac{ds}{J} - \Pr Nb \int_{-1}^1 (\sum_{n=1}^{n_e} T_n \frac{d\Psi_n(s)}{ds}) \cdot (\sum_{l=1}^{n_e} C_l \frac{d\Psi_l(s)}{ds}) \Psi_m(s) \frac{ds}{J} \\
& - \Pr Nt \int_{-1}^1 (\sum_{n=1}^{n_e} T_n \frac{d\Psi_n(s)}{ds}) \cdot (\sum_{l=1}^{n_e} T_l \frac{d\Psi_l(s)}{ds}) \Psi_m(s) \frac{ds}{J} \\
& - \Pr MEc \int_{-1}^1 (\sum_{n=1}^{n_e} U_n \Psi_n(s)) \cdot (\sum_{l=1}^{n_e} U_l \Psi_l(s)) \Psi_m(s) J ds, \tag{8.32}
\end{aligned}$$

$$\begin{aligned}
R3_m = & \sum_{e=1}^N [\Pr Le \{ \int_{-1}^1 (\sum_{n=1}^n U_n \Psi_n(s)) (\sum_{e=1}^l \frac{dC_l}{dx} \Psi_l(s)) \Psi_m(s) J ds + \int_{-1}^1 (\sum_{n=1}^n V_n \Psi_n(s)) (\sum_{e=1}^l C_l \frac{d\Psi_l(s)}{ds}) \Psi_m(s) ds \} \\
& + \int_{-1}^1 (\sum_{e=1}^n C_n \frac{d\Psi_n(s)}{ds}) \frac{d\Psi_m(s)}{ds} \frac{ds}{J} + \frac{Nt}{Nb} \int_{-1}^1 (\sum_{e=1}^n T_n \frac{d\Psi_n(s)}{ds}) \frac{d\Psi_m(s)}{ds} \frac{ds}{J}], \tag{8.33}
\end{aligned}$$

$$\begin{aligned}
R4_m = & \sum_{e=1}^N [\Pr Lb \{ \int_{-1}^1 (\sum_{n=1}^n U_n \Psi_n(s)) (\sum_{e=1}^l \frac{dN_l}{dx} \Psi_l(s)) \Psi_m(s) J ds + \int_{-1}^1 (\sum_{n=1}^n V_n \Psi_n(s)) (\sum_{e=1}^l C_l \frac{d\Psi_l(s)}{ds}) \Psi_m(s) ds \} \\
& + \int_{-1}^1 (\sum_{e=1}^n N_n \frac{d\Psi_n(s)}{ds}) \frac{d\Psi_m(s)}{ds} \frac{ds}{J} + Pe\sigma \int_{-1}^1 (\sum_{e=1}^n C_n \frac{d\Psi_n(s)}{ds}) \frac{d\Psi_m(s)}{ds} \frac{ds}{J} \\
& + Pe \int_{-1}^1 (\sum_{e=1}^n N_n \Psi_n(s)) (\sum_{e=1}^l C_l \frac{d\Psi_l(s)}{ds}) \frac{d\Psi_m(s)}{ds} \frac{ds}{J}], \tag{8.34}
\end{aligned}$$

The local testing functions are defined below respectively

$$\Psi_1(s) = (1 - s)/2 \text{ and } \Psi_2(s) = (1 + s)/2, \tag{8.35}$$

Now the integrals in the residuals are solved through Gaussian quadrature formulas. We have to compute such values of U_n , V_n , T_n , C_n and N_n for which $\max(|R|) < 10^{-12}$.

8.3 Results and discussion

8.3.1 Validity of computed results

The flow govern equations are solved with finite element scheme in two-dimensional domain (x, y) . To check the accuracy and validity of the method, we allocated the fix values to controlling physical parameters ($Gr = Re = Ec = Pr = 1.0$, $Nt = Nb = 0.2$, $M = 0.5$, $Le = Lb = Pe = 1.0$, $Nr = Rb = \sigma = 0.1$) and varying the step sizes along x -axis and y -axis. The computed results of interested physical quantities (velocity u , temperature T , concentration C and motile microorganisms density n) are plotted via **Figs. (8.2)-(8.9)**. In **Fig. (8.2)**, we fixed the step size along y (considering number of elements is 300) and varying the step size along x i.e. $dx = 0.05, 0.1, 0.2$. It can be observed from **Fig. (8.2)** that the results of velocity are agreed quite well for different step size. On the other hand, in **Fig. (8.3)**, the step-size along x is fixed while number of elements are varies. It could be seen that by increasing number of elements from 300, the results for velocity profile remained similar. This means that 300 number of elements are enough to compute the results of this problem. **Figs. (8.4)-(8.9)** deliberated the similar results for temperature, concentration and microorganisms density. These results assured the accuracy and validity of the applied method for this set of equations.

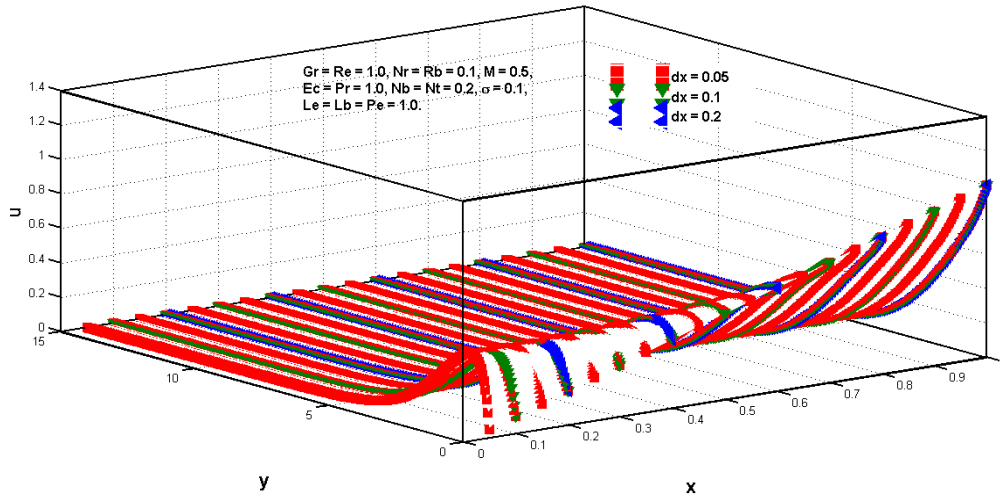


Fig. 8.2: Axial velocity u for different step size along x -axis.

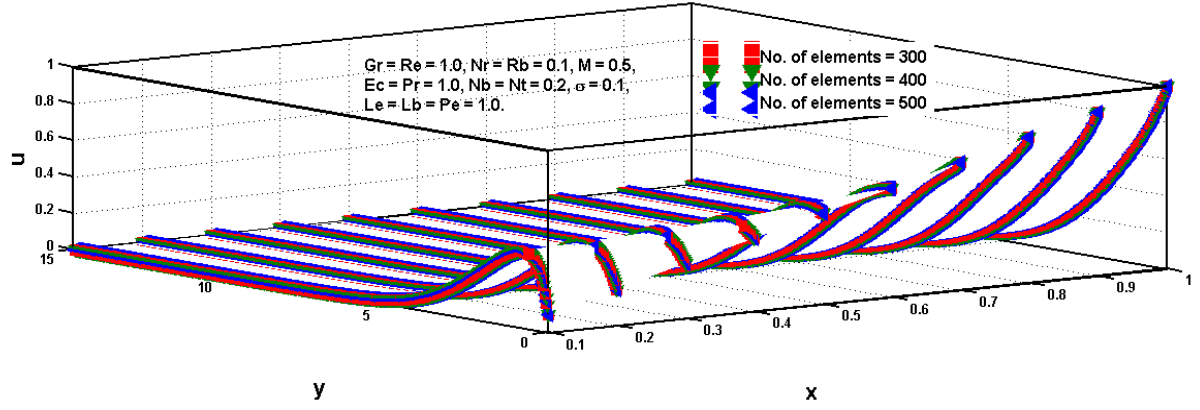


Fig. 8.3: Axial velocity u for different step size along y -axis.

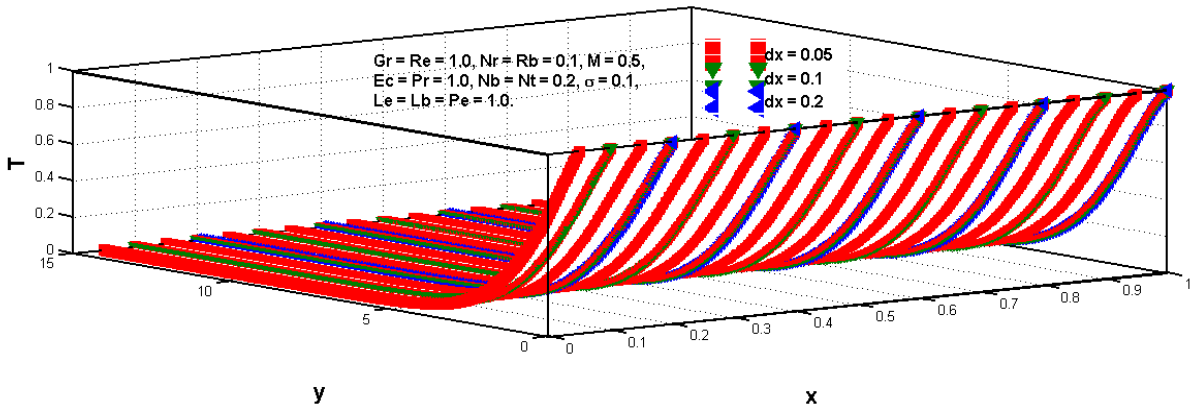


Fig. 8.4: Temperature T for different step size along x -axis.

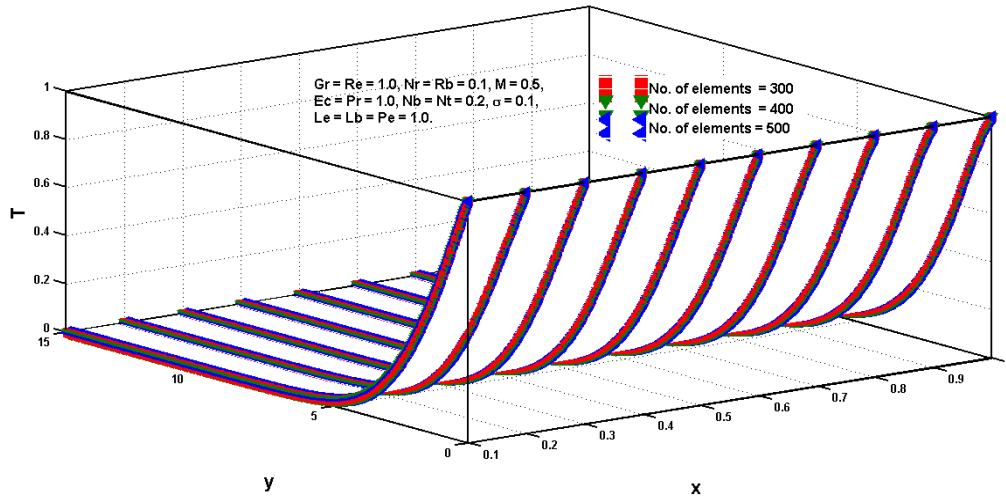


Fig. 8.5: Temperature T for different step size along y -axis.

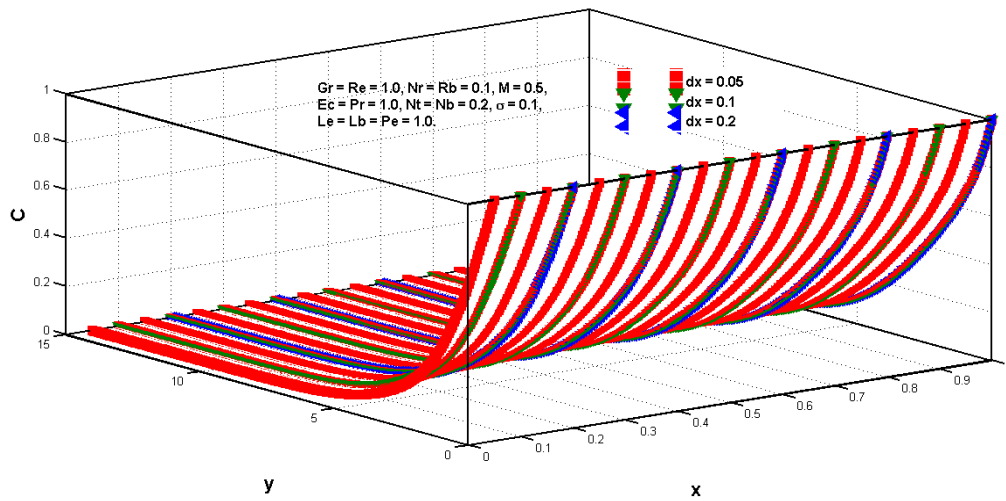


Fig. 8.6: Nanoparticles concentration C for different step size along x -axis.

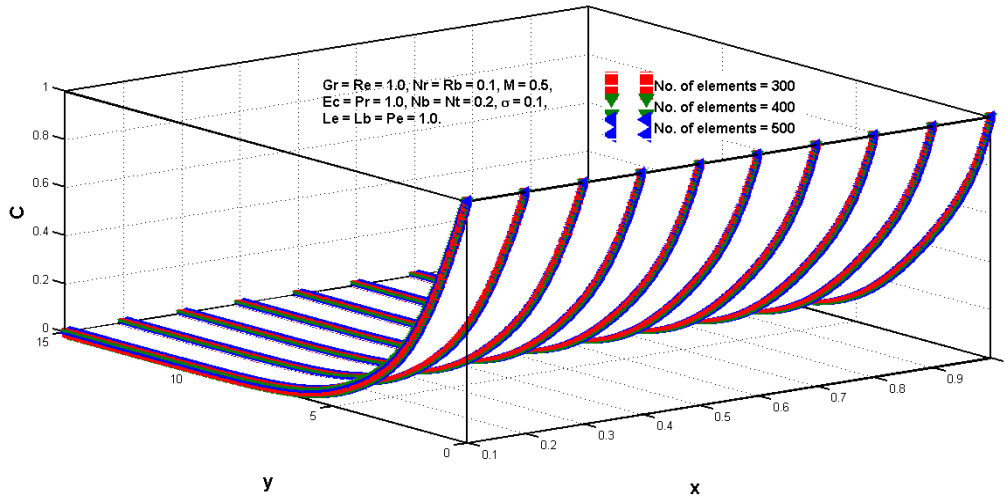


Fig. 8.7: Nanoparticles concentration C for different step size along y -axis.

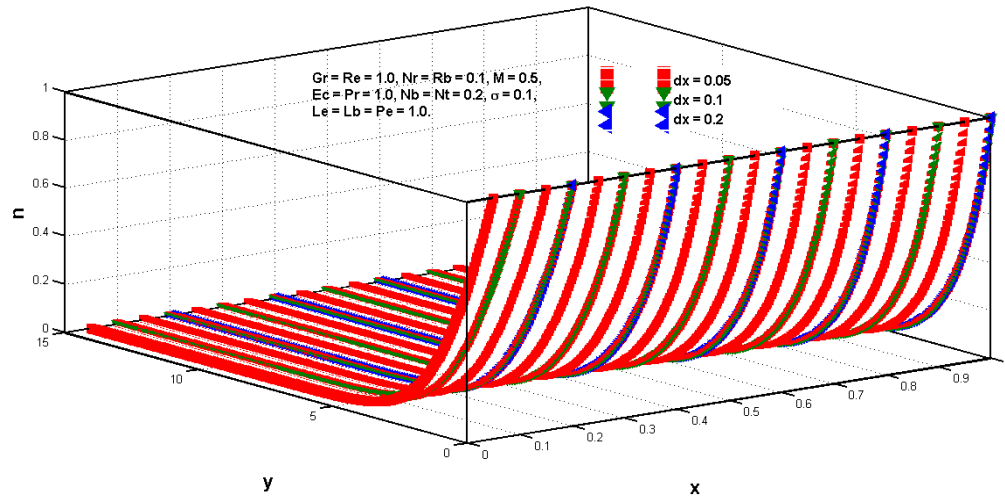


Fig. 8.8: Motile microorganisms density n for different step size along x -axis.

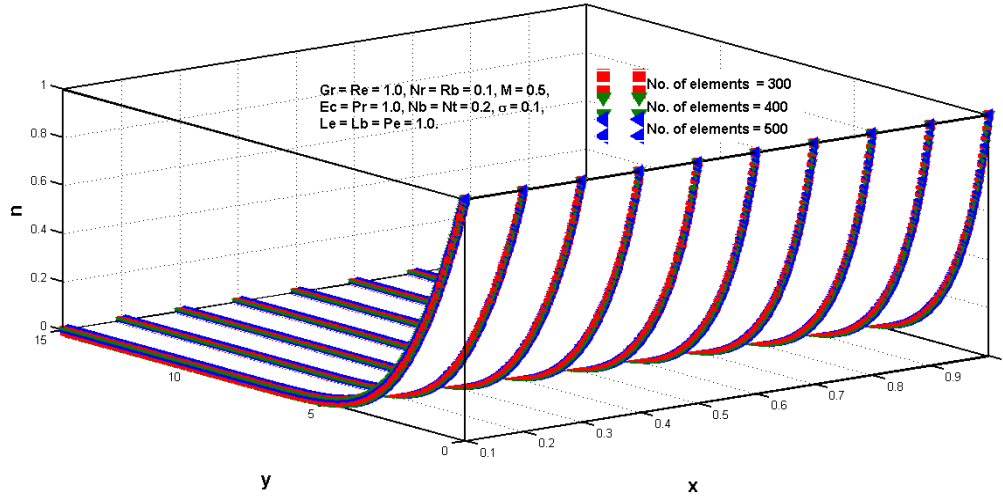


Fig. 8.9: Motile microorganisms density n for different step size along y -axis.

8.3.2 Axial Velocity Profile

Figs. (8.10)-(8.13) reflect the fluid momentum verses controlling parameters (Gr , Nr , Rb and M) on axial velocity. **Fig. (8.10)** delineates the Grashof number impacts on fluid velocity, this figure shows that for increasing values Grashof number the velocity is increasing near the sheet surface while opposite behaviour has been captured in free stream region. **Fig. (8.11)** elaborates buoyancy ratio parameter influences on horizontal velocity. The buoyance ratio parameter accelerates velocity near the surface while velocity is decelerated in far away region. **Fig. (8.12)** depicts bioconvection Rayleigh number effects on horizontal velocity profile. This graph predicts that larger values of bioconvection Rayleigh number opposed the fluid movement in surface vicinity while it increases velocity near the boundary layer region. **Fig. (8.13)** elaborates the Hartmann number effects on axial velocity, it could be seen that Hartmann number decreases the velocity near the surface but its effects are opposite near the boundary layer region.

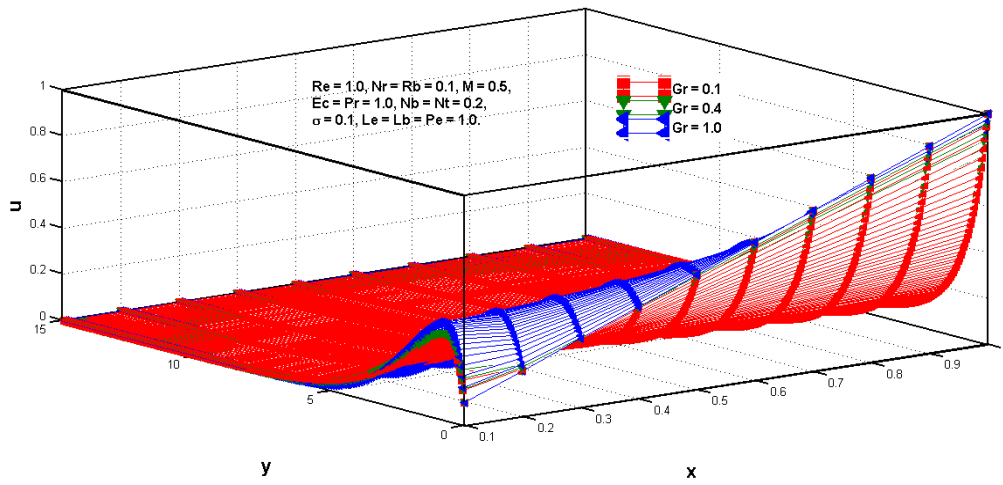


Fig. 8.10: Axial velocity u versus Grashof number Gr .

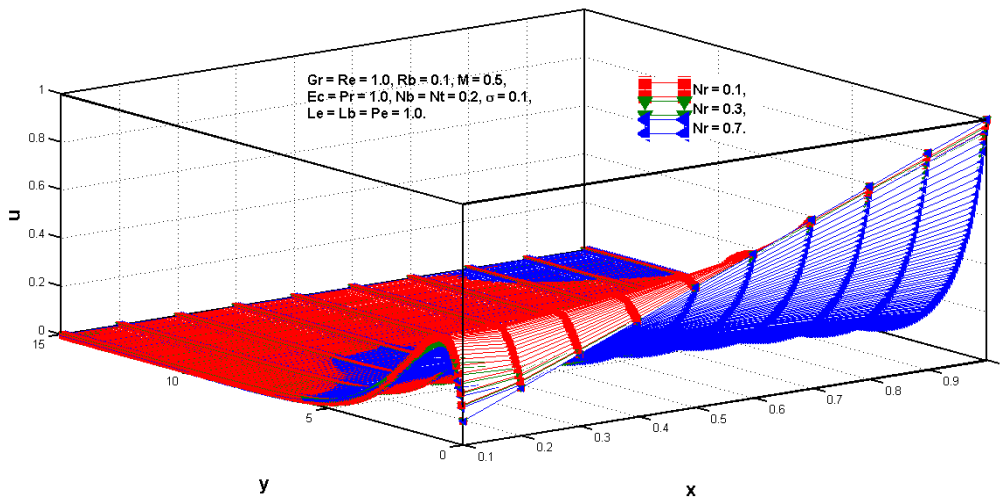


Fig. 8.11: Axial velocity u against buoyancy ratio parameter Nr .

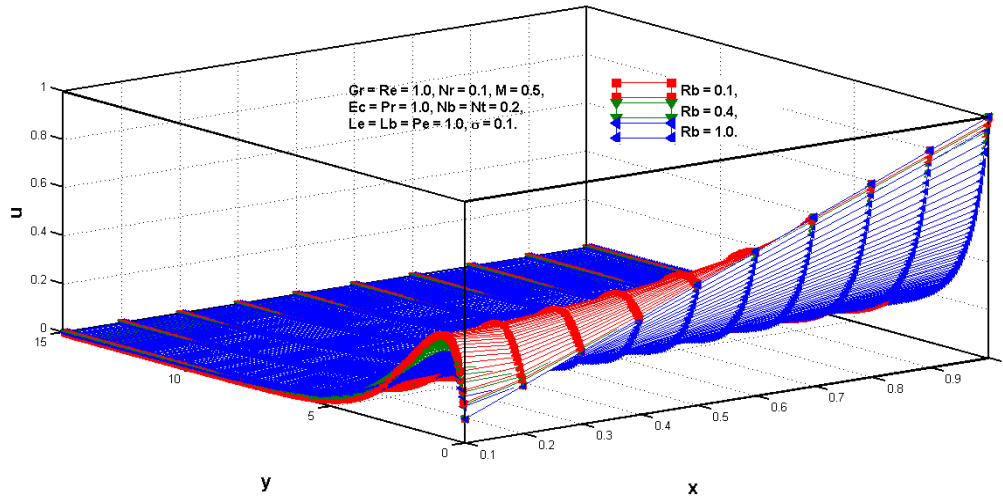


Fig. 8.12: Axial velocity u for different values of bioconvection Rayleigh number Rb .

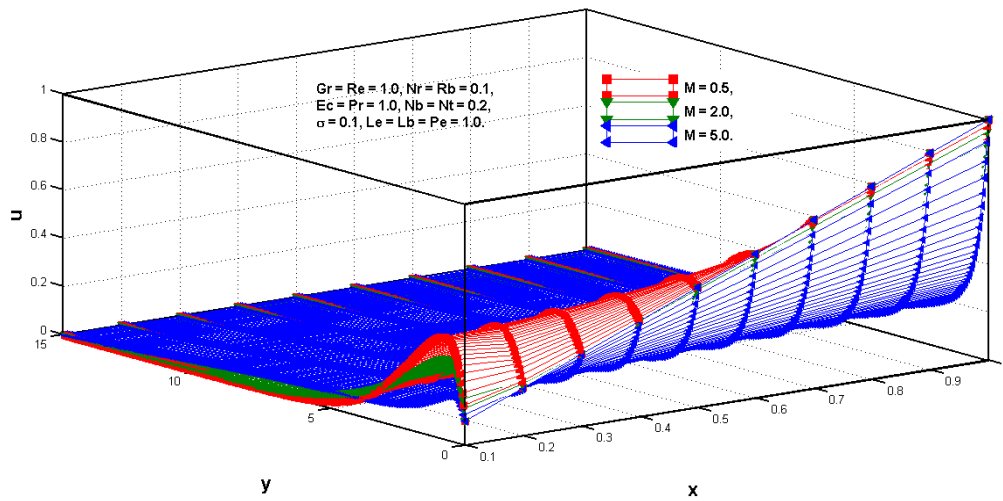


Fig. 8.13: Axial velocity u for different Hartmann number M .

Temperature Profile

Figs. (8.14)-(8.17) disclose the consequences of involving physical parameters (Nb , Nt , Ec and M) on temperature profile. **Fig. (8.14)** validates the interesting results of thermodynamics that Brownian motion causes enhancement in the fluid temperature. **Fig. (8.15)** also suggests that the thermophoresis phenomenon rise fluid temperature in away from surface. Eckert number impacts on temperature are demonstrated through **Fig. (8.16)**. This figure shows that Eckert number rises fluid temperature. **Fig. (8.17)** is responsible to reveal the outcomes of temperature versus Hartmann number. Hartmann number enhances the temperature profile significantly in far away region (see graph).

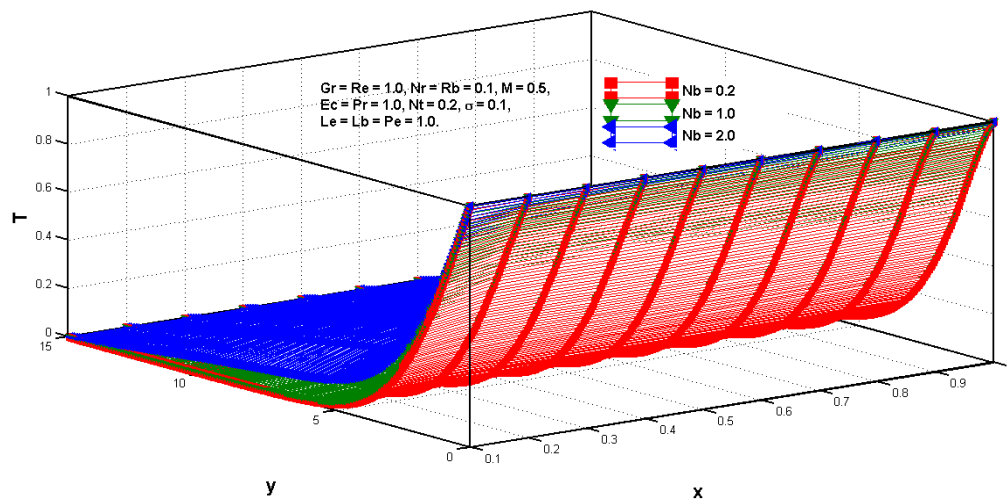


Fig. 8.14: Temperature T for different values of Brownian motion parameter Nb .

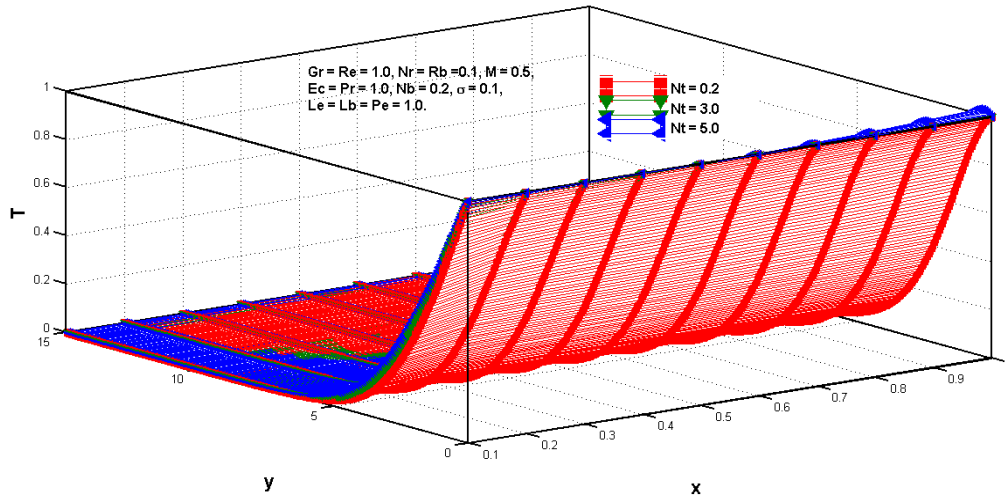


Fig. 8.15: Temperature T for different values of thermophoresis parameter Nt .

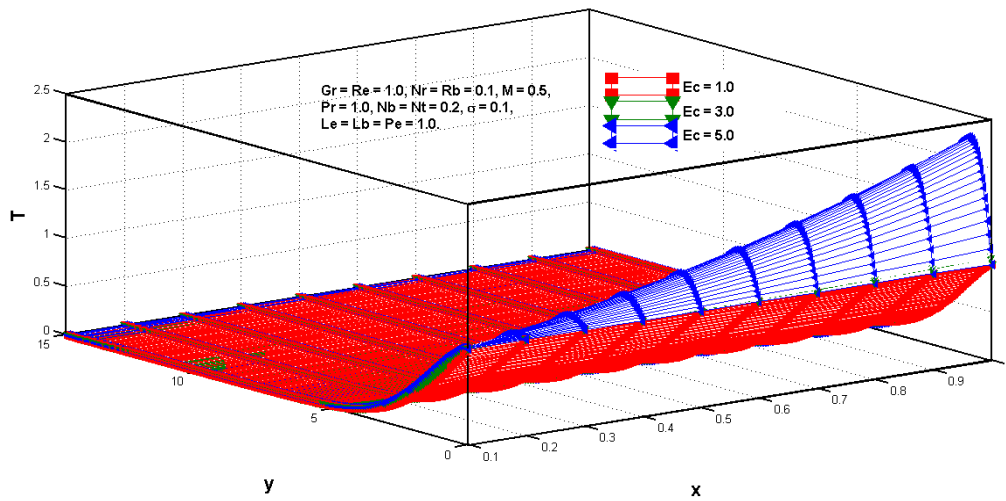


Fig. 8.16: Temperature T for different values of Eckert number Ec .

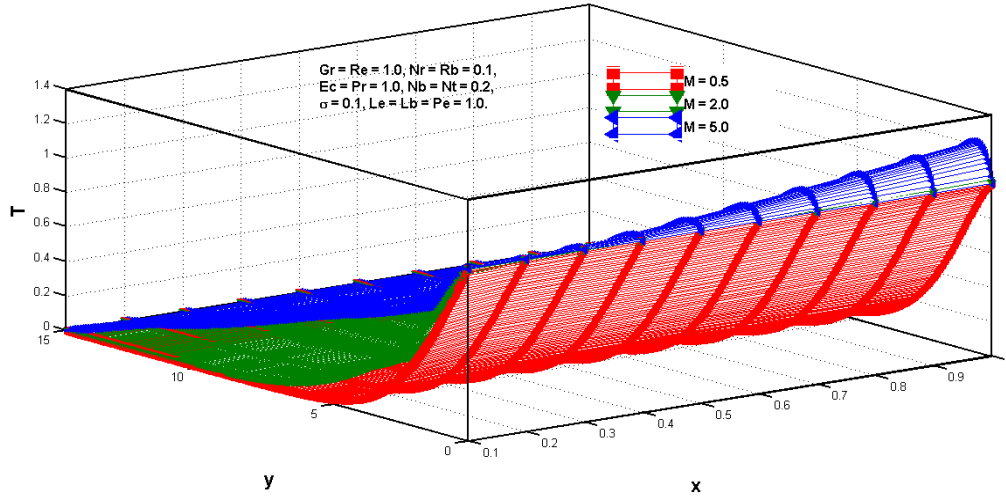


Fig. 8.17: Temperature T for different values of Hartmann number M .

8.3.3 Concentration profile

The outcomes of thermophysical parameters on nanoparticles concentration are captured in **Figs. (8.18)-(8.21)**. **Fig. (8.18)** deliberates the influences of buoyancy ratio parameter on concentration profile. This figure forecasted that the buoyancy ratio parameter enlarges the concentration of nanoparticles in far away region. The consequences of Brownian motion on concentration profile are shown via **Fig. (8.19)**. The computed results reveals that the Brownian motion causes reduction in the concentration profile. The outcomes of nanoparticles concentration against variations in thermophoresis parameter are displayed in **Fig. (8.20)**. This figure shows that the thermophoresis phenomenon enhances the concentration profile. **Fig. (8.21)** discloses that the traditional Lewis number decreases the nanoparticles concentration significantly.

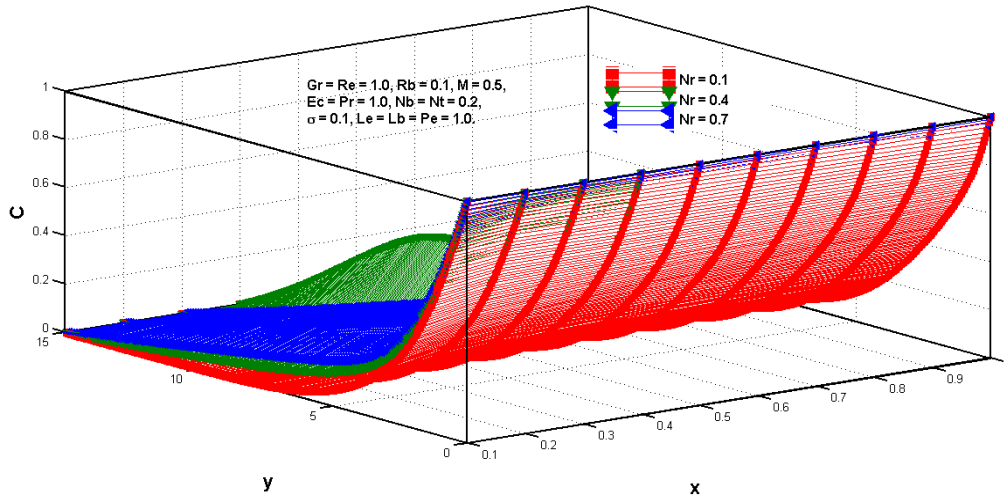


Fig. 8.18: Concentration C for different values of buoyancy ratio parameter Nr .

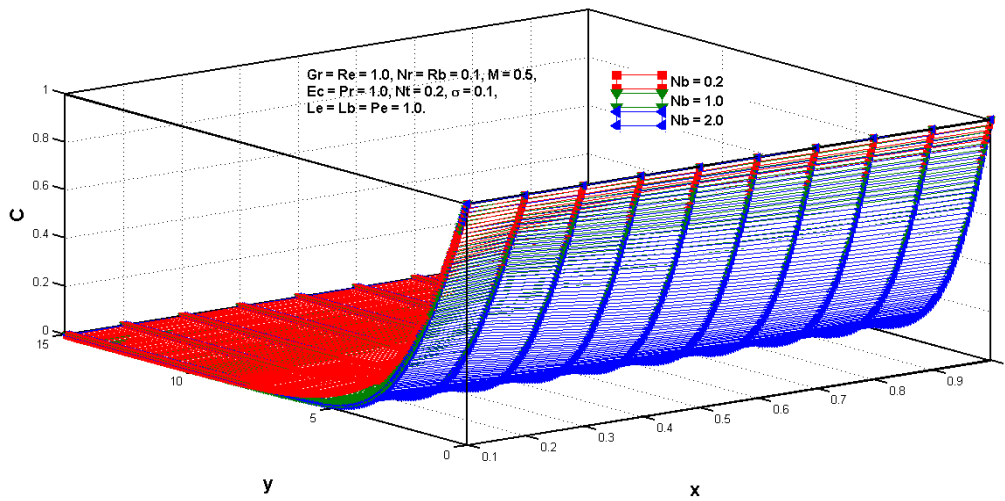


Fig. 8.19: Concentration C for different values of Brownian motion parameter Nb .

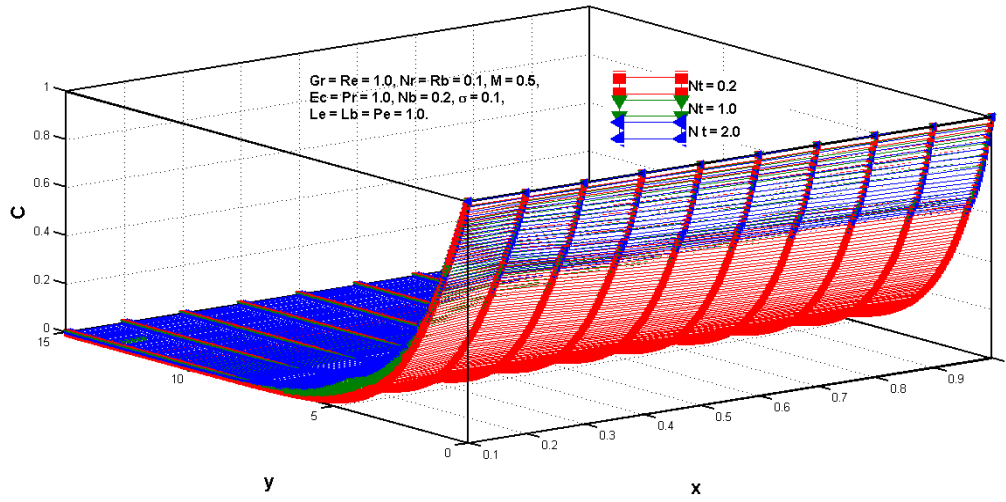


Fig. 8.20: Concentration C for different values of thermophoresis parameter Nt .

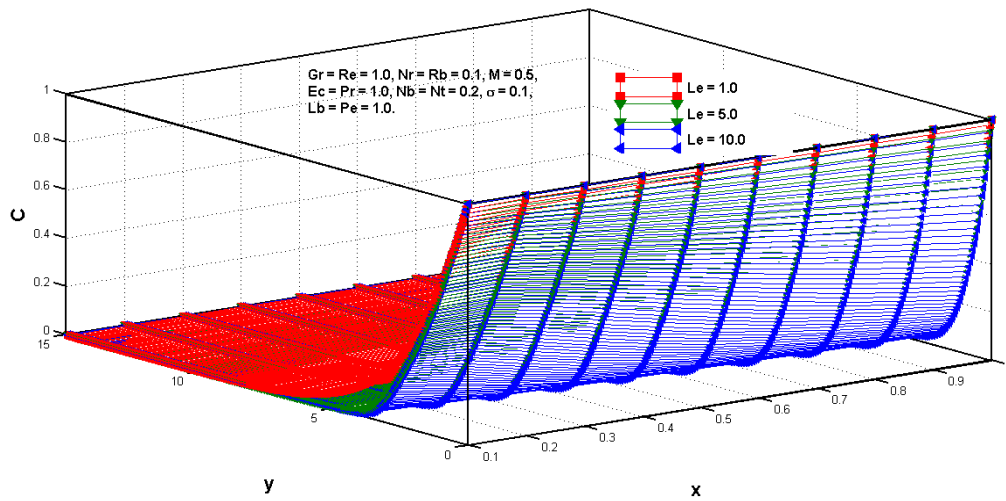


Fig. 8.21: Concentration C for different values of Lewis number Le .

8.3.4 Motile microorganisms density

The impacts of governing parameters on motile microorganisms density are analyzed with the aid of **Figs. (8.22)-(8.25)**. **Fig. (8.22)** manifests that the bioconvection Rayleigh number enhances the density of motile microorganisms. **Fig. (8.23)** displays the effects of bioconvection Lewis number on density of motile microorganisms. One can find that bioconvection Lewis number decreases the density in far away region. **Fig. (8.24)** reflects the variations in density function versus increasing values of bioconvection Peclet number. This figure shows that the bioconvection Peclet number declines the density of microorganisms. **Fig. (8.25)** exhibits the effects of average density parameter on motile microorganism density. It can be observed that by increasing average density of motile microorganisms, the total density decreases.

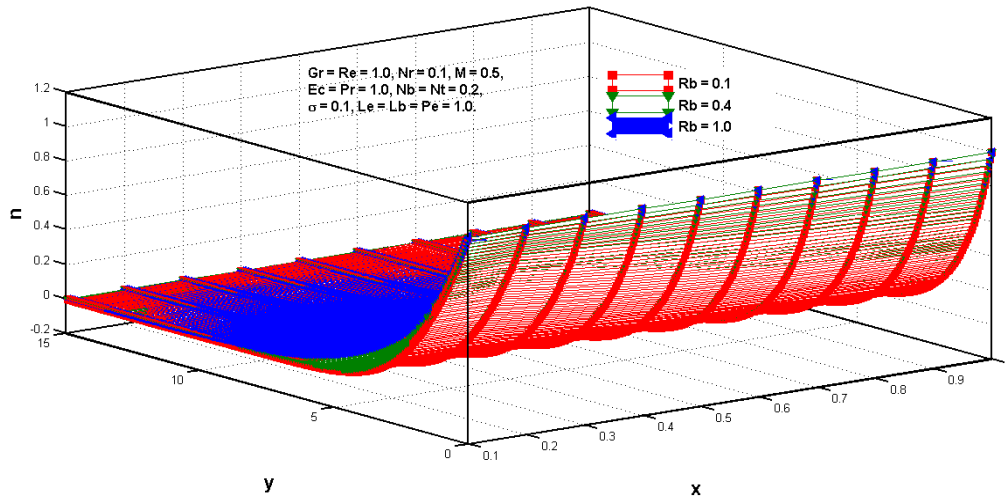


Fig. 8.22: Microorganisms density n for different values of bioconvection Rayleigh number Rb .

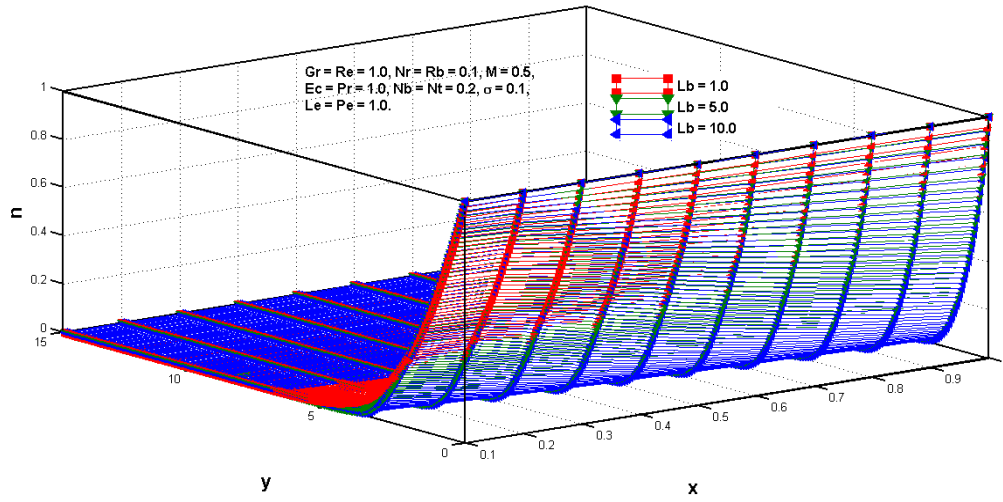


Fig. 8.23: Microorganisms density n for different values of bioconvection Lewis number Lb .

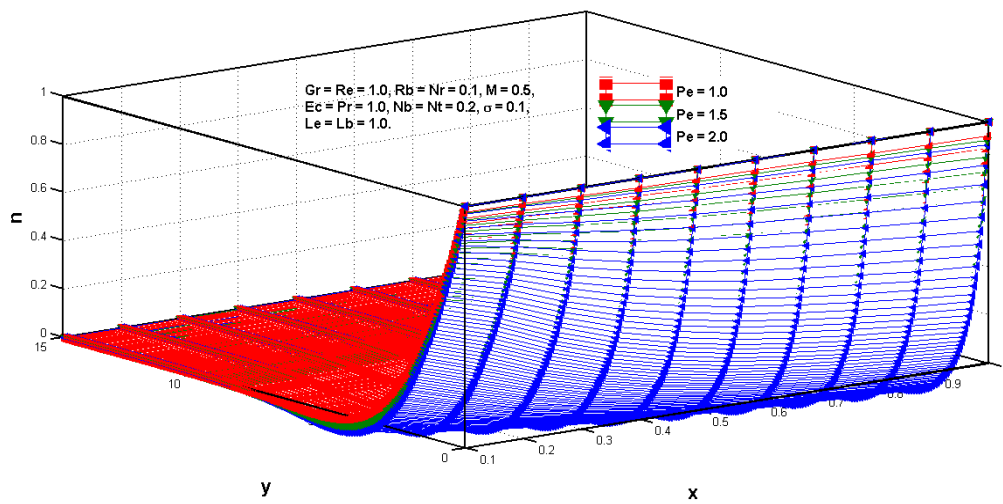


Fig. 8.24: Microorganisms density n for different values of Peclet number Pe .

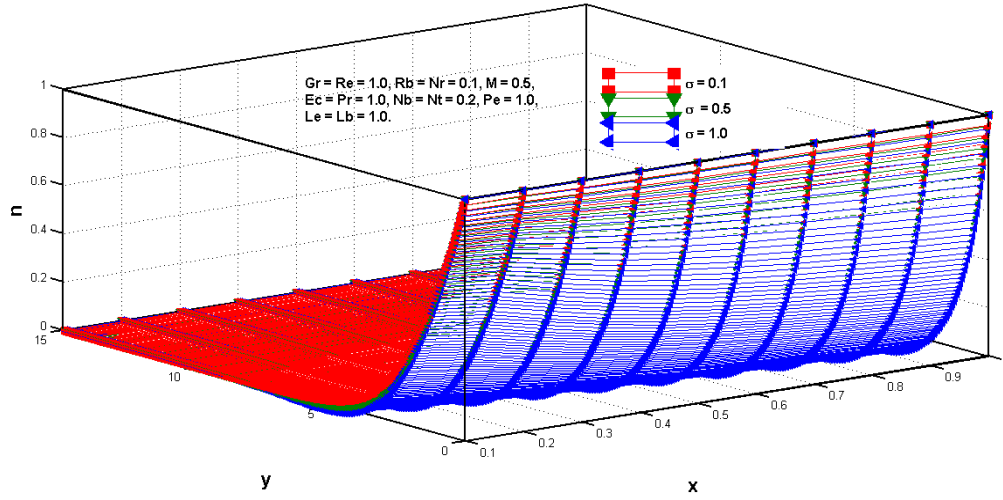


Fig. 8.25: Microorganisms density n for different values of σ .

8.3.5 Wall friction factor, wall heat flux, wall mass flux and wall microorganisms density flux

Tables 8.1-8.4 demonstrate the effects of physical parameters on the interested physical quantities in the vicinity of surface i.e. wall friction factor, wall heat flux, wall mass flux and wall microorganisms density flux. **Table 8.1** consists the numerical values of wall friction factor against variations in the controlling parameters (Gr , Nr , Rb and M). It can be seen that friction of wall is decreased along x -axis, also, one can observed that all physical parameters (Gr , Nr , Rb and M) increase wall friction. **Table 8.2** discloses the consequences of thermophysical parameters on wall heat flux. The heat transfer rate enhances away from the origin along x -axis. This table predicts that the wall heat flux decreases for all thermal parameters. The impacts of governing parameters on wall mass flux could be investigated through **Table 8.3**. One can seen that the physical parameters Nb , Nt and Le enhance the wall mass flux while opposite behaviour is observed versus Nr . Also, it is observed that wall mass flux enlarges as marching along x -axis. **Table 8.4** manifests the outcomes of the physical parameters on the microorganisms density flux at surface. The density flux enhances in the away region along

x -axis from the origin. Also, this table suggests that the physical parameters (Lb , Pe and σ) enhance wall microorganisms density flux, on the other hand, the bioconvection Rayleigh number is declines wall density flux.

Table 8.1: Wall friction factor i.e. $\frac{1}{2} \text{Re}_x^{\frac{1}{2}} C_{f_x}$ by varying parameters (Gr , Nr , Rb and M).

	Gr		Nr		Rb		M	
dx	0.1	1.0	0.1	0.7	0.1	0.7	0.5	2.0
0.1	0.7525	0.9216	0.7525	0.7825	0.7525	0.7847	0.7525	0.8059
0.2	0.1183	0.4557	0.1183	0.1851	0.1183	0.1985	0.1183	0.2027
0.3	-0.1077	0.2973	-0.1077	-0.0232	-0.1077	0.0043	-0.1077	0.0287
0.4	-0.2613	0.1774	-0.2613	-0.1686	-0.2613	-0.1362	-0.2613	-0.1155
0.5	-0.3934	0.0657	-0.3934	-0.2973	-0.3934	-0.2402	-0.3934	-0.2543
0.6	-0.5162	-0.0431	-0.5162	-0.4194	-0.5162	-0.3481	-0.5126	-0.3914
0.7	-0.6341	-0.1505	-0.6341	-0.5379	-0.6341	-0.4534	-0.6341	-0.5275
0.8	-0.7491	-0.2568	-0.7491	-0.6542	-0.7491	-0.5574	-0.7491	-0.6628
0.9	-0.8623	-0.3624	-0.8623	-0.7689	-0.8623	-0.6608	-0.8623	-0.7974
1.0	-0.9744	-0.4673	-0.9744	-0.8825	-0.9744	-0.7637	-0.9744	-0.9313

Table 8.2: Wall heat flux $\text{Re}_x^{-\frac{1}{2}} Nu_x$ against physical parameters (Nb , Nt , Ec and M).

	Nb		Nt		M		Ec	
dx	0.2	2.0	0.2	3.0	0.5	2.0	0.1	5.0
0.1	0.3454	0.1640	0.3454	0.1485	0.3454	0.2278	0.3454	0.2070
0.2	0.3034	0.0579	0.3034	0.0402	0.3034	0.1573	0.3034	0.1284
0.3	0.3008	-0.0247	0.3008	-0.0474	0.3008	0.1224	0.3008	0.0607
0.4	0.2964	-0.1162	0.2964	-0.1519	0.2964	0.0822	0.2964	-0.0248
0.5	0.2884	-0.2170	0.2884	-0.2778	0.2884	0.0363	0.2884	-0.1260
0.6	0.2768	-0.3282	0.2768	-0.4306	0.2768	-0.0456	0.2768	-0.2478
0.7	0.2619	-0.4508	0.2619	-0.6170	0.2619	-0.0739	0.2619	-0.3753
0.8	0.2439	-0.5856	0.2439	-0.8452	0.2439	-0.1386	0.2439	-0.5239
0.9	0.2231	-0.7332	0.2231	-1.1259	0.2231	-0.2100	0.2231	-0.6890
1.0	0.1995	-0.8945	0.1995	-1.4722	0.1995	-0.2881	0.1995	-0.8714

Table 8.3: Wall mass flux i.e. $\text{Re}_x^{-\frac{1}{2}} Sh_x$ against parameters (Nr , Nb , Nt and Le).

	Nr		Nb		Nt		Le	
dx	0.1	0.7	0.2	2.0	0.2	3.0	1.0	10.0
0.1	0.4002	0.3747	0.4002	0.4029	0.4002	0.6027	0.4002	0.4026
0.2	0.3692	0.2952	0.3692	0.3977	0.3692	0.6879	0.3692	0.4336
0.3	0.3766	0.2748	0.3766	0.4362	0.3766	0.8254	0.3766	0.5123
0.4	0.3897	0.2646	0.3897	0.4731	0.3897	0.9992	0.3897	0.5882
0.5	0.3922	0.2572	0.3922	0.5058	0.3922	1.2111	0.3922	0.6668
0.6	0.3998	0.2520	0.3998	0.5348	0.3998	1.4714	0.3998	0.7309
0.7	0.4085	0.2492	0.4085	0.5610	0.4085	0.1937	0.4085	0.7993
0.8	0.4187	0.2428	0.4187	0.5851	0.4187	2.1948	0.4187	0.8663
0.9	0.4307	0.2504	0.4307	0.6077	0.4307	2.6961	0.4307	0.9322
1.0	0.4448	0.2540	0.4448	0.6239	0.4448	3.3241	0.4448	0.9970

Table 8.4: Microorganisms wall density flux i.e. $\text{Re}_x^{-\frac{1}{2}} Nn_x$ by varying physical parameters (Rb , Lb , Pe and σ).

	Rb		Lb		Pe		σ	
dx	0.1	0.7	1.0	10.0	1.0	2.0	0.1	1.0
0.1	0.4698	0.4491	0.4698	0.4117	0.4698	0.5485	0.4698	0.4923
0.2	0.5029	0.4243	0.5029	0.4631	0.5029	0.6422	0.5029	0.5574
0.3	0.5681	0.4574	0.5681	0.5585	0.5681	0.7560	0.5681	0.6560
0.4	0.6236	0.4997	0.6236	0.6485	0.6236	0.8487	0.6236	0.7423
0.5	0.6689	0.5424	0.6689	0.7335	0.6689	0.9220	0.6689	0.8147
0.6	0.7064	0.5831	0.7064	0.8146	0.7064	0.9809	0.7064	0.8760
0.7	0.7382	0.6210	0.7382	0.8927	0.7382	1.0299	0.7382	0.9290
0.8	0.7661	0.6562	0.7661	0.9684	0.7661	1.0725	0.7661	0.9764
0.9	0.7916	0.6889	0.7916	1.0421	0.7916	1.1111	0.7916	1.0201
1.0	0.8154	0.7197	0.8154	1.1137	0.8154	1.1474	0.8154	1.0616

8.4 Concluding remarks

The current chapter focuses on the movement of motile microorganisms in MHD viscous nanofluid flow. The governing mathematical system is solved via numerical approach finite element method. The impacts of flow controlling parameters are depicted on interested physical quantities via graphs. The key findings of analysis are listed below:

- Velocity of fluid flow asymptotically declines versus y -axis and boundary layer is achieved. Additionally, the buoyancy ratio parameter and Grashof number accelerate the fluid velocity while Hartmann number and bioconvection Rayleigh number produce resistance to fluid movement.
- Temperature enlarges against all controlling parameters (Nb , Nt , Ec and M).
- Concentration of nanoparticles increases versus buoyancy ratio parameter and thermophoresis parameter while both magnetic field and Brownian motion are counterproductive on

it.

- Density of motile microorganisms becomes high against larger values of bioconvection Rayleigh number while all other governing parameters (Lb , Pe and σ) decline the density of motile microorganisms.
- Wall friction factor enlarges for increasing values of all physical parameters (Gr , Nr , Rb and M).
- Wall heat flux decreases versus all physical parameters (Nb , Nt , Ec and M).
- Wall mass flux enlarges versus physical parameters Nb , Nt and Le while it declines against buoyancy ratio parameter Nr .
- Flux of microorganisms density enhances against physical parameters (Lb , Pe and σ) while bioconvection Rayleigh number has opposing effects on it.

Bibliography

- [1] A.W. Sisko, The flow of lubricating greases, *Industrial & Engineering Chemistry*, 50(1958)1789-1792.
- [2] F.T. Akyildiz, K. Vajravelu, R.N. Mohapatra, E. Sweet and R.A. Van Gorder, Implicit differential equation arising in the steady flow of a Sisko fluid, *Applied Mathematics and Computation*, 210(2009)189-196.
- [3] Kh.S. Mekhimer and M.A. El Kot, Mathematical modelling of unsteady flow of a Sisko fluid through an anisotropically tapered elastic arteries with time-variant overlapping stenosis, *Applied Mathematical Modelling*, 36(2012)5393-5407.
- [4] S. Nadeem and N.S. Akbar, Peristaltic flow of Sisko fluid in a uniform inclined tube, *Acta Mechanica Sinica*, 26(2010)675-683.
- [5] S. Nadeem, N.S. Akbar and K. Vajravelu, Peristaltic flow of a Sisko fluid in an endoscope: Analytical and numerical solutions, *International Journal of Computer Mathematics*, 88(2011)1013-1023.
- [6] N.S. Akbar, Peristaltic Sisko nano fluid in an asymmetric channel, *Applied Nanoscience*, 4(2014)663-673.
- [7] M. Khan, S. Munawar and S. Abbasbandy, Steady flow and heat transfer of a Sisko fluid in annular pipe, *International Journal of Heat and Mass Transfer*, 53(2010)1290-1297.
- [8] M. Khan, Q. Abbas, and K. Duru, Magnetohydrodynamic flow of a Sisko fluid in annular pipe: A numerical study, *International Journal for Numerical Methods in Fluids*, 62(2010)1169-1180.

- [9] M. Khan and A. Shahzad, On axisymmetric flow of Sisko fluid over a radially stretching sheet, *International Journal of Non-Linear Mechanics*, 47(2012)999-1007.
- [10] M. Khan and A. Shahzad, On boundary layer flow of Sisko fluid over stretching sheet, *Quaestiones Mathematicae*, 36(2013)137-151.
- [11] M.Y. Malik, Arif Hussain, T. Salahuddin, M. Awais and S. Bilal, Numerical solution of Sisko fluid over a stretching cylinder and heat transfer with variable thermal conductivity, *Journal of Mechanics*, 32(2016)593-601.
- [12] R.M. Darji and M.G. Timol, Similarity Solutions of laminar incompressible boundary layer equations of non-Newtonian viscoelastic fluids, *International Journal of Mathematical Archive*, 2(2011)1395-1404.
- [13] N.S. Akbar, S. Nadeem and C. Lee, Biomechanical analysis of Eyring-Prandtl fluid model for blood flow in stenosed arteries, *International Journal of Nonlinear Science and Numerical Simulation*, 14(2013)345-353.
- [14] N.S. Akbar, MHD Eyring-Prandtl fluid flow with convective boundary conditions in small intestines, *International Journal of Biomathematics*, 6(2013), DOI: 10.1142/S1793524513500344.
- [15] H. Alfven, Existence of electromagnetic-hydrodynamic waves, *Nature*, 150(1942)405-406.
- [16] V.J. Rossow, On flow of electrically conducting fluid over a flat plate in the presence of a transverse magnetic field, *NACA Technical Report Server*, NACA-TN-3971, 44(1957)489-508.
- [17] A. Chakrabarti and A.S. Gupta, Hydromagnetic flow and heat transfer over a stretching sheet, *Quarterly of Applied Mathematics*, 37(1979)73-78.
- [18] H.I. Anderson, An exact solution of the Navier-Stokes equations for magnetohydrodynamic flow, *Acta Mechanica*, 113(1995)241-244.
- [19] K.A. Yih, Free convection effect on MHD coupled heat and mass transfer of a moving permeable vertical surface, *International Communications in Heat and Mass Transfer*, 26(1999)95-104.

- [20] S.J. Liao, On the analytic solution of magnetohydrodynamic flows of non-Newtonian fluids over a stretching sheet, *Journal of Fluid Mechanics*, 488(2003)189-212.
- [21] E.M. Abo-Eldahab and A.M. Salem, MHD flow and heat transfer of non-Newtonian power-law fluid with diffusion and chemical reaction on a moving cylinder, *Heat and Mass Transfer*, 41(2005)703-708.
- [22] R. Cortell, A note on magnetohydrodynamic flow of a power-law fluid over a stretching sheet, *Applied Mathematics and Computation*, 168(2005)557-566.
- [23] A. Ishak, R. Nazar and I. Pop, Hydromagnetic flow and heat transfer adjacent to a stretching vertical sheet, *Heat and Mass Transfer*, 44(2008)921-927.
- [24] N.S. Akbar, A. Ebaid and Z.H. Khan, Numerical analysis of magnetic field effects on Eyring-Powell fluid flow towards a stretching sheet, *Journal of Magnetism and Magnetic Materials*, 382(2015)355-358.
- [25] M.Y. Malik and T. Salahuddin, Numerical solution of MHD stagnation point flow of Williamson fluid over a stretching cylinder, *International Journal of Nonlinear Sciences and Numerical Simulation*, 16(2015)161-164.
- [26] M.Y. Malik, T. Salahuddin, Arif Hussain and S. Bilal, MHD flow of tangent hyperbolic fluid over a stretching cylinder: Using Keller box method, *Journal of Magnetism and Magnetic Materials*, 395(2015)271-276.
- [27] M.J. Lighthill, Studies on MHD waves and other anisotropic wave motion, *Philosophical Transactions of the Royal Society London A: Mathematical, Physical & Engineering Sciences*, 252(1960)397-430.
- [28] H. Sato, The Hall effect in the viscous flow of ionized gas between parallel plates under transverse magnetic field, *Journal of the Physical Society of Japan*, 16(1961)1427-1433.
- [29] R.N. Jana, A.S. Gupta and N. Datta, Hall effects on the hydromagnetic flow past an infinite porous flat plate, *Journal of the Physical Society of Japan*, 43(1977)1767-1772.

- [30] G.S. Seth and S.K. Ghosh, Effect of Hall currents on unsteady hydromagnetic flow in a rotating channel with oscillating pressure gradient, *Indian Journal of Pure and Applied Mathematics*, 17(1986)819-826.
- [31] R.C. Chaudhary and A.K. Jha, Heat and mass transfer in elastic-viscous fluid past an impulsively started infinite vertical plate with Hall Effect, *Latin American Applied Research*, 38(2008)17-26.
- [32] A.M. Salem and M. Abd El-Aziz, Effect of Hall currents and chemical reaction on hydro-magnetic flow of a stretching vertical surface with internal heat generation/absorption, *Applied Mathematical Modelling*, 32(2008)1236-1254.
- [33] F.M. Ali, R. Nazar, N.M. Arifin and I. Pop, Effect of Hall current on MHD mixed convection boundary layer flow over a stretched vertical flat plate, *Meccanica*, 46(2011)1103-1112.
- [34] S. Shateyi and S.S. Motsa, Boundary layer flow and double diffusion over an unsteady stretching surface with hall effect, *Chemical Engineering Communications*, 198(2011)1545-1565.
- [35] M.G. Reddy, Influence of thermal radiation, viscous dissipation and Hall current on MHD convection flow over a stretched vertical flat plate, *Ain Shams Engineering Journal*, 5(2014)169-175.
- [36] K.V. Prasad, K. Vajravelu and Hanumesh Vaidya, Hall effect on MHD flow and heat transfer over a stretching sheet with variable thickness, *International Journal for Computational Methods in Engineering Science and Mechanics*, 17(2016)288-297.
- [37] G. Sreedevi, R. Raghavendra Rao, D.R.V. Prasada Rao and A.J. Chamkha, Combined influence of radiation absorption and Hall current effects on MHD double-diffusive free convective flow past a stretching sheet, *Ain Shams Engineering Journal*, 7(2016)383-397.
- [38] S. Chandra and J.C. Misra, Influence of Hall current and microrotation on the boundary layer flow of an electrically conducting fluid: Application to Hemodynamics, *Journal of Molecular Liquids*, 224(2016)818-824.

- [39] P.S. Gupta and A.S. Gupta, Heat and mass transfer on stretching sheet with suction or blowing, *The Canadian Journal of Chemical Engineering*, 55(1977)744-746.
- [40] B.K Dutta and P. Roy, Temperature field in flow over a stretching surface with uniform heat flux, *International Communications in Heat and Mass Transfer*, 12(1985)89-94.
- [41] L.G. Grubka and K.M. Bobba, Heat transfer characteristics of a continuous stretching surface with variable temperature, *ASME Journal of Heat Transfer*, 107(1985)248-250.
- [42] I.A. Hassanien, A.A.Abdullah and R.S.R.Gorla, Flow and heat transfer in a power-law fluid over a non-isothermal stretching sheet, *Mathematical and Computer Modelling*, 28(1998)105-116.
- [43] R. Cortell, Viscous flow and heat transfer over a nonlinearly stretching sheet, *Applied Mathematics and Computation*, 184(2007)864-873.
- [44] H.I. Andersson and V. Kumaran, On sheet-driven motion of power-law fluids, *International Journal of Non-Linear Mechanics*, 41(2006)1228-1234.
- [45] T.C. Chiam, Heat transfer in a fluid with variable thermal conductivity over a linearly stretching sheet, *Acta Mechanica*, 129(1998)63-72.
- [46] M.S. Abel and N. Mahesha, Heat transfer in MHD viscoelastic fluid flow over a stretching sheet with variable thermal conductivity, non-uniform heat source and radiation, *Applied Mathematical Modelling*, 32(2008)1965-1983.
- [47] M.S. Abel, P.S. Datti and N. Mahesha, Flow and heat transfer in a power-law fluid over a stretching sheet with variable thermal conductivity and non-uniform heat source, *International Journal of Heat and Mass Transfer*, 52(2009)2902-2913.
- [48] M. Mishra, N. Ahmad and Z.U. Siddiqui, Unsteady boundary layer flow past a stretching plate and heat transfer with variable thermal conductivity, *World Journal of Mechanics*, 2(2012)35-41.
- [49] R.R. Rangi and N. Ahmad, Boundary layer flow past over the stretching cylinder with variable thermal conductivity, *Applied Mathematics*, 3(2012)205-209.

- [50] P.K. Singh, Boundary layer flow in porous medium past a moving vertical plate with variable thermal conductivity and permeability, *International Journal of Engineering Research and Development*, 1(2012)22-26.
- [51] L. Miao, W.T. Wu, N. Aubry and M. Massoudi, Heat transfer and flow of a slag-type non-linear fluid: Effects of variable thermal conductivity, *Applied Mathematics and Computation*, 227(2014)77-91.
- [52] A.K. Jhankal, MHD boundary layer flow near stagnation point of linear stretching sheet with variable thermal conductivity via He's homotopy perturbation method, *Journal of Applied Fluid Mechanics*, 8(2015)571-578.
- [53] H.C. Brinkman, Heat effects in capillary flow I, *Applied Scientific Research*, 2(1951)120-124.
- [54] T.F. Lin, K.H. Hawks and W. Leidenfrost, Analysis of viscous dissipation effect on thermal entrance heat transfer in laminar pipe flows with convective boundary conditions, *Heat and Mass Transfer*, 17(1983)97-105.
- [55] K. Vajravelu and A. Hadjinicolaou, Heat transfer in a viscous fluid over a stretching sheet with viscous dissipation and internal heat generation, *International Communications in Heat and Mass Transfer*, 20(1993)417-430.
- [56] T. Shigechi, S. Momoki and D. Ganbat, Effect of viscous dissipation on fully developed heat transfer of plane Couette-Poiseuille laminar flow, *Reports of the Faculty of Engineering, Nagasaki University*, 29(1999)153-156.
- [57] S.P. Anjali Devi and B. Ganga, Viscous dissipation effects on non-linear MHD flow in a porous medium over a stretching porous surface, *International Journal of Mathematics and Mechanics*, 5(2009)45-59.
- [58] P.K. Singh, Viscous dissipation and variable viscosity effects on MHD boundary layer flow in porous medium past a moving vertical plate with suction, *International Journal of Engineering Science and Technology*, 4(2012)2647-2656.

- [59] J. Alinejad and S. Samarbakhsh, Viscous flow over nonlinearly stretching sheet with effects of viscous dissipation, *Journal of Applied Mathematics*, 2012(2012), DOI:10.1155/2012/587834.
- [60] M.G. Reddy, P. Padma and B. Shankar, Effects of viscous dissipation and heat source on unsteady MHD flow over a stretching sheet, *Ain Shams Engineering Journal*, 6(2015)1195-1201.
- [61] F. Mabood, S. Shateyi, M.M. Rashidi, E. Momoniat and N. Freidoonimehr, MHD stagnation point flow heat and mass transfer of nanofluids in porous medium with radiation, viscous dissipation and chemical reaction, *Advanced Powder Technology*, 27(2016)742-749.
- [62] W.A. Aissa and A.A. Mohammadein, Joule heating effects on a micropolar fluid past a stretching sheet with variable electric conductivity, *Journal of Computational and Applied Mechanics*, 6(2005)3-13.
- [63] M.A. Alim, Md.M. Alam, and A.A. Mamun, Joule heating effect on the coupling of conduction with MHD free convection flow from a vertical flat plate, *Nonlinear Analysis: Modelling and Control*, 12(2007)307-316.
- [64] K. Kaladhar, Natural convection flow of couple stress fluid in a vertical channel with Hall and Joule heating effects, *Procedia Engineering*, 127(2015)1071-1078.
- [65] D. Harish Babu and P.V. Satya Narayana, Joule heating effects on MHD mixed convection of a Jeffrey fluid over a stretching sheet with power law heat flux: A numerical study, *Journal of Magnetism and Magnetic Materials*, 412(2016)185-193.
- [66] J.A. Fillo, Viscous and Joule heating effects on the heat transfer from a flat plate, *Physics of Fluids*, 11(1968), DOI:10.1063/1.1691924.
- [67] M.A. Hossain, Viscous and Joule heating effects on MHD free convection flow with variable plate temperature, *International Journal of Heat and Mass Transfer*, 35(1992)3485-3487.

- [68] M.F. El-Amin, Combined effect of viscous dissipation and Joule heating on MHD forced convection over a non-isothermal horizontal cylinder embedded in a fluid saturated porous medium, *Journal of Magnetism Magnetic Materials*, 263(2003)337-343.
- [69] S. Das, R.N. Jana and O.D. Makinde, Magnetohydrodynamic mixed convective slip flow over an inclined porous plate with viscous dissipation and Joule heating, *Alexandria Engineering Journal*, 54(2015)251-261.
- [70] S.M. Ibrahim and K. Suneetha, Heat source and chemical effects on MHD convection flow embedded in a porous medium with Soret, viscous and Joules dissipation, *Ain Shams Engineering Journal*, 7(2016)811-818.
- [71] J.B.J. Fourier, *Théorie Analytique De La Chaleur*, Paris, 1822.
- [72] C. Cattaneo, Sulla conduzionedelcalore, *Atti del Seminario matematico e fisico dell'Università di Modena*, 3(1948)83-101.
- [73] C. Cattaneo, A form of heat conduction equation which eliminates the paradox of instantaneous propagation, *Comptes Rendus*, 247(1958)431-433.
- [74] N. Fox, Generalised thermoelasticity, *International Journal of Engineering Science*, 7(1969)437-445.
- [75] B. Straughan and F. Franchi, Benard convection and the Cattaneo law for heat conduction, *Proceedings of the Royal Society of Edinburgh Section A: Mathematics*, 96(1984)175-178.
- [76] G. Lebon and A. Clout, Benard-Marangoni instability in a Maxwell-Cattaneo fluid, *Physics Letters A*, 105(1984)361-364.
- [77] P. Haupt, *Continuum Mechanics and Theory of Materials*, Springer, Berlin, (2002).
- [78] C.I. Christov, On frame indifferent formulation of the Maxwell-Cattaneo model of finite-speed heat conduction, *Mechanics Research Communications*, 36(2009)481-486.
- [79] M. Ciarletta and B. Straughan, Uniqueness and structural stability for the Cattaneo-Christov equations, *Mechanics Research Communications*, 37(2010)445-447

- [80] B. Straughan, Thermal convection with the Cattaneo-Christov model, *International Journal of Heat and Mass Transfer*, 53(2010)95-98.
- [81] B. Straughan, Porous convection with Cattaneo heat flux, *International Journal of Heat and Mass Transfer*, 53(2010)2808-2812.
- [82] V. Tibullo and V. Zampoli, A uniqueness result for the Cattaneo-Christov heat conduction model applied to incompressible fluids, *Mechanics Research Communications*, 38(2011)77-79.
- [83] T. Salahuddin, M.Y. Malik, Arif Hussain, S. Bilal and M. Awais, MHD flow of Cattaneo-Christov heat flux model for Williamson fluid over a stretching sheet with variable thickness: Using numerical approach, *Journal of Magnetism and Magnetic Materials*, 401(2016)991-997.
- [84] M.Y. Malik, Mair Khan, T. Salahuddin and Imad Khan, Variable viscosity and MHD flow in Casson fluid with Cattaneo-Christov heat flux model: Using Keller box method, *Engineering Science and Technology, an International Journal*, 19(2016)1985-1992.
- [85] A. Tanveer, S. Hina, T. Hayat, M. Mustafa and B. Ahmad, Effects of the Cattaneo-Christov heat flux model on peristalsis, *Engineering Applications of Computational Fluid Mechanics*, 10(2016)373-383.
- [86] S.U.S. Choi, Enhancing thermal conductivity of fluids with nanoparticles, *The Proceedings of the 1995, ASME International Mechanical Engineering Congress and Exposition, San Francisco, USA, ASME, FED 231/MD*, 66(1995)99-105.
- [87] S.U.S. Choi, Z.G. Zhang, W. Yu, F.E. Lockwood and E.A. Grulke, Anomalous thermal conductivity enhancement in nanotube suspensions, *Applied Physics Letters*, 79(2001), DOI:10.1063/1.1408272.
- [88] H.U. Kang, S.H. Kim and J.M. Oh, Estimation of thermal conductivity of nanofluid using experimental effective particle volume, *Experimental Heat Transfer*, 19(2006)181-191.
- [89] D.H. Yoo, K.S. Hong and H.S. Yang, Study of thermal conductivity of nanofluids for the application of heat transfer fluids, *Thermochimica Acta*, 455(2006)66-69.

- [90] S.E.B. Maiga, S.J. Palm, C.T. Nguyen, G. Roy and N. Galanis, Heat transfer enhancement by using nanofluids in forced convection flow, *International Journal of Heat and Fluid Flow*, 26(2005)530-546.
- [91] X.Q. Wang and A.S. Mujumdar, A review on nanofluids-Part I: Theoretical and numerical investigation, *Brazilian Journal of Chemical Engineering*, 25(2008)613-630.
- [92] J. Buongiorno, Convective transport in nanofluids, *ASME Journal of Heat Transfer*, 128(2005)240-250.
- [93] N. Bachok, A. Ishak and I. Pop, Boundary-layer flow of nanofluids over a moving surface in a flowing fluid, *International Journal of Thermal Sciences*, 49(2010)1663-1668.
- [94] W.A. Khan and I. Pop, Boundary-layer flow of a nanofluid past a stretching sheet, *International Journal of Heat and Mass Transfer*, 53(2010)2477-2483.
- [95] P. Rana and R. Bhargava, Flow and heat transfer of a nanofluid over a nonlinearly stretching sheet: A numerical study, *Communications in Nonlinear Science and Numerical Simulation*, 17(2012)212-226.
- [96] K. Zaimi, A. Ishak and I. Pop, Boundary layer flow and heat transfer over a nonlinearly permeable stretching/shrinking sheet in a nanofluid, *Scientific Reports*, 4(2014), DOI: 10.1038/srep04404
- [97] F. Mabood, W.A. Khan and A.I.M. Ismail, MHD boundary layer flow and heat transfer of nanofluids over a nonlinear stretching sheet: A numerical study, *Journal of Magnetism and Magnetic Materials*, 374(2015)569-576.
- [98] M.Y. Malik, Imad Khan, Arif Hussain and T. Salahuddin, Mixed convection flow of MHD Eyring-Powell nanofluid over a stretching sheet: A numerical study, *AIP Advances*, 5(2015), DOI:10.1063/1.4935639.
- [99] S. Naramgari and C. Sulochana, MHD flow over a permeable stretching/shrinking sheet of a nanofluid with suction/injection, *Alexandria Engineering Journal*, 55(2016)819-827.
- [100] T. Cebeci and P. Bradshaw, *Physical and computational aspects of convective heat transfer*, Springer-Verlag New York, (1984)407-413

- [101] C.Y. Wang, Free convection on a vertical stretching surface, *Journal of Applied Mathematics and Mechanics(ZAMM)*, 69(1989)418-420.
- [102] R.S.R. Gorla and I. Sidawi, Free convection on a vertical stretching surface with suction and blowing, *Applied Scientific Research*, 52(1994)247-257.
- [103] T. Fang, J. Zhang and Y. Zhong, Boundary layer flow over a stretching sheet with variable thickness, *Applied Mathematics and Computation*, 218(2012)7241-7252.
- [104] M.M. Khader and A.M. Megahed, Boundary layer flow due to a stretching sheet with a variable thickness and slip conditions, *Journal of Applied Mechanics and Technical Physics*, 56(2015)241-247.
- [105] W.A. Khan, O.D. Makinde and Z.H. Khan, MHD boundary layer flow of a nanofluid containing gyrotactic microorganisms past a vertical plate with Navier slip, *International Journal of Heat and Mass Transfer*, 74(2014)285-291.
- [106] W.N. Mutuku and O.D. Makinde, Hydromagnetic bioconvection of nanofluid over a permeable vertical plate due to gyrotactic microorganisms, *Computers & Fluids*, 95(2014)88-97.
- [107] K. Das, P.R. Duari and P.K. Kundu, Nanofluid bioconvection in presence of gyrotactic microorganisms and chemical reaction in a porous medium, *Journal of Mechanical Science and Technology*, 29(2015)4841-4849.
- [108] J.R. Cash and A.H. Carp, A variable order Runge-Kutta method for initial value problems with rapidly varying right-hand sides, *ACM Transactions on Mathematical Software* 16(1990)201-222.